EVALUATION OF THE SEISMIC PERFORMANCE OF A LOW-RISE SPECIAL MOMENT-RESISTING STEEL FRAME STRUCTURE DESIGNED ACCORDING TO THE TURKISH BUILDING EARTHQUAKE CODE (2018)

A THESIS SUBMITTED TO
THE GRADUATE SCHOOL OF NATURAL AND APPLIED SCIENCES
OF
MIDDLE EAST TECHNICAL UNIVERSITY

BY

SÜMEYYE SELEN TEMİZER

IN PARTIAL FULFILLMENT OF THE REQUIREMENTS
FOR
THE DEGREE OF MASTER OF SCIENCE
IN
CIVIL ENGINEERING

SEPTEMBER 2024

Approval of the thesis:

EVALUATION OF THE SEISMIC PERFORMANCE OF A LOW-RISE SPECIAL MOMENT-RESISTING STEEL FRAME STRUCTURE DESIGNED ACCORDING TO THE TURKISH BUILDING EARTHQUAKE CODE (2018)

submitted by **SÜMEYYE SELEN TEMİZER** in partial fulfillment of the requirements for the degree of **Master of Science** i**n Civil Engineering, Middle East Technical University** by,

Prof. Dr. Naci Emre Altun
Dean, **Graduate School of Natural and Applied Sciences** ________________

Prof. Dr. Erdem Canbay
Head of the Department, **Civil Engineering** ________________

Prof. Dr. Afşin Sarıtaş
Supervisor, Civil Engineering, METU ________________

Examining Committee Members:

Prof. Dr. Cem Topkaya
Civil Engineering Dept., METU ________________

Prof. Dr. Afşin Sarıtaş
Civil Engineering Dept., METU ________________

Prof. Dr. Alp Caner
Civil Engineering Dept., METU ________________

Prof. Dr. Murat Altuğ Erberik
Civil Engineering Dept., METU ________________

Assist. Prof. Dr. Ertan Sönmez
Civil Engineering Dept., Atılım University ________________

Date: 06.09.2024

I hereby declare that all information in this document has been obtained and presented in accordance with academic rules and ethical conduct. I also declare that, as required by these rules and conduct, I have fully cited and referenced all material and results that are not original to this work.

Name Last name : Temizer, Sümeyye Selen

Signature :

ABSTRACT

EVALUATION OF THE SEISMIC PERFORMANCE OF A LOW-RISE SPECIAL MOMENT-RESISTING STEEL FRAME STRUCTURE DESIGNED ACCORDING TO THE TURKISH BUILDING EARTHQUAKE CODE (2018)

Temizer, Sümeyye Selen
Master of Science, Civil Engineering
Supervisor : Prof. Dr. Afşin Sarıtaş

September 2024, 120 pages

On February 6, 2023, seismic events with epicenters in Pazarcık and Elbistan led to the collapse of numerous buildings. This study examines methods to enhance the seismic performance of moment-resisting steel-framed buildings, focusing on the structures in Defne, Antakya. A hypothetical building, designed per the 2018 Turkish Building Earthquake Code and 2018 Steel Structure Design, Calculation, and Construction Principles, was analyzed using nonlinear plastic hinge and link models in SAP2000 with earthquake data from station 3129 (Defne, Antakya). The study evaluated different structural configurations, including bare frames, continuous infill walls, and no infill walls on the first floor, as well as basement floor implementation.

The results indicate that continuous infill walls significantly reduce lateral displacements, while the absence of infill walls on the first floor negatively affects structural behavior. Consequently, the continuity of the infill walls across all floors is highly recommended, especially in high seismic zones. Furthermore, the inclusion of a basement floor improves overall performance by reducing the lateral displacement and plastic hinging in the first-floor columns. Also, using a higher steel grade in columns than in beams and limiting the axial load capacity usage in columns below 50% in design enhances the building's resilience under major seismic events. These findings provide insights into improving the seismic design of special moment-resisting frames, which can be integrated into future revisions of regulations.

Keywords: Earthquake, Seismic Design, Time-History Analysis, Infill Wall, Basement Floor

ÖZ

2018 TÜRKİYE DEPREM YÖNETMELİĞİNE GÖRE TASARLANAN ALÇAK KATLI SÜNEKLİK DÜZEYİ YÜKSEK ÇELİK ÇERÇEVE BİR YAPININ SİSMİK PERFORMANS DEĞERLENDİRMESİ

Temizer, Sümeyye Selen
Yüksek Lisans, İnşaat Mühendisliği
Tez Yöneticisi: Prof. Dr. Afşin Sarıtaş

Eylül 2024, 120 sayfa

6 Şubat 2023'te merkez üssü Pazarcık ve Elbistan olan sismik olaylar çok sayıda binanın yıkılmasına yol açtı. Bu çalışma, Defne, Antakya'daki yapılara odaklanarak, süneklik düzeyi yüksek çelik çerçeve yapıların sismik performansını artırmaya yönelik yöntemleri incelemektedir. 2018 Türk Bina Deprem Yönetmeliği ve 2018 Çelik Yapı Tasarım, Hesap ve Yapım Esasları'na göre tasarlanan varsayımsal bir bina, 3129 (Defne /Antakya) istasyonundan alınan deprem verileriyle SAP2000'de doğrusal olmayan plastik mafsal ve bağlantı modelleri kullanılarak analiz edilmiştir. Çalışmada çıplak çerçeveler, sürekli dolgu duvarlar ve birinci katta dolgu duvar olmamasının yanı sıra bodrum kat uygulaması da dahil olmak üzere farklı yapısal konfigürasyonlar değerlendirilmiştir.

Sonuçlar, sürekli dolgu duvarların yanal yer değiştirmeleri önemli ölçüde azalttığını, birinci katta dolgu duvarların bulunmamasının ise yapısal davranışı olumsuz etkilediğini göstermektedir. Bu sebeple, özellikle yüksek deprem bölgelerinde dolgu duvarların tüm katlarda devamlılığı önemle tavsiye edilmektedir. Ayrıca, yapıya bodrum katının dahil edilmesi, birinci kat kolonlarındaki yanal yer değiştirmeyi ve mafsal bölgelerindeki plastikleşmeyi azaltarak genel deprem performansını artırmaktadır. Ayrıca kolonlarda kirişlere göre daha yüksek, çelik kalitesi kullanılması ve kolonlarda eksenel yük kapasite kullanımının tasarımda %50'nin altında sınırlandırılması, binanın yüksek sismik olaylara karşı dayanıklılığını artırmaktadır. Bu bulgular, yönetmeliklerin gelecekteki revizyonlarına entegre edilebilecek süneklik düzeyi yüksek çerçevelerin sismik performansının iyileştirilmesine yönelik bilgiler sunmaktadır.

Anahtar Kelimeler: Deprem, Sismik Tasarım, Zaman Tanım Analizi, Dolgu Duvar, Bodrum Katı

To my family,

ACKNOWLEDGMENTS

I would like to express my deepest gratitude to my supervisor, Prof. Dr. Afşin Sarıtaş, for his guidance, advice, criticism, encouragement, and insight throughout the research. It was a great pleasure for me to work under his kind supervision. I am deeply grateful for his mentorship and dedication.

I am equally thankful to my co-advisor (unofficial) Dr. Halil Fırat Özel for his advice and support. It is very valuable that he answered all my questions with great patience and gave his time to guide me.

I would like to extend my deep thanks to my manager, Mr. Serkan Şahin. I completed my thesis while I was working in the Mitaş Industry. His endless support and contributions are gratefully acknowledged. He always has a willingness to share his experience. I am very fortunate to have his companionship and supportive work environment.

I would like to express my sincere gratitude for the unwavering support and encouragement of my colleague, Mr. Altan Zervent. He always approached me with the warmth and sincerity of an older brother. He thoughtfully and patiently answered all my questions, significantly contributing to the progress of my thesis. I deeply appreciate the enthusiasm that he shared in each step of my progress and for letting me know that he is always there to facilitate my work.

I'm really thankful for all the support from Assoc. Prof. Dr. Alper Aldemir during my time as an undergraduate, in my Master's program, and even throughout my business journey. His vast knowledge and genuine interest in my development have been truly invaluable.

Last but not least, I would like to express my heartfelt thanks to my family, Nalan Gemalmaz, Enver Temizer, and my fiancé Rasim Sarı. The love and support they have given me throughout my life are priceless.

TABLE OF CONTENTS

LIST OF TABLES

TABLES

LIST OF FIGURES

FIGURES

LIST OF ABBREVIATIONS

ABBREVIATIONS

Design, Calculation, and Construction Principles of Steel Structures **DCCPSS2018**

Turkish Building Earthquake Code 2018 **TBEC2018**

Moment Resisting Frame **MRF**

Load and Resistance Factor Design **LRFD**

Strong Column Weak Beam **SCWB**

Drift Ratio **DR**

CHAPTER 1

INTRODUCTION

1.1 General

A significant portion of Anatolia, located in the Alp-Himalaya fold belt, is situated within the first and second-degree seismic zones. The first-degree seismic zone encompasses areas near tectonic basins and active fault lines. In these regions, earthquakes typically lead to considerable loss of lives and extensive property damage.. The second-degree seismic zone, in comparison to the first-degree zone, causes less damage.

The presence of these seismic zones in Anatolia indicates that its geological development is not yet complete. The seismic zones in Turkey include the Western Anatolian Seismic Zone, the Southeastern Anatolian Seismic Zone, and the North Anatolian Seismic Zone.

One of Turkey's most active fault systems, the North Anatolian Fault System (NAFS), which forms the boundary between the Anatolian and Arabian Plates, opposes the westward movement of the Anatolian block. Current GPS data indicates a slip rate of 11±2mm/year for the present-day movement.

On February 6, 2023, two earthquakes occurred on the Southeast Anatolian Fault Line in Turkey, with epicenters in Kahramanmaraş/Pazarcık and Kahramanmaraş/Elbistan, respectively, with magnitudes of 7.7 Mw (Latitude: 37.288 N, Longitude: 37.043 E) and 7.6 Mw (Latitude: 38.089 N, Longitude: 37.239 E), happening 9 hours apart. These earthquakes deeply affected 11 regions in Turkey and were felt across a broad geography, including Syria, Lebanon, Cyprus, Iraq, and Egypt.

Official figures indicate that over 50,000 people lost their lives, with 58,000 buildings collapsed and more than 200,000 buildings severely damaged. About 97% of the buildings that collapsed were constructed prior to 2000, with around 5,000 buildings constructed after 2000 being identified as collapsed or having suffered significant damage.

Besides the damage incurred by old buildings, it has been observed that even newly constructed structures exhibited surprisingly poor performance. In this study, a 4-story steel building that is designed in compliance with the TBEC2018 and ‘Design, Calculation and Construction Principles of Steel Structures’ released in 2018 regulations are utilized through a nonlinear time-history analysis, and its performance during the Kahramanmaraş earthquakes will be evaluated. This building is designed by taking the reference to the building described in Example C-1 in the 'Turkish Building Earthquake Regulations (TBEC-2018) Training Presentations' book written by Erkan Özer, Cavidan Yorgun, and Cüneyt Vatansever in October 2018. Since it was designed for the Istanbul/Maslak region, the structure in the study is designed for the Hatay/Defne region to investigate the seismic response to the Kahramanmaraş earthquake in a realistic manner. The structural elements are designed according to TBEC2018 and DCCPSS2018 for the Hatay/Defne region and have been changed to comply with the relative floor displacement rule. The design principles followed have been shared in Chapter 2.

The buildings are analyzed using a well-known design and analysis program SAP2000 (Version 25.2.0) by Computer and Structures Inc. The assessment of the building's responses to seismic impacts has been conducted within the framework of the Turkey Building Earthquake Regulations 2018 (TBEC2018) rules. During the assessment, the hinge rotation limitations are considered. For this reason, before moving on to the assessment part, the SAP2000 “Auto Hinge” properties, which are installed to capture the nonlinear behavior of column and beam structural elements, are verified. The response on the hinge rotation on a single column under static pushover and nonlinear time-history analysis, including whether a tensile or compressive axial load on the column, is checked according to ASCE41-17. The hinge verification is presented in Chapter 3.

Also, in order to capture a structural overall behavior in a more realistic way, the infill walls used in the building are implemented in the model and considered in the assessment. 3 different buildings are generated - one with bare frame, one with continuous infill wall across all stories, and one with no infill wall in the 1st story. An additional assessment of the material strength is performed. The buildings are generated with different material strengths and their performance under the same seismic data are examined. When the material quality is increased, the change in the structural behavior is interpreted based on the 6 buildings in total. The infill wall modeling and the analysis results conducted with the data of station 3129 are shown in Chapter 4 and Chapter 5, respectively.

In addition to the infill wall investigation, the impact of basement floor use on the building seismic performance is examined. The basement floor is implemented by doubling the 1st floor. The same moment releases and the same geometrical configuration as the 1st floor is used for the basement floor. The shear wall effect and surrounding ground are simulated by using the lateral supports. The basement wall is added to the 6 aforementioned configurations. The models and the analysis results are shared in Chapter 6.

Non-linear time history analyses have been performed, taking into account the earthquake data of Station 3129 (Lat:36.19117, Long:36.1343) located in Defne/Antakya. The buildings are analyzed using a commercial design and analysis program SAP2000. After conducting a thorough analysis of these 6 different building's responses to the Kahramanmaraş earthquake, an assessment will be made to evaluate the suitability of the current standards in the context of the design parameters. Recommendations will be presented to enhance the overall structural seismic response in Chapter 7.

1.2 Soil Properties and Earthquake Data

The earthquake data used in this thesis is taken from station 3129 (Lat:36.19117, Long:36.1343) in the Defne district in the Hatay Province of Turkiye. https://tadas.afad.gov.tr/ showcases the station's features, summarized in Table 1-1, and its location is depicted in Figure 1-1.

Table 1-1: Station Information of 3129

Station Code:	3129
Location:	Lat:36.19117, Long:36.1343
District / City:	Defne/Antakya
Lithology Class:	Clastic Rocks
Average seismic shear-wave velocity from the surface to a depth of 30 meters, $(Vs)_{30}$ (m/s):	447

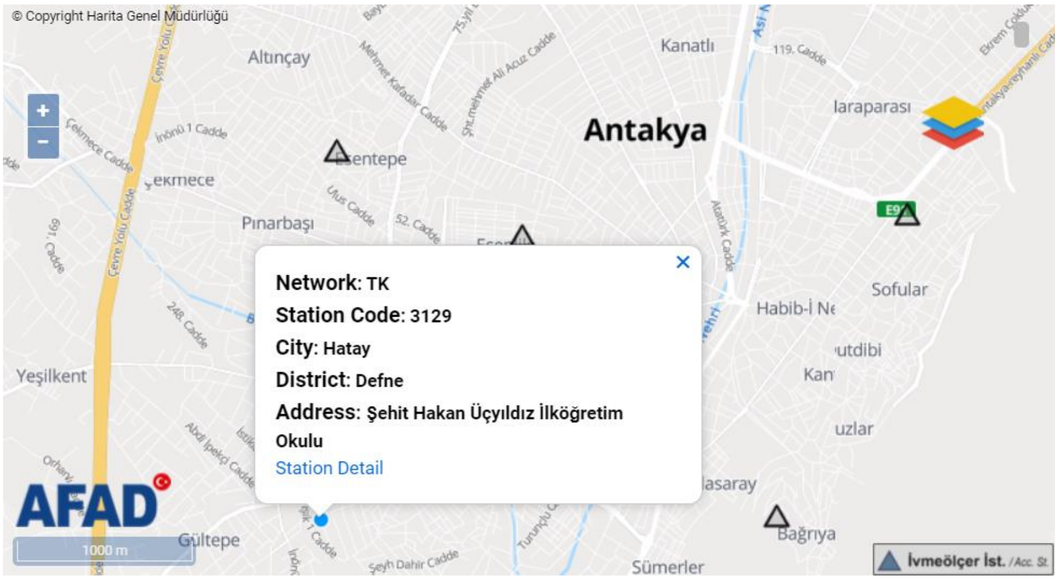

Figure 1-1: The location of the station 3129

Table 1-2 can be used to determine local soil classes defined as ZA, ZB, ZC, ZD, and ZE, as stated in TBEC2018 Section 16.4.1. Site-specific research and evaluation are required for ZF soils.

Table 1-2: Local soil classes specified in TBEC2018

Local Soil Class	**Soil Type**	**Vs30 (m/s)**
ZA	Rocks or other rock-like geological formulations	>1500
ZB	Slightly weathered rocks	760-1500
ZC	Very dense sand, gravel, and hard clay or weathered rocks with many cracks	360-760
ZD	Medium-dense layers of sand, gravel, or very solid clay	180-360
ZE	Loose sand, soft clay	<180
ZF	Soils requiring site-specific investigations	

With the $(Vs)_{30}$ value of 447 m/s for station 3129, the local soil class can be determined as ZC, which represents the very dense sand, gravel, and hard clay or weathered rocks with many cracks.

The earthquake records are plotted in Figure 1-2. The peak ground acceleration (PGA) values of the East-West, North-South, and Up-Down Acceleration records belonging to the 6 Feb 2023 Pazarcık Earthquake are 1.222g, 1.3777g, and 0.07382g, respectively. The PGA values for the location taken from the AFAD hazard map of Turkiye are 0.452g and 0.89g for the 475- and 2475 return periods, corresponding to DD-1 and DD-2, respectively. Considering this specific earthquake and location, the PGA value used in design should be increased by at least 2.70.

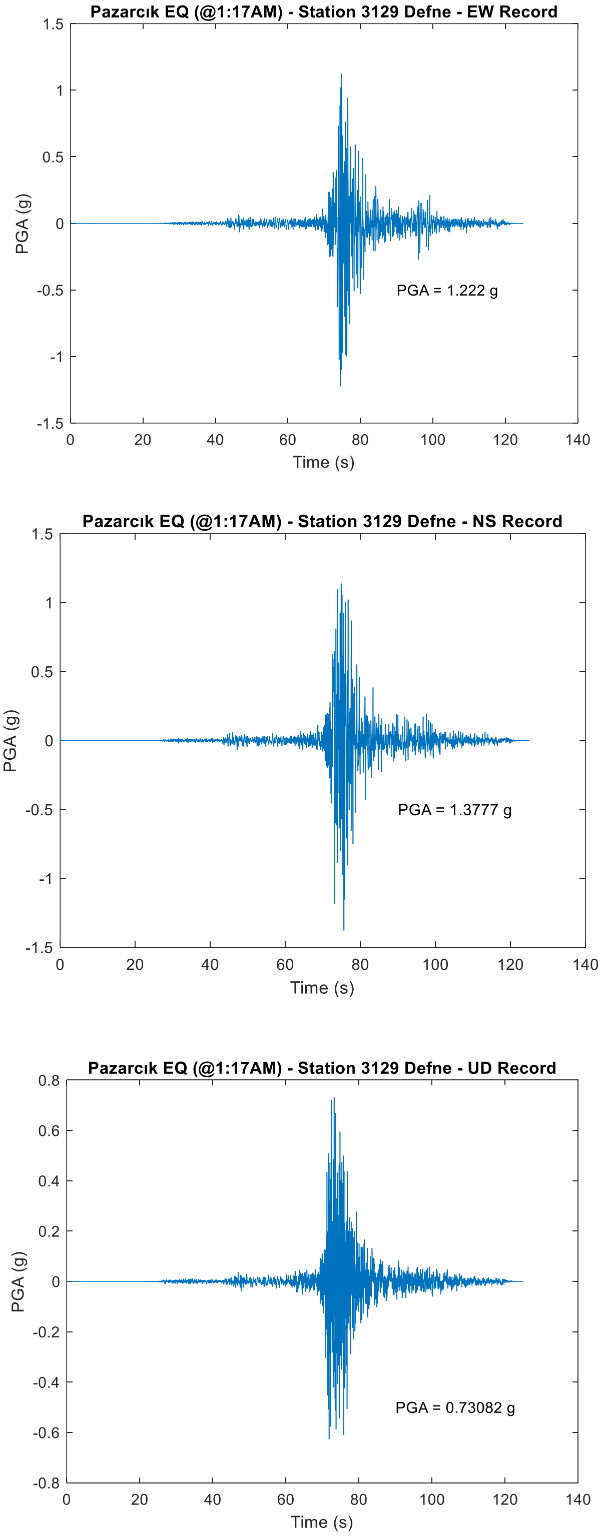

Figure 1-2: Pazarcık earthquake acceleration records of station 3129 (EW record, NS record, and UD record from up to down)

Upon comparing the design spectra of DD-1 and DD-2 to the spectra obtained from the Pazarcık Earthquake in Figure 1-3, it becomes evident that there is a substantial discrepancy between the design response spectra and earthquake spectral acceleration. This observation highlights the need for a closer examination and possibly a re-evaluation of design parameters.

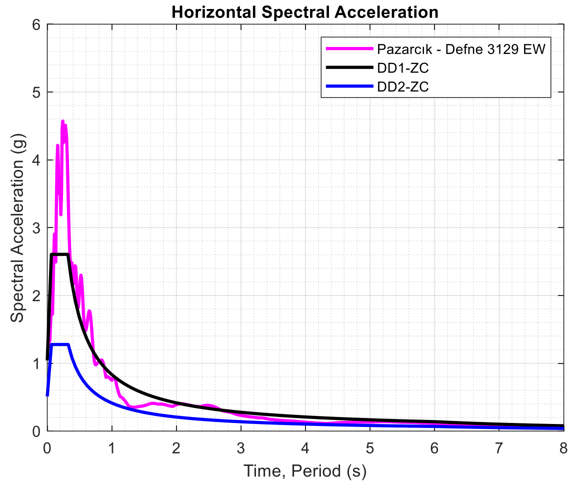

a)

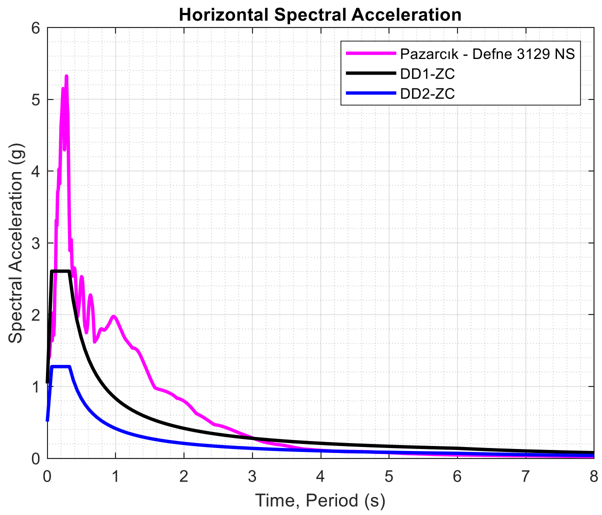

b)

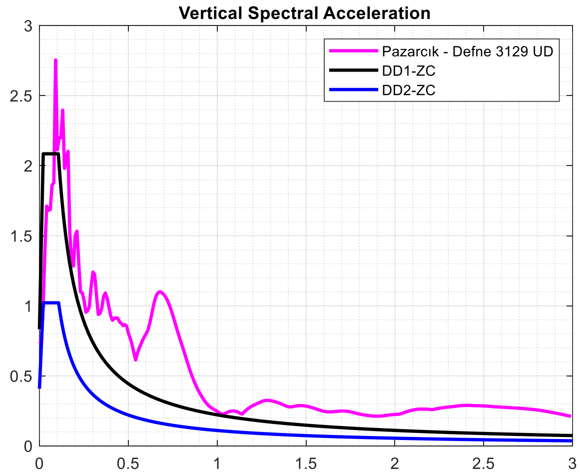

c)

Figure 1-3: Comparison of Pazarcık EQ - Defne 3129 AFAD DD-1 and DD-2 Design Response Spectra with a) EW Records b)NS Records c) UD Records

1.3 Literature Review

Countries follow certain norms and guidelines for designing steel constructions. There are similarities between Turkey's seismic code and other contemporary codes, particularly the American seismic code ASCE.

M. Zorlu et. al. (2017) conducted a study comparing the Building Earthquake Codes released in 2007 and 2016. They evaluated two different buildings of 4 and 9-story within the framework of TBEC2007 and TBEC2016 Building Earthquake Codes. The cross-section conditions of the building elements were examined under seismic loads according to the regulations. In TBEC-2007, the relative story drift ratio limit ($\delta_{i,max}/h_i$) is determined as 0.002. However, according to TBEC-2016, relative story drift limit values are determined depending on whether flexible joint detail is used or not. M. Zorlu et. al. also states at the end of the study that the element sizing is very similar when the sample buildings are designed according to the TBEC2016 and ASCE07.

The Turkish Statistical Institute reports that approximately half of the 3,478,575 buildings in earthquake-prone provinces of Hatay, Adana, Diyarbakır, Elazığ, Gaziantep, Osmaniye, Malatya, Kahramanmaraş, Adıyaman, Kilis, and Şanlıurfa were built in 2000 or later.

There are studies examining the causes of the destruction in the Kahramanmaraş earthquake in detail. In the study conducted by B. Binici et al. (2023), in which detailed studies were carried out, especially on highly damaged or collapsed reinforced concrete buildings, it is stated that TEC1975, which is based on buildings built before 2000 in Turkey, is inadequate compared to the 1998, 2007 and 2018 regulations published later. Several factors contribute to these issues. Firstly, TEC1975's design, which relies on low seismic forces and solely on the equivalent lateral force method, is not robust enough. There's also a notable lack of expertise in employing the strong column-weak beam approach, alongside a disregard for the impacts of higher mode effects and structural irregularities. Furthermore, it has been observed that the design response spectra in the Hatay region surpass both the DD-2 level (designated for a design-basis earthquake with a recurrence interval of 475 years) and the DD-1 level (for a rare earthquake with a recurrence interval of 2475 years), raising concerns about building designs in the area. Between the 0-0.5s and 0.5-1.5s period ranges, the values are 1.75 and 4.65 times above the spectral acceleration values calculated according to the TBEC2018, respectively. The comprehensive assessment of the collapse causes has identified that the primary factor is the creation of soft stories, which occur when the first floor is utilized for commercial purposes. Other significant factors include a poor understanding of how lateral forces are distributed to vertical structural components, the underestimation of seismic requirements, and the lack of detailed examination of the local soil conditions before building constructed. These were contributing factors to the building collapses during the Kahramanmaraş earthquakes.

According to Hacettepe University's Earthquake Investigation Report, in certain areas, the measured earthquake recordings surpass the seismic code. The acceleration demands during earthquakes, especially in Hatay province, are around 2.5 times more than the elastic design acceleration value taken into account in seismic codes with 475-year return periods in 1975, 2007, and 2018 Earthquake Standards. The acceleration demands are found to be higher in the Kahramanmaraş Pazarcık district than even 2475-year return period. According to the same study, Hacettepe University faculty members have seen vertical acceleration levels during earthquakes have reached about 3g. Vertical acceleration was not taken into account in specifications from 1974 to 1988; however, in designs that have been in use after 1988, the maximum vertical acceleration is limited to 2g. Nonetheless, a vertical acceleration of 3g observed in Hatay province led to more devastation during the earthquake.

M. N. Aydınoğlu et al. specifically address the inadequate inspections of pre-2000 buildings, such as the use of unsorted aggregates from the seas directly in concrete, lack of cement production knowledge, and the lack of vibrator use in their study analyzing the destruction in Antakya. When the high demand for acceleration is added to all these deficiencies, it is not surprising that the buildings before 2000 were demolished. Even newly completed buildings that were built after 2000 have collapsed and sustained major damage. In the same study, despite these high acceleration demands, some reasons for some buildings that did not collapse are explained as follows: Structures may be capable of far greater strength than what codes specify. Building collapse might have been avoided by excessive steel reinforcing, material strengths above code standards, and beneficial reinforcement effects at column-beam connections. Differences in ground accelerations and velocities amongst buildings might have lessened the effect of the earthquake on structures. Furthermore, weak soil properties might have affected the buildings with short periods less than what the specifications assumed.

A. Yakut et. al. (2023) wrote in their review article on high-risk buildings in Turkey that strengthening techniques such as base insulation, adding external walls with adequate anchors use of high-quality materials (ready-mixed concrete, quality steel, etc.), and improving foundation systems can also be effective in reducing the risk of earthquakes. The article also noted that the seismic forces (response spectra) calculated from the measurements recorded at the AFAD stations in various Hatay locations (Antakya, Arsuz, Hassa, Kırıkhan) exceeded the design response spectra outlined by the Turkish Earthquake Regulation. It is emphasized that some of the damage may have occurred for this reason, even if the buildings were built in accordance with the earthquake regulations.

The study conducted by A. Aldemir (2024) et al. focuses on investigating the seismic performance of medium-rise reinforced concrete frame buildings in Turkey, particularly during the Kahramanmaraş earthquakes. The authors designed structures based on past earthquake regulations and standards (1968, 1975, 1998, and 2007 with TS500), created numerical models for analysis, and assessed the seismic performance of 88 different buildings. It is found that buildings designed based on past earthquake regulations are insufficient in seismic resistance and prone to collapse during seismic events. The research highlighted the importance of updated design approaches to enhance structural safety and prevent failures in such high-risk seismic zones. Even the buildings designed with the method of 'Strong Column-Weak Beam', the structural elements were insufficient to meet the moment-shear force demand due to the high acceleration values during the Kahramanmaraş earthquake. A. Aldemir et. al. also recommend the addition of a rule to standards mandating the implementation of shear walls in buildings located in seismic zones 1 and 2.

Another study conducted by A. Aldemir et. al. (2024) investigates the seismic performance of medium-rise steel frame buildings in Hatay province during the 2023 Kahramanmaras earthquakes. It highlights that most buildings designed according to past earthquake regulations are inadequate in seismic resistance. A 5-story building designed according to the TEC2007 is considered in this study. The study considered 11 different positions and directions for each building type, using data from AFAD stations to ensure a comprehensive analysis. Seismic data from AFAD stations in

Hatay province is utilized as a time-history function. The findings show that 10 out of 11 buildings were prone to collapse during the Kahramanmaraş earthquake. The research emphasizes the importance of updating building codes and regulations to enhance seismic resilience. A. Aldemir et al. also indicated that it should be mandatory in the regulations to implement steel bracing to the moment resisting frames in the high-risk seismic zones.

The research by A.M. Elkady et al. (2012) explores the dynamic stability of narrow, deep steel columns located in areas prone to seismic activity. This study focuses particularly on how combined axial loads and bending moments affect these columns. It centers on the W24x16 column cross-section, which is often employed in the construction of special moment resisting frames (MRFs) designed for earthquake zones. Considerations in the study also cover geometric imperfections and residual stresses. Key aspects include the rapid deterioration in strength and stiffness of the columns, as well as the occurrence of axial shortening with increasing axial load demands. The decrease in strength of the W24x16 column under the specific loading condition where P/Py equals 0.5 is mainly due to the P-Delta effect, as shown in Figure 1-4.

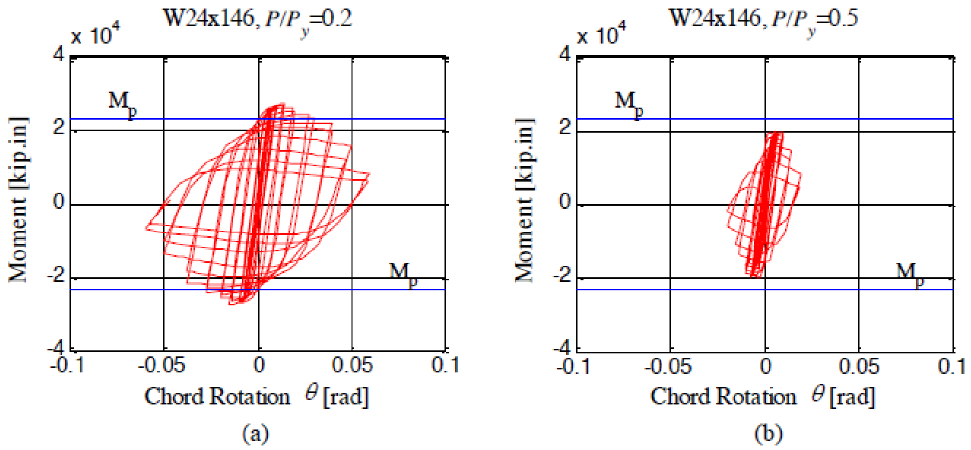

Figure 1-4: Predicted end moment-chord rotation of a fixed-fixed W24x146 steel column subjected to the hysteretic load (A.M. Elkady et al. 2012)

The increase in axial load ratio causes rapid bending strength deterioration, leading to a significant decrease in the column's bending moment resistance capacity. Additionally, the progression of axial shortening in the column accelerates as the P/Py ratio increases, further contributing to the loss of bending strength. This indicates that as the axial load demand approaches 50% of the critical load, the column experiences a more pronounced decline in strength, ultimately affecting its overall structural performance. The P-Delta effect causes strength and stiffness deterioration in the column, making it more vulnerable to failure under increasing axial load demands. Additionally, when P/Py=0.50, the ductility ratio of the column, which is the plastic component of the rotation over yielding rotation, appears to be significantly larger than the assumed zero plastic rotation capacity based on the ASCE41 provisions. Also, with an increase in axial load, the plastic hinge of the steel column shifts away from the column base. This can be explained by the P-Delta effects, which cause the point of maximum moment to move away from the column end.

According to the 2018 Steel Specification, in all elements where bending rigidity affects structural stability, bending rigidities will be additionally multiplied by a τ_b coefficient depending on the level of axial force. The limit for multiplication is P/Py=0.5. When P/Py $\leq$ 0.5, the τ_b coefficient is applied as 1.0. In cases where P/Py>0.5, Eq. 1-1 is applied for τ_b.

$$\boldsymbol{\tau_b = 4(\alpha P/P_y) * (1 - \alpha P/P_y)} \qquad \text{(Eq. 1-1)}$$

α is 1.0 for the ‘Load and Resistance Factor Design’ method that will be used in this study. The specification also states that if the P/Py ratio is greater than 0.5, the τ_b coefficient can be applied as 1.0 provided by applying 0.001Yi additional fictitious loads for all horizontal and vertical load combinations.

Masonry infill walls significantly enhance the capacity of steel frames to resist lateral loads and dissipate energy, thereby increasing the resilience of the structure against seismic activities. However, they can lead to stress concentration at connections and introduce uncertainties in structural response. (W. Jing-Ren et. Al. 2022) Traditionally deemed non-structural components, their role in seismic assessment frameworks is evolving as they have been shown to substantially affect the performance of moment-resisting frames. The elastic properties of masonry infills, such as Young's modulus, vary according to the materials used (brick and mortar), influencing overall behavior. Lastly, the aspect ratio of masonry infill walls is critical, as it affects the distribution of stresses and damage patterns during loading events. There are two main methods for modeling these infill walls: micro-modeling and macro-modeling:

Micro-modeling entails detailed simulations that precisely capture the mechanical behavior of the infill materials and their interaction with the frame, requiring substantial computational resources. While this method provides accurate insights, it may not be practical for large-scale structures. On the other hand, macro-modeling simplifies the representation of infill walls, often using equivalent strut models. This method is more computationally efficient and focuses on the overall structural response. Equivalent strut models are used to simply capture the wall’s compressive behavior under lateral loads.

In their research, J-R. Wu et al. (2012) employed models featuring a single strut to investigate and compare both micro and macro modeling techniques for infill walls. They refined these models through calibration with genetic algorithm outcomes. To enhance the dataset and accurately capture the force-displacement characteristics of masonry infill walls, they supplemented their experimental findings with data derived from numerical simulations. The initial database was established by analyzing data from prior experimental trials of nine prototypes featuring infill walls of varying heights and lengths. This analysis aimed to observe the behavior of masonry infills within steel frames in detail. Following this, a genetic algorithm was formulated, incorporating three main steps: (i) collecting data from earlier experimental studies on an existing infilled MRF, (ii) creating a calibrated micro-model, which is used as a reference model for the macro-model, (iii) generating a macro-model with a single-strut and calibrate the parameters according to the database obtained from the micro-model. The micro-modeling FE analysis is done using the ABAQUS program, and the model is calibrated according to the experimental data. The stress contour of masonry infills at the end of the FE analysis proves that the aspect ratio of the infills (L_{infill}/H_{infill}) has a significant influence on the response of the infill walls. As depicted in the Figure 1-5, Model-7 demonstrates the most significant off-diagonal strut, compensating for the majority of the stress loss. Model 3 and Model 6 likewise reveal a decrease in strength, underscoring the effect of aspect ratio on performance.

Model	E_{adj}(MPa)	L(mm)	H(mm)	L_{Infill}(mm)	H_{Infill}(mm)	$(L/H)_{Infill}$(-)
Model-1	6135	3506	2575	3500	2325	1.505
Model-2	6135	2906	2575	2900	2325	1.247
Model-3	6135	2306	2575	2300	2325	0.989
Model-4	6150	3506	2389	3500	2139	1.636
Model-5	6150	2906	2389	2900	2139	1.356
Model-6	6150	2306	2389	2300	2139	1.075
Model-7	6165	3506	2203	3500	1953	1.792
Model-8	6165	2906	2203	2900	1953	1.485
Model-9	6165	2306	2203	2300	1953	1.178

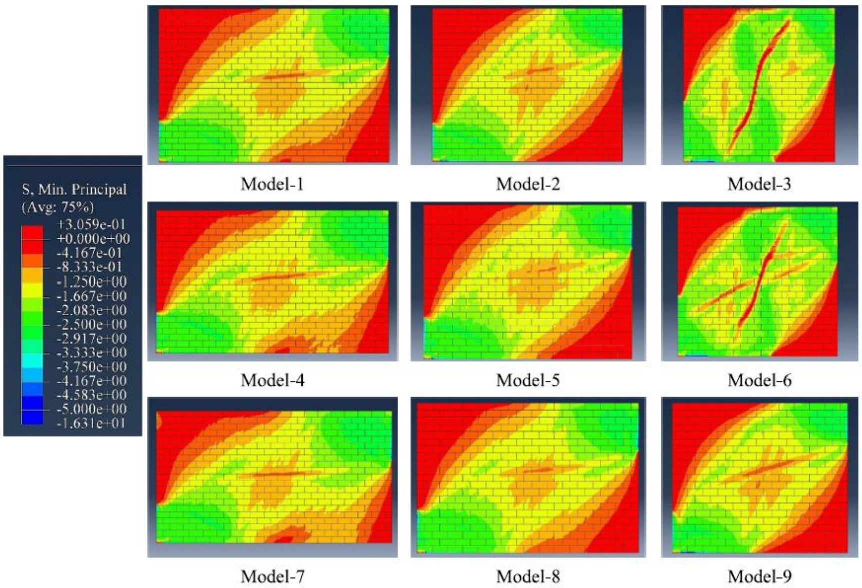

Figure 1-5: Stress Contour of Masonry Fills (J.R. Wu et al. 2012)

The micro-modeling with a single strut method is generated in OpensSees. The column hinges are modeled according to a distributed plasticity approach, and beams are modeled according to lumped plasticity. The masonry struts are modeled using truss elements with a compression axial hinge with the quadrilinear force-displacement relationship, which includes the linear elastic behavior, reduced stiffness due to cracking, strength softening, and residual strength of the infills. Since the aspect ratio plays a key role in the formation of compressive struts, this parameter is taken as a main predictor in the regression analysis mainly for the Elastic stiffness, K_h, and the width of the masonry strut, b_m.

$$Elastic\ Stiffness, \qquad K_h = \alpha E_m t_m \frac{L_m}{H_m} \qquad \text{(Eq. 1-2)}$$

$$Strut\ Width, \qquad b_m = \alpha \left(\frac{L_m}{H_m}\right) \frac{d_m}{\cos^2 \theta} \qquad \text{(Eq. 1-3)}$$

Since the peak force is found to be in a good correlation with the width of the wall, Lm, the peak force formula is derived in Eq. 1-4.:

$$Peak\ Force, \qquad F_{h,max} = \beta f_m t_m L_m \qquad \text{(Eq. 1-4)}$$

Also, the yielding and residual forces are related to the peak force of the infills:

$$Yielding\ Force, \qquad F_{h,y} = a_1 * F_{h,max} \qquad \text{(Eq. 1-5)}$$

$$Residual\ Force, \qquad F_{h,r} = a_2 * F_{h,max} \qquad \text{(Eq. 1-6)}$$

The displacement parameters are:

$$Yield\ Displacement, \qquad d_{h,y} = \frac{F_{h,y}}{K_h} \qquad \text{(Eq. 1-7)}$$

$$Peak\ Displacement, \qquad d_{h,max} = b_1 * d_{h,y} \qquad \text{(Eq. 1-8)}$$

$$Residual\ Displacement, \qquad d_{h,res} = b_2 * d_{h,y} \qquad \text{(Eq. 1-9)}$$

The six coefficients (α, β, a1, a2, b1, and b2) are established through regression analysis. Each model in this analysis shows an R^2 value exceeding 0.8, demonstrating a robust fit to the curve. In the conclusion part, J.-R. Wu et al. indicate that the single strut model 80% underestimates the shear force demand and 50% underestimates the bending moment demand relating to the local responses in the columns. However, in simulating the global responses of the MRF structures, the validated single strut macro-modeling with the validated parameters is in very good agreement with the micro-modeling.

In 2021, M. Mohammedi et al. pointed out that while placing UnReinforced Masonry (URM) in specific parts of a structure can boost its lateral strength and better its capacity to dissipate energy, it might also lead to the possibility of critical failures, especially at more severe limit states.

M. Mohammedi et al. (2021) carried out an evaluation of Unreinforced Masonry (URM) infills when subjected to 15 different seismic events. This assessment incorporated the design of a four-story and a two-story building. They explored three architectural variations: a bare frame, a frame incorporating infill walls at each level, and a frame with a soft-first-story design. To model the infill walls, they utilized a three-strut macro-model developed by Pashaie and Mohammadi, which had previously been corroborated through experiments. The model accounted for axial trilinear behavior in each strut, with the struts functioning solely in compression (Figure 1-6). Within each frame bay, two sets of struts were arranged, each containing three struts. The dimension of these struts was determined by the a_M value in Eq. 1-10, which refers to the width of the equivalent strut as proposed by Mainestone in 1974.

$$\boldsymbol{a_M = 0.175 * (\lambda h_c)^{-0.4} * r_{inf}} \qquad \text{(Eq. 1-10)}$$

r_{inf} is the length of the off-diagonal of infill wall, λ is the relative stiffness of the infill wall to the columns, and h_c is the height of the column. The displacement-axial force relationship of the struts is calculated with the formulas 1-11, 1-12, 1-13, 1-14:

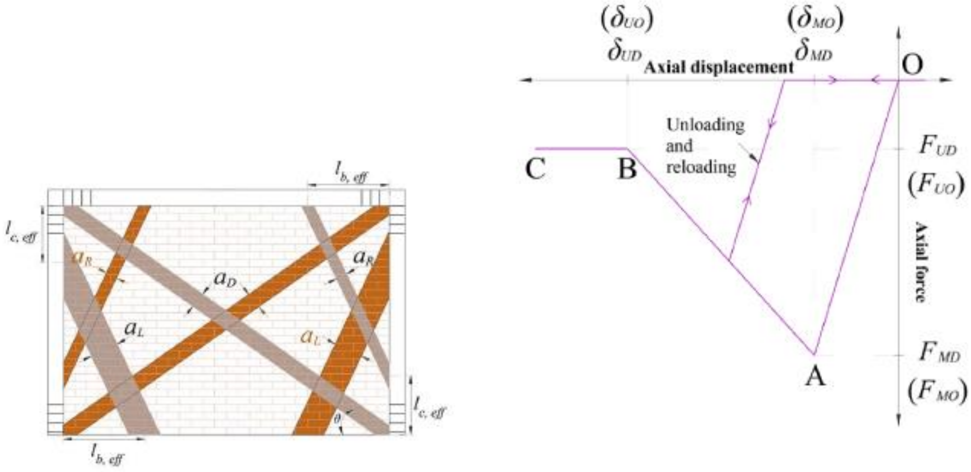

Figure 1-6: Macro-modelling of infill struts and force-displacement curve (M. Mohammadi et. al. 2021)

$$F_{MD} = f_c * a_d * t_{inf} \quad \text{(Eq. 1-11)}$$

$$F_{UD} = 0.25 * F_{MD} \quad \text{(Eq. 1-12)}$$

$$\delta_{MD} = 12.4 * 10^{-4} * \sin(2\theta) * L_{Dstrut} \quad \text{(Eq. 1-13)}$$

$$\delta_{UD} = 0.4 * \arctan(\mu) * \delta_{MD} \quad \text{(Eq. 1-14)}$$

After calibrating the struts to be used in the buildings, the Incremental Dynamic Analysis (IDA) is used for the nonlinear dynamic analysis of the structures. 15 earthquake motion records are scaled to several levels of seismic intensity to investigate the entire structural behavior in a broad range, from the elastic stage to the nonlinear stage and collapse of the structure.

In the conclusion part of the study held by Mohammadi et al. (2021), although infills are found to enhance seismic performance at the IO and LS levels, this effect is less significant in taller structures. At the CP performance level, infills affect the seismic behavior of the frame negatively since the infilled two-story frame and the four-story frame with a soft first story are found to be the weakest models. Therefore, it is strongly recommended that the infill walls be included in the design process.

Using the basement floor lowers the center of gravity of the building, providing better stability during an earthquake. At the same time, damages occurring in the substructure absorb the energy and cause a better earthquake performance in the superstructure.

In the study carried out by J.A. Mercado et. al (2018), the seismic performance of hypothetical two-story buildings was evaluated, specifically focusing on structures with zero, one, or two basement levels. The research aimed to extend previous findings regarding the influence of basements on the seismic response of buildings. The buildings' seismic responses were compared under two earthquake conditions, Operating Level Earthquake (OLE) and Contingency Level Earthquake (CLE), including parameters such as settlements, horizontal displacements, and peak story accelerations. OLE and CLE earthquakes represent the exceedance probability of 50% in 50 years (72-year return period) and 10% in 50 years (475-year return period), respectively.

The study utilized numerical simulations to demonstrate that structures with basement levels generally exhibited improved seismic performance, as they reduced the extent of damaging effects compared to buildings without basement levels. The main findings of the study highlight that the presence of at least one basement level significantly improves the seismic performance of low-rise buildings during earthquakes. The research demonstrated that structures with basements experience smaller seismic-induced settlements and more favorable horizontal displacements compared to those without basements. Buildings without a basement level experienced significant seismic-induced settlements, while the inclusion of one basement level reduced settlements by approximately 70%, and two basement levels resulted in reductions of about 90%. Additionally, horizontal displacements were generally small and not significantly affected by the presence of basement levels during the Operating Level Earthquake (OLE). However, larger displacements were noted in the Contingency Level Earthquake (CLE) for buildings without basements.

Additionally, peak story accelerations were higher in buildings with basement levels, with values reaching up to 0.45 g for two basement levels, which is 18.4% higher than the zero basement level. This underlines the importance of accurately modeling substructures in seismic analyses to obtain realistic predictions of performance during seismic events. Overall, the findings emphasize the critical role that basement levels play in enhancing the resilience of buildings subjected to seismic forces.

P. Jones et al. (2010) examine the relative safety of high-rise and low-rise buildings with steel moment-resisting frames (SMF) in the Los Angeles region under the threat of high seismic hazards. It focuses on both recorded and simulated ground motions to assess the deformation demands on typical SMF structures, specifically six- and twenty-storey buildings designed for earthquake resistance according to the 1994 Uniform Building Code (UBC). The study aims to highlight the differences in how tall and short structures respond to seismic events, considering the effects of brittle and ductile connections. In this study, the basement walls are not explicitly modeled. Instead, their effects are incorporated by fixing the lateral movement of the perimeter nodes at the ground floor. This approach simplifies the model while still considering the impact of the basement on the overall structure's lateral stability.

The study conducted by N. Çağlar et al. (2021) focuses on the influence of basement stories on the seismic response of reinforced concrete (RC) buildings situated on near-surface alluvial soft soil. Two-dimensional finite element models of RC buildings and the surrounding soil were modeled, with the soil considered a homogeneous elastoplastic media according to the Mohr-Coulomb failure criterion. Seven different models with different structural slenderness ratios (H/B) with and without basement floors were prepared using PLAXIS 2D for the study. In total, 14 distinct models are assessed. Initially, the settlement beneath static loads was analyzed, followed by a time-history dynamic analysis with the Marmara Earthquake acceleration record to assess the earthquake responses based on lateral displacements of structures. The comparison of models with and without a basement story revealed significant differences in their responses under static and dynamic loads. Specifically, when the slenderness ratio (H/B) was set to 2.00, the vertical displacements measured for the RC building without a basement were 68.73 cm, whereas the displacement for the building with a basement was only 1.05 cm. This dramatic reduction in vertical displacement highlights the beneficial impact of a basement in enhancing the stability of structures built on soft soils. Overall, the findings indicate that increasing the height of RC buildings without basements negatively impacts their seismic response. Additionally, the analysis revealed that buildings without basement stories are more susceptible to damage under both static and dynamic conditions, underscoring the importance of incorporating basement levels for better earthquake resilience.

1.4 Objective and Scope

The objective of this study is to examine the factors contributing to the collapse of structures during the Kahramanmaraş Earthquake on February 6, 2023. This will be done by evaluating a low-rise special moment-resisting steel structure with 3 different configurations and utilizing 2 different material strengths, i.e., 6 different model cases in total, designed according to the Turkish Building Earthquake Code (2018) and for the ZC Soil Class. The aforementioned building is a 4-story building designed with the reference of the study described in Example C-1 in the 'Turkey Building Earthquake Regulations (TBEC-2018) Training Presentations' book written by Erkan Özer, Cavidan Yorgun, and Cüneyt Vatansever in October 2018. It is designed directly for the Antakya/Hatay region, and the only change compared to the reference model is the column cross-sections to ensure the story drift ratio limit. This study involves subjecting the aforementioned 6 structures to seismic forces by using the nearest monitoring station data (Station 3129, Lat:36.19117, Long:36.1343) located in Defne/Antakya. All analyses and evaluations are conducted with a commercial software, SAP2000. In order to capture the inelastic behavior of the building, the P-M2-M3 and P-M3 hinges are placed at the end of the columns and beams, respectively. The inelastic behavior that will potentially occur in the joint region is omitted, assuming that the joint region is well-designed and does not contribute to additional energy dissipation from this region. It is accepted that the predominant damage will be occurred at the beam and column ends. The verification of the plastic hinges is done using a 4-meter simple cantilever column model. The pushover analysis and dynamic analysis results show that the 'Nonlinear Beam Column' hinge models supplied by SAP2000 can be used in the assessments. Furthermore, the influence of infill walls is investigated on the overall structural behavior. The infill walls are simulated by using link elements, representing compression-only truss members. Additionally, the implementation of the basement floor with the aforementioned 6 different model configurations is examined based on the Performance Levels the building undergoes. Following the analysis, it was determined that the PGA values recommended by AFAD require further examination and rectification. It was observed that not having an infill wall on the 1st floor, which indicates a soft floor, has a significantly negative impact on the overall seismic response of the building. Additionally, having the basement floor improves seismic performance by restricting lateral movement and absorbing energy. Based on these findings, it is recommended that these suggestions be incorporated into the latest regulations to enhance the seismic performance of low-rise special moment frames.

The outline of the thesis can be described as follows:

- Chapter 2 focuses on the design of the building according to TBEC 2018 and DCCSPP 2018.
- Chapter 3 includes the verification of the 'Auto hinge' model utilized in the models according to ASCE41-17.
- Chapter 4 presents the implementation of the infill wall on the model to capture a more realistic behavior of the structure.
- Chapter 5 shows the results of the analysis and findings of the seismic performance of the 6 different configurations of a building.

- Chapter 6 includes the basement floor implementation effects on the seismic response of the structures by analyzing the 6 buildings.
- Chapter 7 captures the summary and conclusion of the study by making a comparison between the 6 aforementioned models.

CHAPTER 2

DESIGN OF THE BUILDING ACCORDING TO THE TURKISH EARTHQUAKE BUILDING CODE (2018)

The building included in this study is designed according to TBEC2018, and the design principles will be shown in this section.

The reference building to follow the same design methodology is taken from the book 'Turkish Building Earthquake Regulation (TBEC-2018) Education Presentations' by Erkan Özer, Cavidan Yorgun, and Cüneyt Vatansever (2018) and is designed to be used for office purposes for the Maslak region of Istanbul and designed for the ZA Soil type. The load-carrying system of the building in both directions consists of steel frames with high ductility levels (special moment resisting frames), which are defined in TBEC2018 Section 9.3.

The new building is designed for office purposes, taking the first building as a reference, and is designed for the Defne/Antakya region. The station selected for time-history data (station 3129) is located in the Defne/Antakya region. The soil class of this region is ZC. Therefore, the ground effect coefficients Fs and F1 are 1.5 times greater than the soil class ZA in which the first building is located. The spectral acceleration coefficient SS and S1 values of the Defne/Antakya region are 1.8 times greater than the spectral acceleration coefficient of the Maslak/Istanbul region. For this reason, the Equivalent Earthquake Load is approximately 2.7 times greater for the second building.

Structural analyses of the load-carrying system of the building are carried out using the General Analysis Method, the details of which are explained in DCCPSS2018 Section 6.3. Accordingly, while the relative story drifts and deflection checks are based on unreduced element stiffnesses, the required strengths of the elements are obtained by taking into account reduced element stiffnesses, hence the second-order effects. The second-order effects on the required strength of the elements are taken into account by performing an Approximate Second-Order Analysis described in DCCPSS2018 Section 6.5.

In the analysis and dimensioning, the Load and Resistance Factor Design (LRFD) method described in DCCPSS2018 Section 5.3.1 is used.

When the effective relative story drifts are taken into account during the design (TBEC2018 Section 4.9.1), it is found that the column dimensions are insufficient compared to the reference building. For this reason, the column cross-section is enlarged to HE 500B for all floors for the newly designed building. In the building to be designed, S235, which is the most commonly used material quality in terms of availability in the Turkish and European markets, is preferred.

The 3D view of the building is given in Figure 2-1. Plan and profile views of the building are given in Figure 2-2.

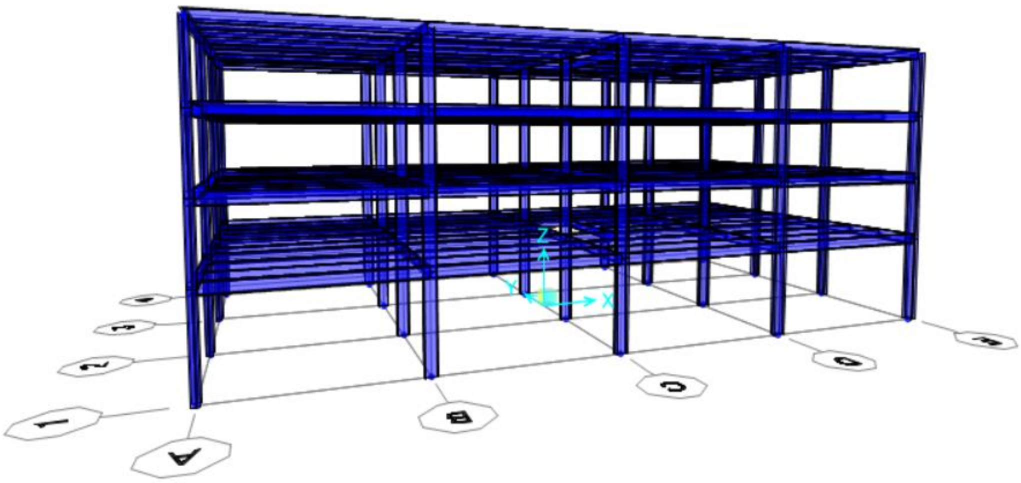

Figure 2-1: The 3D view of the building

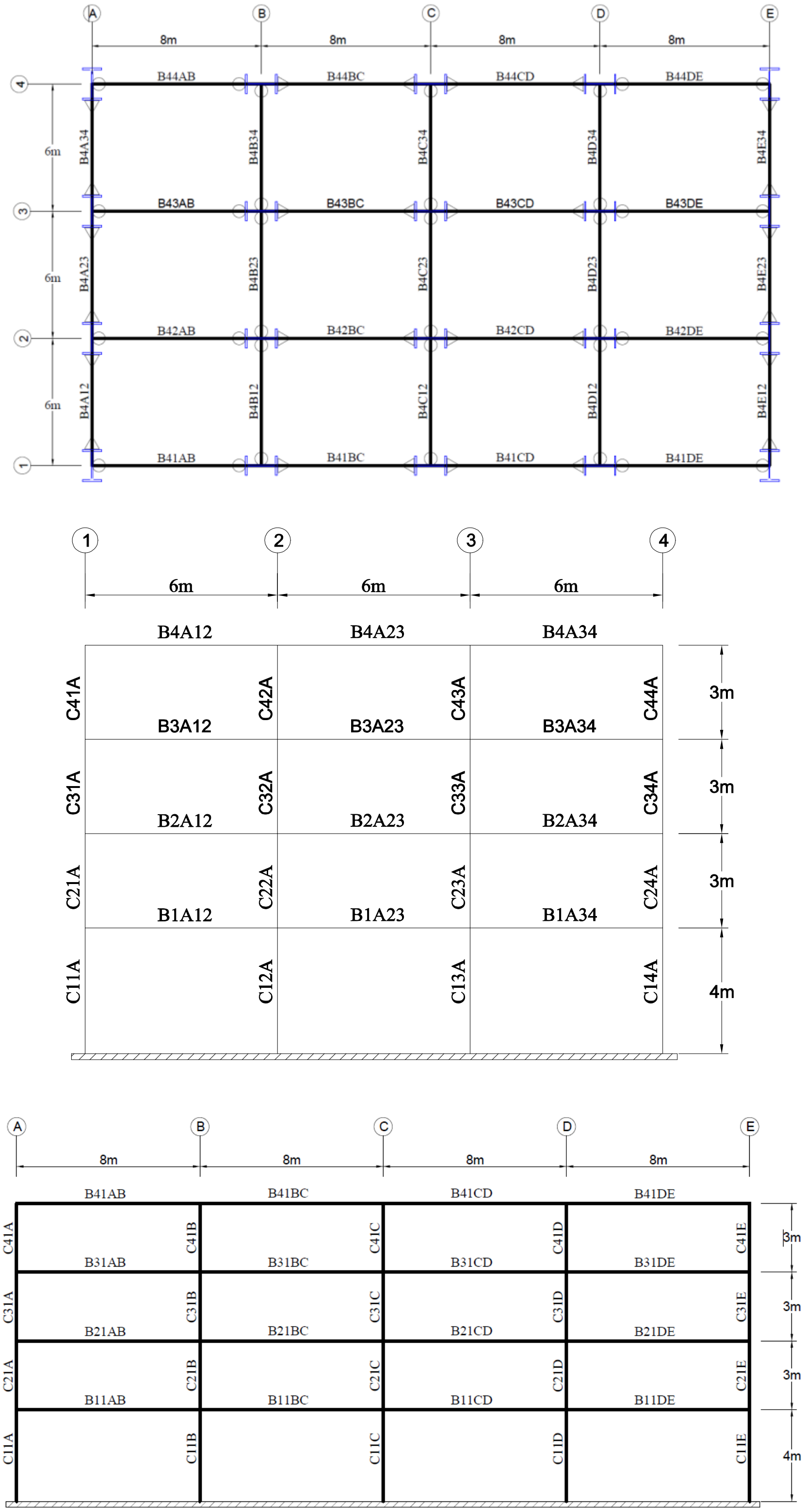

Figure 2-2: The plan and profile views of the building

2.1 Design of the Special Moment-Resisting Steel Frame

The section design of the load-carrying system is based on the TBEC 2018 and DCCPSS 2018.

2.1.1 Dead and Live Loads

As this building will be designed concerning the first building, the dead loads and live loads are considered to be similar to the first building.

Roof Deck:

Roof Dead Load	Distributed Load
Covering	0.5 kN/m²
Izolation	0.4 kN/m²
Corrugated deck sheet + reinforced concrete floor	2.1 kN/m²
Suspended floor + equipment installation	0.5 kN/m²

Dead Load	G	= 3.5 kN/m²
Live Load	Qr	= 2.0 kN/m²
Snow Load	S	= 0.6 kN/m²
Parapet Load	Gd	= 2.0 kN/m

Floor:

Floor Dead Load	Distributed Load
Covering	0.5 kN/m²
Corrugated deck sheet + reinforced concrete floor	2.1 kN/m²
Suspended floor + equipment installation	0.5 kN/m²

Partition wall	1.0 kN/m²

Dead Load	G	=	4.1 kN/m²
Live Load	Q	=	2.0 kN/m²
Outside Wall Load	Gd	=	3.0 kN/m

2.1.2 Earthquake Loads

2.1.2.1 Earthquake Ground Motion Levels

The earthquake ground motion levels are considered in the design of buildings under seismic actions in Section 2.1 of TBEC2018. Code considers four different seismic intensity levels DD-1, DD-2, DD-3, and DD-4.

DD-1 corresponds to the ground motion level for which the probability of exceeding the spectral magnitudes in 50 years is 2%. The recurrence period is 2475 years. DD-1 can be described as a very rare earthquake ground motion. This earthquake ground motion is also considered as the largest earthquake ground motion.

DD-2 refers to the uncommon seismic activity that has a 10% chance of exceeding specific spectral amplitudes within a 50-year timeframe and recurs approximately every 475 years. This seismic activity is known as the standard design earthquake ground motion..

DD-3 denotes a category of earthquake ground motion characterized by a 50% chance of exceeding the spectral magnitudes within a 50-year span and a recurrence interval of 72 years. This category is also commonly referred to as frequent earthquake ground motion.

DD-4 denotes an earthquake ground motion that occurs very frequently, characterized by a 68% chance of exceeding spectral magnitudes over 50 years (and a 50% chance over 30 years), with a return period of 43 years. This is also referred to as a service earthquake ground motion.

2.1.2.2 Building Occupancy Class (BKS) and Building Importance Factor (I)

Building Occupancy Class (BKS), which is the coefficient depending on the usage purpose of the building, is determined according to the table Earthquake Design Classes defined in Section 3.2. of TEBC2018.

Table 2-1: Earthquake Design Classes

Building Use Class	Building Usage Purpose	Building Importance Factor
BKS = 1	**Buildings that need to be used after an earthquake, buildings where people stay for a long time and intensely, buildings where valuable goods are stored and buildings containing dangerous substances** **a)** Buildings that must be used immediately after an earthquake (Hospitals, dispensaries, health centers, fire brigade buildings and facilities, PTT and other communication facilities, transportation stations and terminals, energy generation and distribution facilities, province, district and municipality administration buildings, first aid and disaster planning stations)) **b)** Schools, other educational buildings and facilities, dormitories and dormitories, military barracks, prisons, etc. **c)** museums **d)** Toxic, explosive, flammable, etc. with features buildings where substances are located or stored	1.5
BKS = 2	Shopping malls, sports facilities,cinema, theatre, concert halls, places of worship, etc.	1.2
BKS = 3	Other buildings that are not included in the definitions given for BKS=1 and BKS=2 (Houses, workplaces, hotels, building type industrial structures, etc.)	1.0

Since the building to be designed will be used in a workplace purpose, the Building Use Class, BKS=3 and the building importance factor, I=1.0.

2.1.2.3 Building Usage Class (DTS)

The horizontal elastic design spectral accelerations Sae(T), which represent the values of the horizontal elastic design acceleration spectrum for any earthquake ground motion level considered in Section 2.3.4.1 of TBEC2018, are defined as the ordinates dependent on the natural vibration period, in terms of gravitational acceleration (g). The horizontal design spectrum is shown in Figure 2-3.

$$S_{ae}(T) = \left(0.4 + 0.6\frac{T}{T_A}\right)S_{DS} \qquad (0 \le T \le T_A)$$

$$S_{ae}(T) = S_{DS} \qquad (T_A \le T \le T_B)$$

$$S_{ae}(T) = \frac{S_{D1}}{T} \qquad (T_B \le T \le T_L)$$

$$S_{ae}(T) = \frac{S_{D1}T_L}{T^2} \qquad (T_L \le T)$$

where,

$$T_A = 0.2\frac{S_{D1}}{S_{DS}} \quad ; \quad T_B = \frac{S_{D1}}{S_{DS}} \qquad T_L = 6\ \text{s}$$

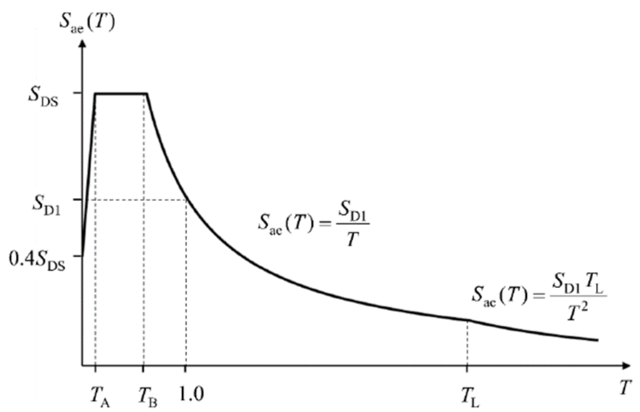

Figure 2-3: Horizontal elastic design spectrum (TBEC2018)

Within the scope of the Turkey Earthquake Hazard Maps (https:tdth.afad.gov.tr/), the parameters obtained to determine the Earthquake Design Class (DTS) at the DD-2 (design level earthquake) ground motion level are as follows:

Short-time period map spectral acceleration coefficient (S_S) = 1.064

1 sec. period map spectral acceleration coefficient (S_1) = 0.276

Local soil impact coefficients FS and F1, depending on the local soil class, are given in Table 2-2, respectively. Linear interpolation can be made for intermediate values of map spectral acceleration coefficients defined in Table 2-2.

Table 2-2: Local soil impact coefficients for different period zones

Yerel Zemin Sınıfı	Kısa periyot bölgesi için *Yerel Zemin Etki Katsayısı* F_S					
	$S_S \le 0.25$	$S_S = 0.50$	$S_S = 0.75$	$S_S = 1.00$	$S_S = 1.25$	$S_S \ge 1.50$
ZA	0.8	0.8	0.8	0.8	0.8	0.8
ZB	0.9	0.9	0.9	0.9	0.9	0.9
ZC	1.3	1.3	1.2	1.2	1.2	1.2
ZD	1.6	1.4	1.2	1.1	1.0	1.0
ZE	2.4	1.7	1.3	1.1	0.9	0.8
ZF	*Sahaya özel zemin davranış analizi yapılacaktır* (**Bkz.16.5**).					

Yerel Zemin Sınıfı	1.0 saniye periyot için *Yerel Zemin Etki Katsayısı* F_1					
	$S_1 \le 0.10$	$S_1 = 0.20$	$S_1 = 0.30$	$S_1 = 0.40$	$S_1 = 0.50$	$S_1 \ge 0.60$
ZA	0.8	0.8	0.8	0.8	0.8	0.8
ZB	0.8	0.8	0.8	0.8	0.8	0.8
ZC	1.5	1.5	1.5	1.5	1.5	1.4
ZD	2.4	2.2	2.0	1.9	1.8	1.7
ZE	4.2	3.3	2.8	2.4	2.2	2.0
ZF	*Sahaya özel zemin davranış analizi yapılacaktır* (**Bkz.16.5**).					

Since the local soil class for the second building is ZC, the $S_S \ge 1.50$, and $0.20 < S_1 < 0.30$, the F_S and F_1 values can be listed as follows:

Local ground impact coefficient for short period (F_S) = 1.2

Local ground impact coefficient for 1 sec. period (F_1) = 1.5

According to the TBEC2018 Section 2.3.2.2, the short-time period design spectral acceleration coefficient (S_{DS}) and 1 sec. period design spectral acceleration coefficient (S_{D1}) will be calculated using Eq. 2.1 and Eq.2-2 according to TBEC2018.

$$S_{DS} = S_s * F_s = (1.064)(1.2) = 1.277 \qquad \text{(Eq. 2-1)}$$

$$S_{D1} = S_1 * F_1 = (0.276)(1.5) = 0.414 \qquad \text{(Eq. 2-2)}$$

Horizontal design spectrum periods:

$$T_A = 0.2 * \left(\frac{S_{D1}}{S_{DS}}\right) = 0.2 * \left(\frac{0.414}{1.277}\right) = 0.065\ s$$

$$T_B = \frac{S_{D1}}{S_{DS}} = \frac{0.414}{1.277} = 0.324\ s$$

$$T_L = 6\ s$$

Earthquake Design Classes (DTS), which are important for design under seismic events, are determined according to Table 2.3, and they depend on the Building Usage Classes and the short-period design spectral acceleration coefficient (S_{DS}) specified in Section 2.3.2.2 for DD-2 earthquake motion level.

Table 2-3: Building Usage Classification

Acceleration Design Spectrum Factor (S_{DS}) for DD-2 Earthquake level and short period	**Building Usage Classification**	
	BKS = 1	**BKS = 2, 3**
$S_{DS} < 0.33$	DTS 4a	DTS = 4
$0.33 \leq S_{DS} < 0.5$	DTS = 3a	DTS = 3
$0.5 \leq S_{DS} < 0.75$	DTS = 2a	DTS = 2
$0.75 \leq S_{DS}$	DTS = 1a	DTS = 1

From the values of S_{DS}=1.1.277, which is greater than 0.75, and BKS=3 values, the Earthquake Design Class (DTS) can be determined as 1.

2.1.2.4 Building Height Class

Buildings are divided into eight classes in terms of height to account for the influence of the height of the buildings under seismic actions in Section 3.3.2. in TBEC2018, the building height class should be determined using the DTS and BYS values of the building in Table 2-4.

Table 2-4: Building Height Class

Building Height Class	Building Allowable Height According to Earthquake Design Classes and Building Height Category (m)		
	DTS = 1, 1a, 2, 2a	DTS = 3, 3a	DTS = 4, 4a
BYS = 1	$H_N > 70$	$H_N > 91$	$H_N > 105$
BYS = 2	$56 < H_N \leq 70$	$70 < H_N \leq 91$	$91 < H_N \leq 105$
BYS = 3	$42 < H_N \leq 56$	$56 < H_N \leq 70$	$56 < H_N \leq 91$
BYS = 4	$28 < H_N \leq 42$	$42 < H_N \leq 56$	
BYS = 5	$17.5 < H_N \leq 28$	$28 < H_N \leq 42$	
BYS = 6	$10.5 < H_N \leq 17.5$	$17.5 < H_N \leq 28$	
BYS = 7	$7 < H_N \leq 10.5$	$10.5 < H_N \leq 17.5$	
BYS = 8	$H_N \leq 7$	$H_N \leq 10.5$	

The aforementioned building's total height is 13.0 m. By considering H_N=13 and DTS=1, the building height class (BYS) is determined as 6.

2.1.2.5 Determination of Seismic Performance

According to TBEC in 2018, the ability of existing buildings to withstand seismic activity with four different categories. These states are defined as follows: "Immediate Occupancy Performance Level," "Limited Damage Performance Level," "Controlled Damage Performance Level," and "Collapse Prevention Performance Level" (Figure 2-4).

The Immediate Occupancy (QC) performance level is characterized by either the absence of structural damage in the building's elements or only negligible damage being present.

The Limited Damage (LD) performance level reflects a scenario where structural damage to the building is minimal. It can be said that linear behavior remains limited.

Controlled Damage (CD) performance level means that damage that is not too serious, widespread, and can be repaired in the majority of parts of the building's structural system to ensure life safety.

The Collapse Prevention (CP) performance level is identified as the stage prior to structural failure, characterized by substantial damage to the structural components responsible for carrying the building's load. The objective at this performance level is to ensure that the building avoids any form of complete or partial collapse.

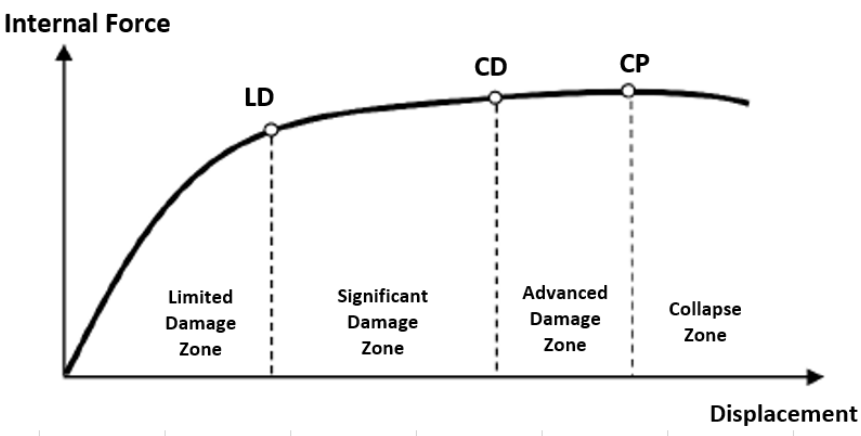

Figure 2-4: Performance State Zones

For given seismic intensity levels, nominal performance targets are determined for earthquake design classes DTS = 1, 2, 3, 3a, 4, 4a, and advanced performance targets determined for earthquake design classes DTS = 1a, 2a are given in Table 25.

Table 2-5: Target Performance Levels

(a) New Reinforced Concrete, Prefabricated Reinforced Concrete and Steel Buildings (Except High- Buildings BYS ≥ 2

Earthquake Level	(1) DTS = 1.1a , 2 2a , 3, 3a, 4, 4a		(2) (2) DTS = 1a , 2a	
	Normal Performance Target	Evaluation/Design Approach	Advanced Performance Target	Evaluation/Design Approach
DD-3	—	—	Limited Damage	Deformation-Based Design
DD-2	Controlled Damage	Force-Based Design	Controlled Damage	Force-Based Design
DD-1	—	—	Controlled Damage	Deformation-Based Design

(b) New Constructed or Existing High-Rise Buildings (BYS = 1)

Earthquake Level	DTS = 1, 2, 3, 3a, 4, 4a		DTS = 1a, 2a	
	Normal Performance Target	Evaluation/Design Approach	Advanced Performance Target	Evaluation/Design Approach
DD-4	Immediate Occupancy	Force-Based Design	—	—
DD-3	—	—	Limited Damage	Deformation-Based Design
DD-2	Controlled Damage	Force-Based Design	Controlled Damage	Force-Based Design
DD-1	Prevention of Collapse	Deformation-Based Design	Controlled Damage	Deformation-Based Design

(c) Existing Reinforced Concrete, Prefabricated Reinforced Concrete and Steel Buildings (Except Tall Buildings – BYS ≥ 2)

Earthquake Level	DTS = 1, 2, 3, 3a, 4, 4a		DTS = 1a, 2a	
	Normal Performance Target	Evaluation/Design Approach	Advanced Performance Target	Evaluation/Design Approach
DD-3	—	—	Limited Damage	Deformation-Based Design
DD-2	Controlled Damage	Deformation-Based Design	—	—
DD-1	—	—	Controlled Damage	Deformation-Based Design

With the DTS=1 and for the earthquake ground motion level DD-2, the performance target of the aforementioned steel building is determined as Normal Performance Target: Controlled Damage (CD), and the Evaluation/Design Approach is determined as Force-Based Design.

2.1.2.6 Inspection of the Irregularities

Irregularities will be checked in accordance with TBEC 3.6. There are no irregularities in the building since any protrusions, discontinuities, or large gaps in the floors do not exist, and the horizontal load-carrying systems are placed regularly. Similarly, the absence of discontinuities or abrupt changes in stiffness within the vertical supports, and consistency of the floor masses along the building height, there are no vertical irregularities.

In accordance with TBEC 3.6.2.1, torsional irregularity (A1 type irregularity) and stiffness irregularity between adjacent floors (B2 type irregularity) will be examined in order to determine the earthquake calculation method according to TBEC 4.6.2. This examination can be done by considering the conditions in the first row of table below, whose earthquake design class is determined as DTS = 1 and building height class is determined as BYS = 6.

Table 2-6: Buildings to which Equivalent Earthquake Load method are applicable

Building Type	Allowable Building Height	
	DTS=1, 1a, 2, 2a	DTS=3, 3a, 4, 4a
The buildings where the torsional irregularity coefficient, $\eta_{bi} \leq 2.0$ for each floor and there is no B2 type irregularity	BYS ≥ 4	BYS ≥ 5
All other buildings	BYS ≥ 5	BYS ≥ 6

In this case, it must be shown that the type A1 torsional irregularity coefficient, $\eta_{bi} \leq 2.0$ for each floor, and that there is no type B2 stiffness irregularity in the building. The control of these conditions, respectively, is summarized in Tables 2-7, 8, 9, and 10. The displacement values presented in the tables below result from the system's analysis, conducted after completing the final sizing of the load-supporting system.

Table 2-7: Check of B1 Type Torsional Irregularity in X Direction

Floor	$\left(\Delta_i^{(X)}\right)_{max}(m)$	$\left(\Delta_i^{(X)}\right)_{ort}(m)$	$\eta_{bi}^{(X)}$	Requirement
Roof	0.0051	0.0048	1.06	≤ 2.0
3	0.0069	0.0065	1.06	≤ 2.0
2	0.0076	0.0071	1.07	≤ 2.0
1	0.0066	0.0062	1.06	≤ 2.0

Table 2-8: Check of A1 Type Torsional Irregularity in Y Direction

Floor	$\left(\Delta_i^{(Y)}\right)_{max}$	$\left(\Delta_i^{(Y)}\right)_{ort}$	$\eta_{bi}^{(Y)}$	Requirement
Roof	0.0059	0.0049	1.19	≤ 1.2
3	0.0081	0.0068	1.19	≤ 1.2
2	0.0093	0.0093	1.18	≤ 1.2
1	0.0086	0.0072	1.19	≤ 1.2

Table 2-9: Check of the B2 Type Rigidity Irregularity in X Direction

Floor	$\left(\Delta_i^{(X)}\right)_{ort}$	h_i	$\dfrac{\left(\Delta_i^{(X)}\right)_{ort}}{h_i}$	$\dfrac{\left(\Delta_{i-1}^{(X)}\right)_{ort}}{h_{i-1}}$	$\eta_{ki}^{(X)}$	Requirement
Roof	0.0048	3	0.0016	0.0022	1.35	≤ 2.0
3	0.0065	3	0.0022	0.0024	1.09	≤ 2.0
2	0.0071	3	0.0024	0.0016	1.53	≤ 2.0
1	0.0062	4	0.0016			

Table 2-10: Check of the B2 Type Rigidity Irregularity in Y Direction

Floor	$\left(\Delta_i^{(Y)}\right)_{ort}$	h_i	$\dfrac{\left(\Delta_i^{(Y)}\right)_{ort}}{h_i}$	$\dfrac{\left(\Delta_{i-1}^{(Y)}\right)_{ort}}{h_{i-1}}$	$\eta_{ki}^{(Y)}$	Requirement
Roof	0.0049	3	0.0016	0.0023	1.38	≤ 2.0
3	0.0068	3	0.0023	0.0026	1.16	≤ 2.0
2	0.0079	3	0.0026	0.0018	1.46	≤ 2.0
1	0.0072	4	0.0018			

Upon examining Tables 2-7 and 2-8, it is observed that the torsional irregularity coefficient of type A1, denoted as ɳbi, for the building at each level complies with the requirement that ɳbi must be less than or equal to 2.0. Furthermore, the building does not exhibit any B2-type rigidity irregularities. These findings indicate that the building adheres to the specifications listed in the first row of Table 2-6, thereby qualifying it for the application of the Equivalent Earthquake Load Method.

2.1.2.7 Determination of Natural Period of Building

The aforementioned building was modeled using the SAP2000 program, and the natural dominant periods of the building in the orthogonal directions are 1.11975 s and 1.03693 s. However, according to the rule specified in TBEC2018 Section 4.7.3.3, the natural dominant vibration period of the building will not be greater than 1.4 times the empirical T_{PA} period, calculated with Eq. 2-3.

$$T_{PA} = C_t * H_N^{\frac{3}{4}} \qquad \text{(Eq. 2-3)}$$

Ct value is specified as 0.08 for the buildings whose load-carrying system is moment-resisting frames, and H_N is the total height of the building (TBEC2018 4.7.3.4a).

$$T_{PA}^{X} = 1.4 * 0.08 * 13^{\frac{3}{4}} = 0.7668\ s$$

$$T_{PA}^{Y} = 1.4 * 0.08 * 13^{\frac{3}{4}} = 0.7668\ s$$

Since the dominant natural frequency of the building is greater than the T_{PA} values, the natural frequency values are determined as 0.7668 s.

$$T_P^X = T_P^Y = 0.7668\ s.$$

2.1.2.8 Seismic Load Reduction Coefficient (Ra(T))

Based on Table 4.1 in TBEC20181, the Structural Load Carrying System Response Coefficient, R, is given as 8, and the Overstrength Factor, D, is given as 3 for special moment-resisting steel frames with high ductility level in accordance with the allowable building height class, BYS =6≥3. The earthquake load reduction coefficient, Ra(T), should be calculated by taking Tp = 0.7668 s for both directions.

Elastic seismic loads obtained in terms of spectral acceleration coefficient should be divided by the Seismic Load Reduction Factor, Ra. By doing this, the specific nonlinear behavior of the structural system under the seismic actions is considered. According to Section 4.2.1.2 in TBEC2018, The Seismic Load Reduction Factor, Ra, to be used as a basis for reducing linear elastic seismic loads, is calculated as with Eq. 2-4 and Eq. 2-5.

$$R_a(T) = \frac{R}{I} \qquad T > T_B \qquad \text{(Eq. 2-4)}$$

$$R_a(T) = D + \left(\frac{R}{I} + D\right)\frac{T}{T_B} \qquad T \leq T_B \qquad \text{(Eq. 2-5)}$$

Since T=0.768 s > 0.324 s,

$$R_a\left(T_P^{(X)}\right) = R_a\left(T_P^{(Y)}\right) = \frac{R^{(X)}}{I} = \frac{R^{(Y)}}{I} = \frac{8}{1} = 8$$

2.1.2.9 Equivalent Static Lateral Earthquake Load (V_{tE})

In conventional design approaches, the equivalent static lateral force method is more preferred compared to spectrum or time-history analysis due to its simplicity.

Regarding the selection of the calculation method to be applied under seismic actions, it is understood that this method applies to buildings with regular mass and stiffness distribution in plan and elevation. Also, building height class is considered.

As outlined in TBEC2018, Section 4.7.1, Eq. 2-6 will be used to calculate the total Equivalent Earthquake Load (base shear force), V_{tE}, acting on the whole building in the direction of the earthquake.

$$V_{tE}^{(X)} = m_t * S_{aR}\left(T_P^{(x)}\right) \geq 0.04 * m_t * I * S_{DS} * g \qquad \text{(Eq. 2-6)}$$

$$T_B = 0.324\ s < T = 0.767\ s \ \leq T_L = 6\ s$$

$$S_{ae}(T) = \frac{S_{D1}}{T} = \frac{0.414}{0.767} = 0.540$$

$$S_{aR}(T) = \frac{S_{ae}(T)}{R_a(T)} = \frac{0.540}{8} = 0.0675$$

$$V_{tE}^{(X)} = V_{tE}^{(Y)} = 1423.95 * 0.0675 * 9.81 = 0.04 * 1423.95 * 1 * 1.2768 * 9.81$$

$$V_{tE}^{(X)} = V_{tE}^{(Y)} = 942.756\ kN \geq 713.424\ kN$$

According to Section 4.7.2 in TBEC2018, the overall equivalent earthquake load is determined by summing the equivalent earthquake loads on each floor of the building. For the X and Y directions, the equivalent earthquake load on the building's top floor, denoted as Δ_{FNE}, is calculated using Eq. 2-7 and Eq. 2-8.:

$$\Delta F_{NE}^{(X)} = 0.0075 * N * V_{tE}^{(X)} = 0.0075 * 4 * 942.756 = 28.283\ kN \qquad \text{(Eq. 2-7)}$$

$$\Delta F_{NE}^{(Y)} = 0.0075 * N * V_{tE}^{(Y)} = 0.0075 * 4 * 942.756 = 28.283\ kN \qquad \text{(Eq. 2-8)}$$

The remaining part of the total equivalent load, except the force on the top floor, will be distributed to the floors of the building based on Eq. 2-9 as specified in TBEC 2018.

$$F_{iE}^{(X)} = \left(V_{tE}^{(X)} - \Delta F_{NE}^{(X)}\right) * \frac{m_i * H_i}{\sum_{j=i}^{N} m_j * H_j} \qquad \text{(Eq. 2-9)}$$

$$F_{iE}^{(X)} = F_{iE}^{(Y)} = (942.756 - 28.283) * \frac{m_i * H_i}{\sum_{j=i}^{N} m_j * H_j} \qquad \text{(Eq. 2-10)}$$

The equivalent earthquake load acting on each floor is given in Table 2-11. The equivalent earthquake load acting on the top floor also includes the top floor force, ΔF_{NE}.

Table 2-11: The equivalent earthquake loads applied on the floors

Floor	$m_i\ (kg)$	$H_i\ (m)$	$\frac{m_i * H_i}{\sum_{j=i}^{N} m_j * H_j}$	$F_{iE}^{(X)}\ (kN)$	$F_{iE}^{(Y)}\ (kN)$
Roof	321.34	13.00	0.35	349.57	349.57
3	366.91	10.00	0.31	282.20	282.20
2	366.91	7.00	0.22	197.54	197.54
1	368.79	4.00	0.12	113.46	113.46

2.1.2.10 Horizontal Earthquake Effect

In the earthquake calculation of the load-carrying system under the influence of a horizontal earthquake, earthquake loads defined in the horizontal (X) and (Y) directions perpendicular to each other will be combined as Eq. 2-11 and Eq. 2-12, according to TBEC 2018 4.4.2.1.

$$E_{\mathrm{d}}^{(\mathrm{H})} = \pm E_{\mathrm{d}}^{(\mathrm{X})} \pm 0.3 E_{\mathrm{d}}^{(\mathrm{Y})} \qquad \text{(Eq. 2-11)}$$

$$E_{\mathrm{d}}^{(\mathrm{H})} = \pm 0.3 E_{\mathrm{d}}^{(\mathrm{X})} \pm E_{\mathrm{d}}^{(\mathrm{Y})} \qquad \text{(Eq. 2-12)}$$

While $E_d^{(X)}$ and $E_d^{(Y)}$ are the earthquake effects calculated separately in the perpendicular X and Y directions, respectively; $E_d^{(H)}$ includes both direction effects and symbolizes the design basis horizontal earthquake effects.

2.1.2.11 Vertical Earthquake Effect

According to TBEC 2018 Section 4.4.3, the vertical earthquake effect shall be considered in the earthquake calculation. The vertical earthquake effect for this building will be approximately taken into account with Eq. 2-13 in accordance with TBEC Section 4.4.3.2:

$$E_d^{(Z)} \approx \frac{2}{3} * S_{DS} * G \qquad \text{(Eq. 2-13)}$$

Load combinations, including earthquake effects to be taken as basis in the design of load-carrying system elements, are given in TBEC208 4.4.4.1. If the Design with Load and Resisting Factors (LRFD) approach is applied in steel buildings, Equation 4.11 will be used with 1.2 G instead of G, and Equation 4.11 will be used as is.

$$G + Q + 0.2S + E_d^{(H)} + 0.3E_d^{(Z)} \qquad \text{(Eq. 2-14)}$$

$$0.9G + H + E_d^{(H)} - 0.3E_d^{(Z)} \qquad \text{(Eq. 2-15)}$$

where Q is defined as the live load, S as the snow load, and H as the lateral ground impulse. When implementing the Design with Load and Resisting Factors Approach (LRFD), if the live load, Q, is less than or equal to 5.0 kN/m², the Q value in the first equation may be decreased to 50%.

The vertical effect calculation is as shown in Eq. 2-16 and Eq. 2-17:

$$G\left(1.2+0.3*\frac{2}{3}*S_{DS}\right)=G\left(1.2+0.3*\frac{2}{3}*1.277\right)=1.455\ G \qquad \text{(Eq. 2-16)}$$

$$G\left(0.9-0.3*\frac{2}{3}*S_{DS}\right)=G\left(0.9-0.3*\frac{2}{3}*1.277\right)=0.645\ G \qquad \text{(Eq. 2-17)}$$

Therefore, the new equations, including the vertical effects, are shown in Eq. 2-18 and Eq. 2-19:

$$1.455G+0.5Q+0.2S+E_d^{(H)} \qquad \text{(Eq. 2-18)}$$

$$0.645G+H+E_d^{(H)} \qquad \text{(Eq. 2-19)}$$

2.1.2.12 Value of the Accidental Eccentricity for the Horizontal Earthquake Loads

The floors are modeled as rigid diaphragms, assuming the lack of A2 and A3 type irregularities in the building and that no significant deformations will occur within the floor. Value of the accidental eccentricity, defined as a fraction of the width of the considered story in the perpendicular direction to the seismic event; according to TBEC 2018 Section 4.5.10, to consider the additional eccentricity effect, the equivalent earthquake loads acting on the floors in such buildings are shifted to the points determined by +5% and -5 of the building width perpendicular to the earthquake direction. Similarly, equivalent seismic loads shall be applied at the center of mass. In this example, additional eccentricities in the X and Y directions are calculated in Eq. 2-20 and Eq. 2-21:

$$e^{(X)}=\pm 0.05\times 32.00=\pm 1.60\ m \qquad \text{(Eq. 2-20)}$$

$$e^{(Y)}=\pm 0.05\times 18.00=\pm 0.90\ m \qquad \text{(Eq. 2-21)}$$

2.1.3 Load Combinations

Internal forces result from the analysis of the building's structural system under dead and live loads, and earthquake forces will be combined in the following combinations in accordance with DCCSPP 5.3.1, TBEC 4.4, and TBEC 9.2.5.

Vertical Load Combinations:

- $1.4\ (G + N_G)$
- $1.2\ (G + N_G) + 1.6\ (Qr + N_{Qr})$
- $1.2\ (G + N_G) + 1.6\ (S + N_S)$
- $1.2\ (G + N_G) + 1.6\ (Q + N_Q) + 0.5\ (Qr + N_{Qr})$
- $1.2\ (G + N_G) + 1.6\ (Q + N_Q) + 0.5\ (S + N_S)$
- $1.2\ (G + N_G) + 1.6\ (Qr + N_{Qr}) + 1.0\ (Q + N_Q)$
- $1.2\ (G + N_G) + 1.6\ (S + N_S) + 1.0\ (Q + N_Q)$

Vertical Load + Earthquake Load Combinations:

- $1.455G + 0.2Q + 0.2S \pm E_d^{(X)} \pm 0.3E_d^{(Y)}$
- $1.455G + 0.2Q + 0.2S \pm 0.3E_d^{(X)} \pm 0E_d^{(Y)}$
- $0.645G \pm E_d^{(X)} \pm 0.3E_d^{(Y)}$
- $0.645G \pm 0.3E_d^{(X)} \pm 0E_d^{(Y)}$

The effects of geometric preliminary imperfections on structural stability can be taken into account using fictitious forces as specified in SDDCPP Section 6.2.2.2. These fictitious loads will act on the original undeformed system. Fictitious loads, N_G, N_Q, $N_{Qr,}$ and N_S, included in the above vertical load combinations, will be calculated as Eq. 2-22.:

$$N_i = 0.002 * \alpha * Y_i \qquad \text{(Eq. 2-22)}$$

α=1.0 for the LRFD approach, N_i is the fictitious load affecting the ith floor, and Y_i is the total vertical load affecting the ith floor.

Table 2-12: Fictitious Loads for Each Floor

Floor	$G\ (kN)$	$N_G\ (kN)$
Roof	2340.15	4.68
3	2740.94	5.78
2	2740.94	5.78
1	2759.34	5.82

According to TBEC 2018 4.3.5, increased earthquake loadings will be considered in the design of steel structural elements. In increased earthquake loadings, the internal forces resulting from earthquake effects are increased by multiplying the Overstrength Factor, D. The overstrength factor for the special moment-resisting steel frames with high ductility levels was previously determined to be 3.0.

2.1.4 Analysis of the Building Structural System

The required strengths of the structural system elements were carried out using the **General Analysis Method**, the details of which are explained in DSSCPP2018 Section 6.3. Accordingly, the required strengths of the elements are obtained by structural analyses considering reduced element stiffnesses and second-order effects. The second-order effects on the required strength of the elements are taken into account by performing an **Approximate Second-Order Analysis**, the details of which are described in DSSCPP Section 6.5. Unreduced element stiffnesses are used for relative story drifts and deflection controls. Structural analyses were carried out using SAP2000 software.

2.1.4.1 Relative Storey Drifts

Relative story drift is checked according to TBEC2018 Section 4.9.1.

For any column, the calculation of reduced relative floor drift, $\Delta_i^{(X)}$, which describes the difference in horizontal displacement between two consecutive floors, is as shown in Eq. 2-23:

$$\Delta_i^{(X)} = u_i^{(X)} - u_{i-1}^{(X)} \qquad \text{(Eq. 2-23)}$$

In the given equation, u_i and u_{i-1} represent the highest horizontal displacements experienced due to reduced earthquake loads at the ends of any column on two consecutive floors of the building in the X direction. In this example, the maximum values of u_i displacements for each earthquake direction are determined by reduced earthquake loads, the specific numerical values of which are provided in Tables 2-13 and 2-14. These loads are applied with an additional eccentricity of ±5%.

TBEC2018 says in Section 4.9.1.1 that the rule given in Section 4.7.3.2 shall not be considered in the computation of total equivalent earthquake load while calculating the relative story drifts. However, for ease of calculation and to stay on the safe side, the total equivalent earthquake load previously calculated for this building will be utilized, and it will be shown that horizontal displacement conditions are met for these loads.

For the X direction, the effective relative story drift in the columns on the ith floor of the building, $\delta_i^{(X)}$, is calculated as shown in Eq. 2-24:

$$\delta_i^{(X)} = \frac{R}{I}\Delta_i^{(X)} \qquad \text{(Eq. 2-24)}$$

Under reduced earthquake loads applied with an added 5% eccentricity in perpendicular X and Y directions, horizontal displacements u_i obtained by analysis of the building system and reduced relative storey drifts, $\Delta_i^{(X)}$, $\Delta_i^{(Y)}$ between consecutive floors are given in the table below.

According to TBEC 4.9.3.1(b), for each earthquake direction, in the columns on any ith floor of the building, the maximum value within the floor of the effective relative floor drifts, $\delta_{i,max}^{(X)}$ and $\delta_{i,max}^{(Y)}$, are calculated based on the equation below will meet the following condition in Eq. 2-25:

$$\frac{\lambda \delta_{i,max}^{(X)}}{h_i} \leq 0.016\,\kappa \qquad \text{(Eq. 2-25)}$$

λ and κ values will be determined according to the TBEC2018 Section 4.9.1.

λ represents the ratio of the elastic design spectral acceleration of the DD-3 earthquake ground motion to the elastic design spectral acceleration of the DD-2 earthquake ground motion for the dominant vibration period of the building in the considered earthquake direction. The equation is shown in Eq. 2-26.

κ is accepted as 1 in reinforcement concrete buildings and 0.5 in steel structures.

$$\lambda = \frac{S_{ae}(T_p)_{DD-3}}{S_{ae}(T_p)_{DD-2}} = \frac{0.164}{0.540} = 0.304 \qquad \text{(Eq. 2-26)}$$

$$\kappa = 0.5 \qquad \text{(Eq. 2-27)}$$

Consequently, relative floor drifts for each floor should not exceed the limit of 0.008.

Table 2-13: Relative story drifts in X direction

Floor	$h_i\ (m)$	$u_i^{(X)}\ (m)$	$\Delta_i^{(X)}$	$\delta_i^{(X)}$	λ	$\frac{\lambda \delta_i^{(X)}}{h_i}$	Requirement
Roof	3	0.0262	0.0051	0.0408	0.3043	0.0041	≤0.008
3	3	0.0211	0.0069	0.0552	0.3043	0.0056	≤0.008
2	3	0.0142	0.0076	0.0608	0.3043	0.0062	≤0.008
1	4	0.0066	0.0066	0.0528	0.3043	0.0040	≤0.008

Table 2-14: Relative story drifts in Y direction

Floor	$h_i\ (m)$	$u_i^{(X)}\ (m)$	$\Delta_i^{(X)}$	$\delta_i^{(X)}$	λ	$\frac{\lambda\delta_i^{(X)}}{h_i}$	Requirement
Roof	3	0.0319	0.0059	0.0472	0.3043	0.0048	≤0.008
3	3	0.0260	0.0081	0.0648	0.3043	0.0066	≤0.008
2	3	0.0179	0.0083	0.0744	0.3043	0.0075	≤0.008
1	4	0.0086	0.0086	0.0688	0.3043	0.0052	≤0.008

As is seen in Tables 2-13 and 2-14, the maximum values of λ(δi/hi) are shown in Eq. 2-28 and Eq. 2-29, respectively, and meet the requirement in TBEC2018 Section 4.9.3.1(b).

$$\frac{\lambda\delta_{i,max}^{(X)}}{h_i} = 0.0062 \leq 0.0080 \qquad \text{(Eq. 2-28)}$$

$$\frac{\lambda\delta_{i,max}^{(Y)}}{h_i} = 0.0075 \leq 0.0080 \qquad \text{(Eq. 2-29)}$$

2.1.4.2 Second-Order Effects

In accordance with TBEC 2018 Section 4.9.2, the second order indicator value, $\theta_{II,i}^{(X)}$, corresponding the second order effects, at each ith floor in the considered direction of earthquake, is calculated as Eq. 2-30:

$$\theta_{\mathrm{II,i}}^{(X)} = \frac{\left(\Delta_i^{(X)}\right)_{ave} \sum_{k=i}^{N} w_k}{V_i^{(X)} h_i} \qquad \text{(Eq. 2-30)}$$

$(\Delta_i^{(X)})_{ave}$ = Average value of the reduced relative story drift in the X direction calculated for the column in ith floor

$V_i^{(X)}$ = Reduced shear force in X direction for the ith floor

h_i = the height of the ith floor

w_k = Total weight acting on the kth floor calculated using the live load mass participation coefficient

If the maximum value of $\theta_{II,i}^{(X)}$, $\theta_{II,max}^{(X)}$, calculated for all floors, satisfies the condition in Eq. 2-31, according to TBEC2018 Section 4.9.2.2, the second-order effects on the building will be assessed according to the DCCPSS2018 Section 6.

$$\theta_{\mathrm{II,max}}^{(X)} = 0.12\frac{D}{C_h R} \qquad \text{(Eq. 2-31)}$$

R is the strength reduction factor, and C_h is a coefficient that shows the nonlinear hysteretic response of the structural system and can be determined as 0.5 for reinforcement concrete buildings and 1 for steel structures.

$$\left(\Delta_2^{(Y)}\right)_{ave} = \left(u_2^{(Y)}\right)_{ave} - \left(u_1^{(Y)}\right)_{ave} = 0.079\ m$$

$$\sum_{k=2}^{4} w_k = 2 * 2890.94 + 2340.15 = 8122.04\ kN$$

$$V_2^{(Y)} = 829.30\ kN$$

$$h_2 = 3\ m$$

$$\theta_{\mathrm{II,i}}^{(Y)} = \frac{\left(\Delta_2^{(Y)}\right)_{ave} \sum_{k=2}^{N} w_k}{V_2^{(Y)} h_2} = \frac{0.079 * 8122.04}{829.360 * 3} = 0.0258$$

$$\theta_{\mathrm{II,max}}^{(Y)} = 0.12 * \frac{D}{C_h R} = 0.12 * \frac{3}{(1.00) * 8} = 0.045$$

$$\theta_{\mathrm{II,i}}^{(Y)} = 0.0258 \le \theta_{\mathrm{II,max}}^{(X)} = 0.045$$

Table 2-15: Second Order Effect for the X direction

Floor	$h_i\ (m)$	$\Delta_i^{(X)}\ (m)$	$w_{ki}^{(X)}$	V_i	$\frac{\Delta_i^{(X)} w_{ki}}{h_i V_i}$		$0.12\frac{D}{C_h R}$
Roof	3	0.0048	2340.15	349.57	0.0107	≤	0.045
3	3	0.0065	5231.10	631.76	0.0179	≤	0.045
2	3	0.0071	8122.04	829.30	0.0232	≤	0.045
1	4	0.0062	1103138	942.76	0.0181	≤	0.045

Table 2-16: Second Order Effect in the Y direction

Floor	$h_i\ (m)$	$\Delta_i^{(X)}\ (m)$	$w_{ki}^{(X)}$	V_i	$\frac{\Delta_i^{(X)} w_{ki}}{h_i V_i}$		$0.12\frac{D}{C_h R}$
Roof	3	0.0049	2340.15	349.57	0.0110	≤	0.045
3	3	0.0068	5231.10	631.76	0.0188	≤	0.045
2	3	0.0079	8122.04	829.30	0.0258	≤	0.045
1	4	0.0072	1103138	942.76	0.0211	≤	0.045

2.1.5 Sizing of Structural Members

The design calculations for columns, primary beams, and secondary beams are done as per TBEC2018 and DSSCPP2018.

The cross-sections determined as a result of the detailed dimensioning calculations on a column, secondary beam, and moment-resisting frame beam for all elements of the load-carrying system of the newly designed building are given in Table 2-17.

Table 2-17: Structural Properties of the Designed Building

Load Carrying Members	Cross-Section	Steel Grade
Secondary Beams (all floors)	IPE 360	S235
Beams on B – D axes (all floors)	IPE 400	S235
Beams on A and E axes (all floors)	IPE 450	S235
Beams on 1-4 axes (all floors)	IPE 450	S235
Columns on ±0.00/+13.00 elevations	HE 500B	S235

CHAPTER 3

INITIAL ASSESSMENT OF THE STRUCTURE

Pushover analysis is a method used in structural engineering to estimate the strength and deformation capacity of structures, particularly under seismic loading. It simulates how a structure responds to gradually increasing lateral loads. The goal is to evaluate how a structure responds beyond its elastic limit until it reaches failure. The pushover analysis curve, revealed after the analysis, is a graphical representation of the structure's response to lateral loading, capturing its post-yielding behavior.

3.1 Plastic Hinge Model Verification

A plastic hinge refers to the deformation of the member (column or beam occurring in a virtual location where plastic deformations are concentrated. Plastic hinges help simulate the gradual degradation of the stiffness and strength, allowing engineers to identify potential failure mechanisms. Different hinge properties may be assigned in SAP2000 depending on the expected behavior:

- Moment Hinges Moment hinges simulate bending behavior, where the focus is on the only moment (M) capacity and rotation (ϴ) relationship.
- Axial Hinges: This type of hinge simulates the axial behavior (tension or compression) by focusing on only the axial force (P) and deformation (Δ) relationship.
- P-M2-M3 Hinges: This type of hinge considers the interaction between axial force (P) and two-moment capacities (M2 and M3) at different axes.

Plastic hinges enable the assessment of different performance levels, which are essential in performance-based design and assessment, especially when evaluating buildings according to the codes.

SAP2000 offers a powerful nonlinear static pushover analysis option to investigate the hinge properties and column/beam performance under lateral loading. This process involves modeling the structure with the material and cross-sectional properties, defining hinge properties, applying incremental lateral loads, and tracking the formation of the plastic hinges. In this chapter, a pushover analysis in SAP2000 will be done by taking a sample of 4-meter columns located on the 1st floor of the building. The hinge features and the nonlinear behavior of the column will be examined.

3.2 Modelling the Structure:

In the modeling, for ease of traceability, column C11E, 4 m long, placed along the axes 1/E in the 1st story, will be investigated under a lateral load.

Material Strength

S235 F_y=235 N/mm^2 F_u=360 N/mm^2 DCCPSS2018 Table 2.1A

E=200 GPa G= 76.923 GPa

Cross-Sectional Properties

HE 500B

$I_{2\text{-}2}$=12620 cm^4 $Z_{2\text{-}2}$=1292 cm^3 $r_{2\text{-}2}$=7.27 cm

$I_{3\text{-}3}$=107200 cm^4 $Z_{3\text{-}3}$=4815 cm^3 $r_{3\text{-}3}$=21.18 cm

J=538.40 cm^4 Cw=7018000 cm^6 L=400 cm

Gross Area=239 cm^2

Shear Area in 2 direction = 7250 mm^2

Shear Area in 3 direction = 14000 mm^2

d=500 mm tf=28 mm tw=14.5 mm

bf=300 mm

Section 9.3.3.2.1 Structural Steel Section in ASCE41-17 emphasizes that the design strength can be calculated according to AISC 360, with the strength reduction factor, Φ, of 1 instead of specified in AISC360.

Tension Capacity of the Column:

$$F_t = A_g * F_y = 239 * 10^2\ mm^2 * 235 \frac{N}{mm^2} = 5616.5\ kN$$

Compression Capacity of the Column:

$$F_{cry} = \left[0.658^{\frac{F_y}{F_{ey}}}\right] F_y \qquad F_{ey} = \frac{\pi^2 E}{\left(\frac{L_{ey}}{r_y}\right)^2} = 652.05\ MPa$$

$$F_{cry} = \left[0.658^{\frac{F_y}{F_{ey}}}\right] F_y = \left[0.658^{\frac{235}{625}}\right] * 235 = 200.78\ MPa$$

$$F_c = A_g * F_{cry} = 239 * 10^2\ mm^2 * 200.78 \frac{N}{mm^2} = 4798.64\ kN$$

3.3 Defining Hinge Properties:

In SAP2000, 2 types of hinges are used to model the nonlinear behavior of structural members – deformation-controlled (ductile) and force-controlled (brittle) hinges. Force-controlled hinges refer to elements that are not allowed to exceed their elastic limits by experiencing a significant degradation after yield deformation. Deformation-controlled hinges, on the other hand, refer to elements that are allowed to exceed their elastic limit in a ductile manner. The difference may be seen in more detail in Figure 3-1.

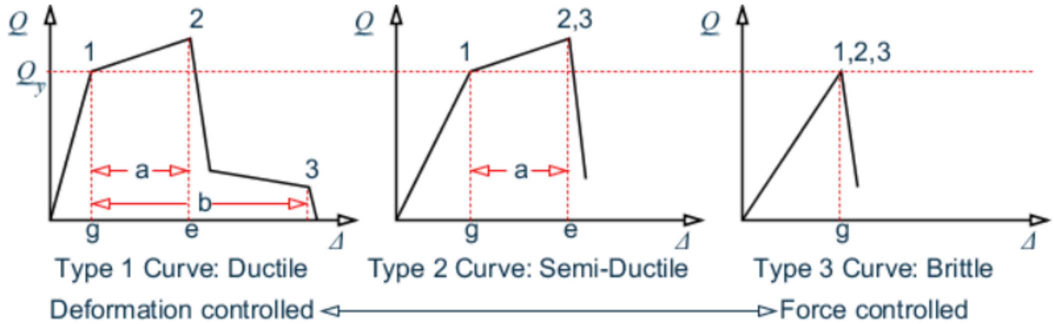

Figure 3-1: Component force vs. deformation curves (FEMA 356)

In this model, P-M2-M3 interacting hinge is selected with a deformation-controlled hinge type to accurately capture the expected ductility of the element.

SAP2000 implements the ASCE41-17 guidelines for the definition and use of column flexural hinges. Figure 3-2 represents the moment-rotation (M- Θ) or force-deformation (P-Δ) relationship based on parameters a, b, and c defined in Table 3-1.

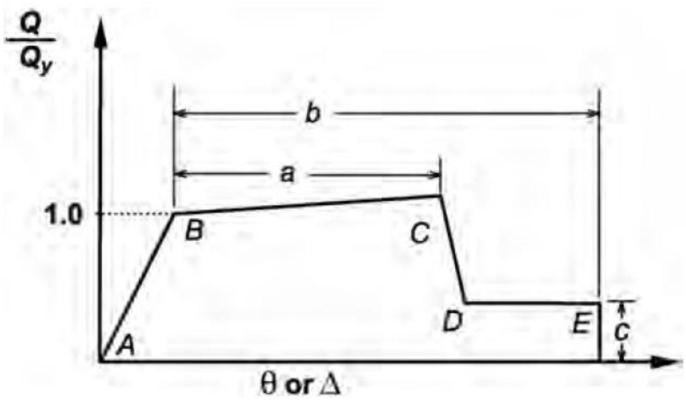

Figure 3-2: Generalized relationship between force and deformation for steel elements or components (ASCE 41-17 Section 9.4.2.2)

ASCE41-17 Section 9.4.2.2.2 Nonlinear Static Procedure says that if the length of the beam or column is equal to 2.6 M_{CE}/V_{CE} or greater, θ_y shall be determined as in Eq. 3-1 by using Eq. 3-2 for M_{CE}:

$$\theta_y = \frac{M_{pce} L(1+\eta)}{6(\tau_b E)I} \quad \text{(Eq. 3-1)}$$

$$M_{CE} = M_{pce} = \begin{cases} for \dfrac{|P|}{P_{ye}} < 0.2 & M_{pe}\left(1 - \dfrac{|P|}{2P_{ye}}\right) \\ for \ \dfrac{|P|}{P_{ye}} \geq 0.2 & M_{pe}\dfrac{9}{8}\left(1 - \dfrac{|P|}{P_{ye}}\right) \end{cases} \quad \text{(Eq. 3-2)}$$

where M_{pe}=expected plastic moment capacity about bending axis, substituting F_{ye} for F_y in Eq. 3-3.

$$M_{pe} = F_y * Z_{3-3} = 1131.25\ kNm \quad \text{(Eq. 3-3)}$$

$$M_{CE} = M_{pce} = M_{pe}(1-0) = 1131.25\ kNm\ for\ P = 0$$

For shear yielding, the expected shear strength, V_{CE}, is calculated as Eq. 3-4:

$$V_{CE} = V_{ye} = \begin{cases} for \dfrac{|P|}{P_{ye}} \leq 0.2 & 0.6F_{ye}A_s \\ for \ \dfrac{|P|}{P_{ye}} > 0.2 & 0.6F_{ye}A_s\sqrt{1 - \left(\dfrac{|P|}{P_{ye}}\right)^2} \end{cases} \quad \text{(Eq. 3-4)}$$

where A_s=effective shear area of the cross-section. A_s in direction 3 is defined as 14000 mm^2.

$$V_{CE} = 0.6 * 235 \frac{N}{mm^2} * 14000\ mm^2 * 10^{-3}\frac{kN}{N} = 1974\ kN\ for\ P = 0$$

$$2.6 * \frac{M_{CE}}{V_{CE}} = 2.6 * \frac{1131.25\ kNm}{1974.00\ kN} = 1.49\ m < L = 4\ m$$

Since 2.6 M_{CE}/V_{CE} is smaller than the length of the column, which is 4 m, θ_y shall be determined as in Eq. 3-1 according to ASCE41-17.

$$\eta = \frac{12EI}{L^2 G A_s} = \frac{12 * 200 * 10^6 \frac{kN}{m^2} * 0.001072\ m^4}{(4\ m)^2 * 76.9 * 10^6 \frac{kN}{m^2} * 0.014\ m^2} = 0.1493$$

$$\tau_b = \begin{cases} for\,\frac{|P|}{P_{ye}} \leq 0.5 & 1.0 \\ for\,\frac{|P|}{P_{ye}} > 0.5 & 4\frac{|P|}{P_{ye}}\left(1 - \frac{|P|}{P_{ye}}\right) \end{cases}$$

$$\tau_b = 1.0\, for\, P = 0$$

$$\theta_y = \frac{1131.25\, kNm * 4\, m * (1 + 0.1493)}{6\left(1.0 * 200 * 10^6 \frac{kN}{m^2}\right) * 0.001072\, m^4} = 0.0040438\, rad$$

Table 3-1: Acceptance Criteria and Modelling Parameters for Nonlinear Procedure of Steel Structural Columns and Beams flexural actions – ASCE41-17

Modeling Parameters
Plastic rotation angle a and b (radians) Residual strength ratio c
Column in Compression
1. Where $\frac{b_f}{2t_f} \leq 0.30\sqrt{\frac{E}{F_{ye}}}$ and For $\frac{P_G}{P_{ye}} < 0.2\,\frac{h}{t_w} \leq 2.45\sqrt{\frac{E}{F_{ye}}}\left(1 - 0.71\frac{P_G}{P_{ye}}\right)$ For $\frac{P_G}{P_{ye}} \geq 0.2\,\frac{h}{t_w} \leq 0.77\sqrt{\frac{E}{F_{ye}}}\left(2.93 - \frac{P_G}{P_{ye}}\right) \leq 1.49\sqrt{\frac{E}{F_{ye}}}$ $a = 0.8\left(1 - \frac{P_G}{P_{ye}}\right)^{2.2}\left(0.1\frac{L}{r_y} + 0.8\frac{h}{t_w}\right)^{-1} - 0.0035 \geq 0$ $b = 7.4\left(1 - \frac{p_G}{P_{ye}}\right)^{2.3}\left(0.5\frac{L}{r_y} + 2.9\frac{h}{t_w}\right)^{-1} - 0.006 \geq 0$ $c = 0.9 - 0.9\frac{P_G}{P_{ye}}$

Table 3-1: (Cont'd): Acceptance Criteria and Modelling Parameters for Nonlinear Procedure of Steel Structural Columns and Beams flexural actions – ASCE41-17

2. Where $\frac{b_f}{2t_f} \geq 0.38\sqrt{\frac{E}{F_{ye}}}$ or For $\frac{P_G}{P_{ye}} < 0.2\ \frac{h}{t_w} \geq 3.76\sqrt{\frac{E}{F_{ye}}}\left(1 - 1.83\frac{P_G}{P_{ye}}\right)$ For $\frac{P_G}{P_{ye}} \geq 0.2\ \frac{h}{t_w} \geq 1.12\sqrt{\frac{E}{F_{ye}}}\left(2.33 - \frac{P_G}{P_{ye}}\right) \geq 1.49\sqrt{\frac{E}{F_{ye}}}$ $a = 1.2\left(1 - \frac{P_G}{P_{ye}}\right)^{1.2}\left(1.4\frac{L}{r_y} + 0.1\frac{h}{t_w} + 0.9\frac{b}{2t_f}\right)^{-1} - 0.0023 \geq 0$ $b = 2.5\left(1 - \frac{p_G}{P_{ye}}\right)^{1.8}\left(0.1\frac{L}{r_y} + 0.2\frac{h}{t_w} + 2.7\frac{b}{2t_f}\right)^{-1} - 0.0097 \geq 0$ $c = 0.5 - 0.5\frac{P_G}{P_{ye}}$
3. Other: Linear interpolation between the values on lines 1 and 2 for both flange slenderness (first term) and web slenderness (second term) shall be performed, and the lower resulting value shall be used.
Columns in Tension
1. For $\frac{\|P_G\|}{P_{ye}} < 0.2$ a=$9\theta_y$ b=$11\theta_y$ c=0.6
2. For $\frac{\|P_G\|}{P_{ye}} \geq 0.2$ a=$13.5(1 - 5/3\|P_G\|/P_{ye}\theta_y \geq 0$ b=$16.5(1 - 5/3\|P_G\|/P_{ye}\theta_y \geq 0$ c=$0.6(1 - 5/3\|P_G\|/P_{ye}) + 0.2 \geq 0.2$
3. Other: Linear interpolation between the values on lines 1 and 2 shall be used.

$$\frac{b_f}{2t_f} = \frac{300}{2*28} = 5.357 \leq 0.30 * \sqrt{\frac{200000}{235}} = 8.75$$

$$\frac{P_G}{P_y} = \frac{0}{235} < 0.2 * \frac{500}{14.5} = 6.897 \leq 2.45 * \sqrt{\frac{200000}{235}}(1 - 0.71 * 0) = 71.47$$

$$a = 0.8 * (1-0)^{2.2} * \left(0.1 * \frac{4}{0.0727} + 0.8 * \frac{0.3}{0.0145}\right)^{-1} - 0.0035 = 0.0327749 \geq 0$$

$$b = 7.4 * (1-0)^{2.3} * \left(0.5 * \frac{4}{0.0727} + 2.9 * \frac{0.3}{0.0145}\right)^{-1} - 0.006 = 0.0785615 \geq 0$$

$$c = 0.9 - 0.9 * 0 = 0.9$$

The modeling parameters are calculated according to the Table 3-1. When the a and b values are scaled in order to place the A, B, C, D, and E points on the graph. The calculated values are similar to what SAP2000 shows in Figure 3-3.

$$\frac{a}{\theta_y} = 8.105, \quad \frac{b}{\theta_y} = 19.428$$

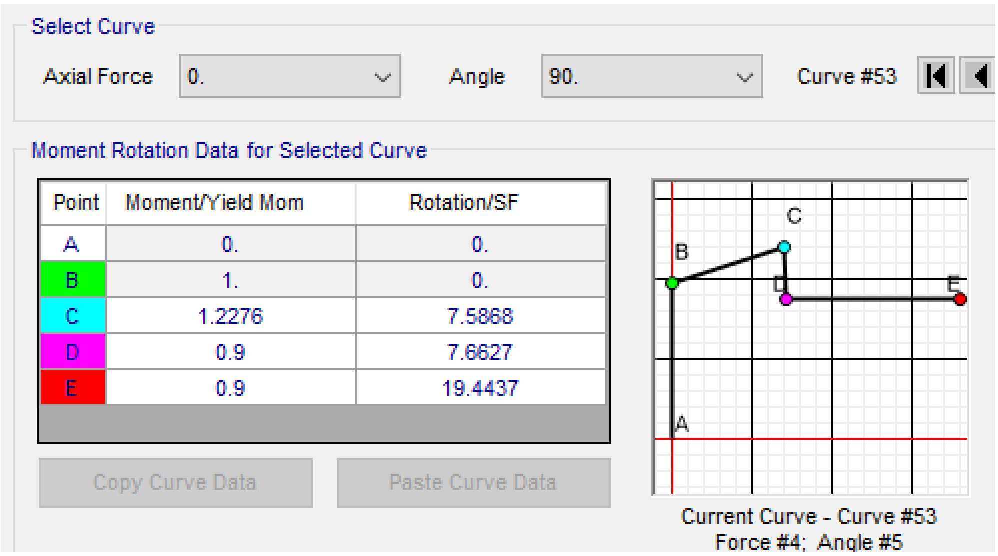

Point	Moment/Yield Mom	Rotation/SF
A	0.	0.
B	1.	0.
C	1.2276	7.5868
D	0.9	7.6627
E	0.9	19.4437

Figure 3-3: The moment rotation data calculated by SAP2000

3.4 Assigning Nonlinear Beam Column Hinge:

Different ‘Hinge Distribution Types’ are used in SAP2000 to simulate the plasticity of the element. The ‘Nonlinear Beam Column’ option refers to the Lumped Plasticity model with the expected hinge length. It is important to note that that the plastic hinge will occur in the middle of the specified length. The ‘User Defined’ option will allow users to define the plastic hinge locations throughout the column length. The ‘Distributed Plasticity’ models the plastic behavior along the length of the element where the plasticity is distributed to different points instead of the lumped plastic hinges at the ends. The plastic hinge distribution will be defined using different approaches such as 5-point Gauss-Lobatto and 7-point Gauss-Legendre. The ‘Equal Spacing’ hinge type, on the other hand, will allow the user to define a certain number of hinges in equal spacing along the length. ‘Continuous Spring Support’ distributes the spring along the length of the frame to represent the nonlinear behavior. These springs can model different types of nonlinear responses, such as stiffness degradation and hysteresis, and may be effective for modeling complex interaction with the surrounding media (e.g., soil-structure interaction).

According to the TBEC2018 Section 5.3.1.2, the 'Lumped Plasticity (Plastic Hinge) Model' can be utilized as a non-linear behavior model for beams and columns modeled as frame (line) finite elements. The plastic hinge length (Lp), which is determined as half of the cross-sectional height (h), results in Lp being 0.5h. In this example, with a calculation of 0.5*500 mm, the hinge length is established at 250 mm. For the implementation of the 'Lumped Plasticity Model,' 'Nonlinear Beam Column' hinge type is selected as depicted in Figure 3-4. The plasticity occurs at the midpoint of the defined hinge length. Therefore, the plastic hinge's position is calculated to be 0.125 meters from the bottom end, achieved by 0.25/2=0.125 m.

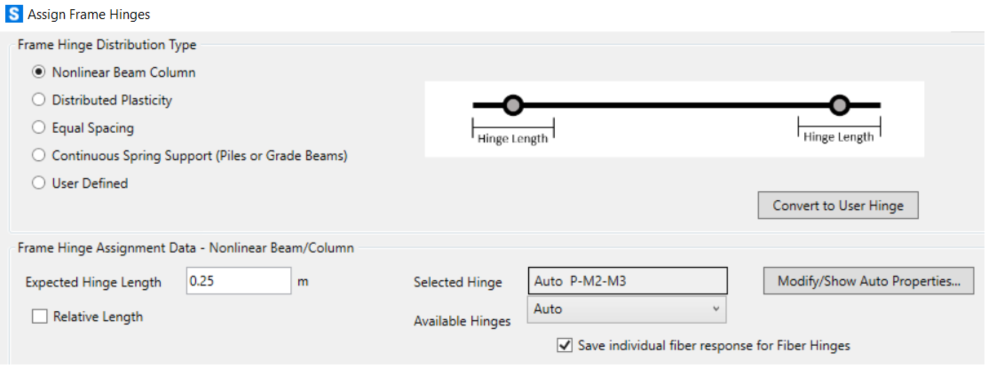

Figure 3-4: Assigning the P-M2-M3 hinge on the bottom end of the column

3.5 Defining the Loads:

Pushover load, or pushover analysis, is a nonlinear static analysis method to evaluate the performance of a structure. It contains applying gradually incremental load to the structure until it reaches the target displacements such as yielding points and rupture points. In this analysis, loads shall be applied incrementally.

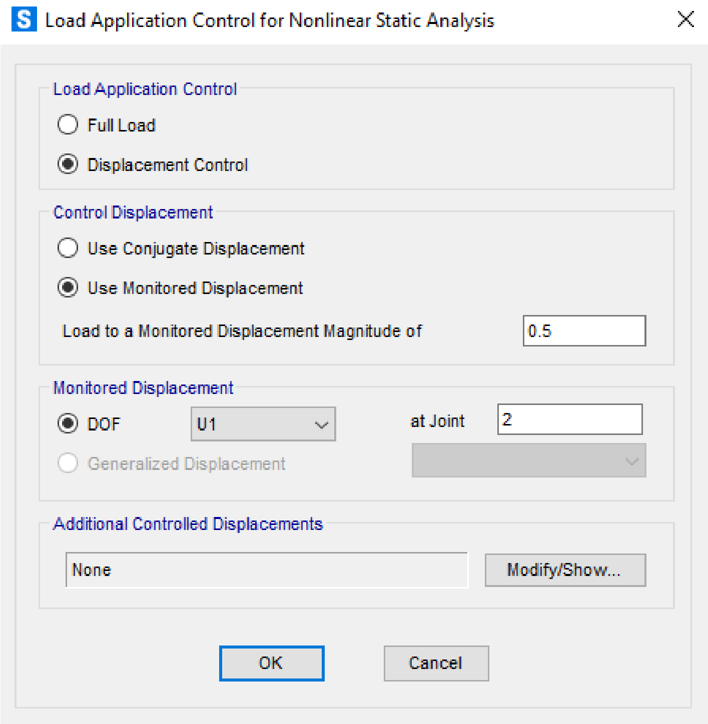

Figure 3-5: Load Application Control Panel

The ‘Conjugate Displacement’ in Figure 3-5 refers to tracking relative displacements between nodes rather than absolute displacements. The ‘Monitored Displacement’, on the other hand, corresponds to tracking the global displacements of the assigned DOF throughout the analysis. In this case, the DOF will be U1, which is in the same direction as the applied load.

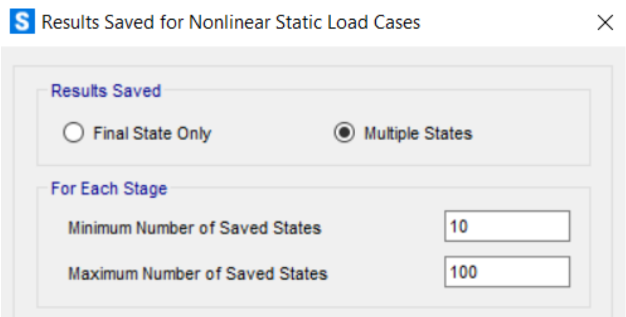

Figure 3-6: Output Saving

The output savings are arranged as in Figure 3-6. If the ‘Final State Only’ is selected, SAP2000 provides the results of only the last step of the analysis, which is the state after all incremental loads have been applied. The ‘Multiple States’ provides the results for various steps throughout the analysis. This option is selected since the intermediate states of the loading and corresponding displacements will be investigated. Minimum and Maximum Number of Saves is determined as 10 and 100, respectively.

For the nonlinear parameters, the solution type is selected as Iterative Event-to-Event since this process combines iterative steps with event-to-event points, providing a more accurate approach. If ‘Iterative Only’ is selected, the analysis proceeds in small increments, solving iteratively each step (using such as Newton-Raphson) to achieve equilibrium at each step. If ‘Event-to-Event only’ is selected, the analysis directly moves from one significant event to the next, reducing the number of steps. Therefore, to ensure the capture of critical events accurately, the ‘Iterative Event-to-Event’ solution is selected.

A 100 kN load is generated for the incremental lateral loading to observe the flexural bending of the column in its strong axis.

3.6 Monitoring Hinge Formation and Progression

When determining first and second failure points (also known as first and second significant events or critical points in pushover analysis), SAP2000 primarily considers various factors related to nonlinear behavior. The first breakdown (or first significant event) is the initial yielding of key structural components. This yielding indicates the beginning of inelastic behavior. The second breakdown (or second significant event) corresponds to further yielding or damage in other structural elements. This can include plastic hinge formations or the yielding of previously unaffected elements. In this case, the second breakdown represents the hinge formation which is the situation of reaching the ultimate capacity. At the second breakdown, the structure (in this case, the column) experiences a substantial reduction in its load-carrying capacity. This is reflected as a noticeable drop in the pushover curve.

The pushover curve of the column is seen in Figure 3-7.

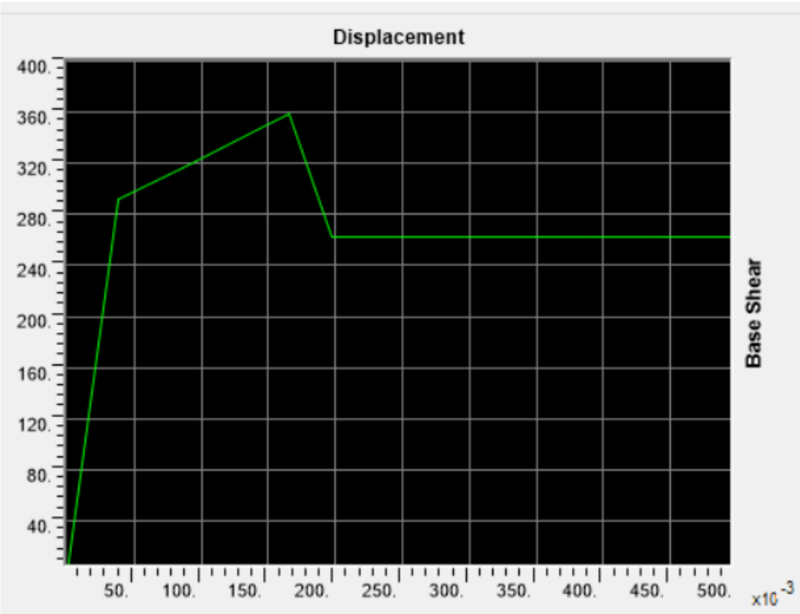

Figure 3-7: Pushover curve of the 4-m long HEB500 column (the units are in kN&m)

The base shear for the first failure point can be calculated as Eq. 3-5:

$$V_{base} = \frac{M_{CE}}{L - \frac{L_p}{2}} = \frac{1131.525\ kNm}{\left(4 - \frac{0.25}{2}\right)m} = 292.01\ kN \qquad \text{(Eq. 3-5)}$$

For the second point, ASCE41-17 states that the beams and columns are permitted to have a strain-hardening slope of 3% of the elastic slope for flexural actions. Therefore, when the 3% of the elastic slope is accepted as a strain-hardening slope, the base shear when the second failure point is achieved is calculated with Eq. 3-6 by using Eq. 3-7:

$$\frac{C_{ordinate} - B_{ordinate}}{a} = \frac{3}{100} * Elastic\ Slope \qquad \text{(Eq. 3-6)}$$

$$Elastic\ slope = \frac{1}{0.0040438} = 247.29 \qquad \text{(Eq. 3-7)}$$

$$\frac{Cordinate - 1}{0.0327749} = 247.29 * \frac{3}{100} \rightarrow C = 1.2431$$

The base shear for the second failure point can be calculated by Eq. 3-8:

$$V_{base@PointC} = \frac{M_{CE@PointC}}{L - \frac{L_p}{2}} \qquad \text{(Eq. 3-8)}$$

$$V_{base@PointC} = \frac{1.2431 * 1131.525\ kNm}{\left(4 - \frac{0.25}{2}\right)m} = 362.99\ kN$$

The hinge moment-rotation curve is seen Figure 3-8.

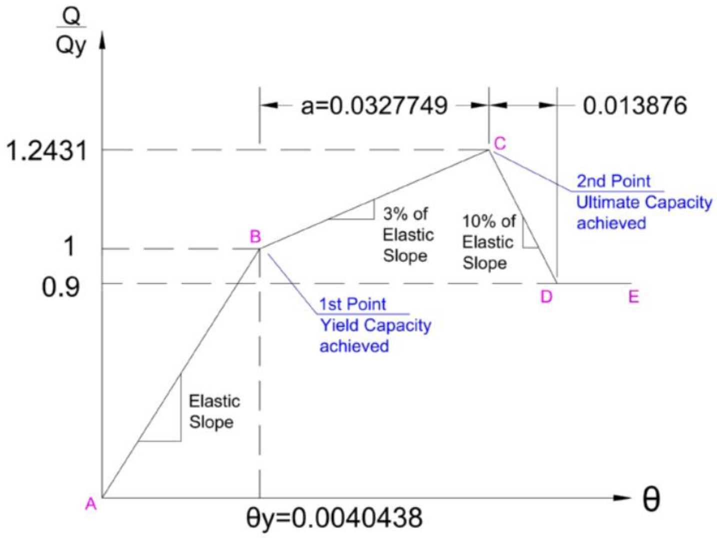

Figure 3-8: The hinge moment-rotation curve

The D point is limited, with a negative stiffness ratio of 10%. This value is recommended to prevent snap-back within the element.

$$\frac{0.9 - 1.2431}{\theta_D - \theta_C} = 247.29 * \left(-\frac{10}{100}\right) \rightarrow \theta_D = 0.050695$$

The values given in the SAP2000 Moment Rotation Data are very close to the calculated values. Therefore, the auto hinge can be utilized to analyze and assess the structure.

3.5. Pushover Analysis with Different Axial Loads

When the axial load of 1700 kN (nearly 35% of the compression capacity) is applied to the column, the hinge values change according to Table 9-7.1 in ASCE41-17.

$$P = 1700\ kN$$

M_{pe}=expected plastic moment capacity about bending axis, substituting F_{ye} for F_y.

$$M_{pe} = F_{ye} * Z_{3-3} = 1131.53\ kNm$$

$$M_{CE} = M_{pce} = M_{pe} * \frac{9}{8} * \left(1 - \frac{1700}{5616.5}\right) = 887.67\ kNm\ for\ P = 1700\ kN$$

For shear yielding, the expected shear strength, V_{CE}:

$$V_{CE} = 0.6 * 235 \frac{N}{mm^2} * 14000\ mm^2 * 10^{-3} \frac{kN}{N} \sqrt{1 - \left(\frac{1700}{5616.5}\right)^2}$$

$$= 1881.4\ kN\ for\ P = 1700\ kN$$

$$2.6 * \frac{M_{CE}}{V_{CE}} = 2.6 * \frac{887.67\ kNm}{1881.4\ kN} = 1.23\ m < L = 4\ m$$

Since 2.6 M_{CE}/V_{CE} is smaller than the length of the column, which is 4 m, θ_y shall be determined as in equation 3-1.

$$\tau_b = 1.0\ for\ P = 0.15 * P_{ye}$$

$$\theta_y = \frac{887.67\ kNm * 4\ m * (1 + 0.1493)}{6\left(1.0 * 200 * 10^6 \frac{kN}{m^2}\right) * 0.001072\ m^4} = 0.00378456\ rad$$

The base shear for the first failure point can be calculated as seen in Eq. 3-9:

$$V_{base} = \frac{M_{CE}}{L - \frac{L_p}{2}} = \frac{887.67\ kNm}{\left(4 - \frac{0.25}{2}\right) m} = 229.08\ kN \qquad \text{(Eq. 3-9)}$$

The calculated values are in parallel with the graphs provided by SAP2000 after the analysis (Figure 3-9 and Figure 3-10).

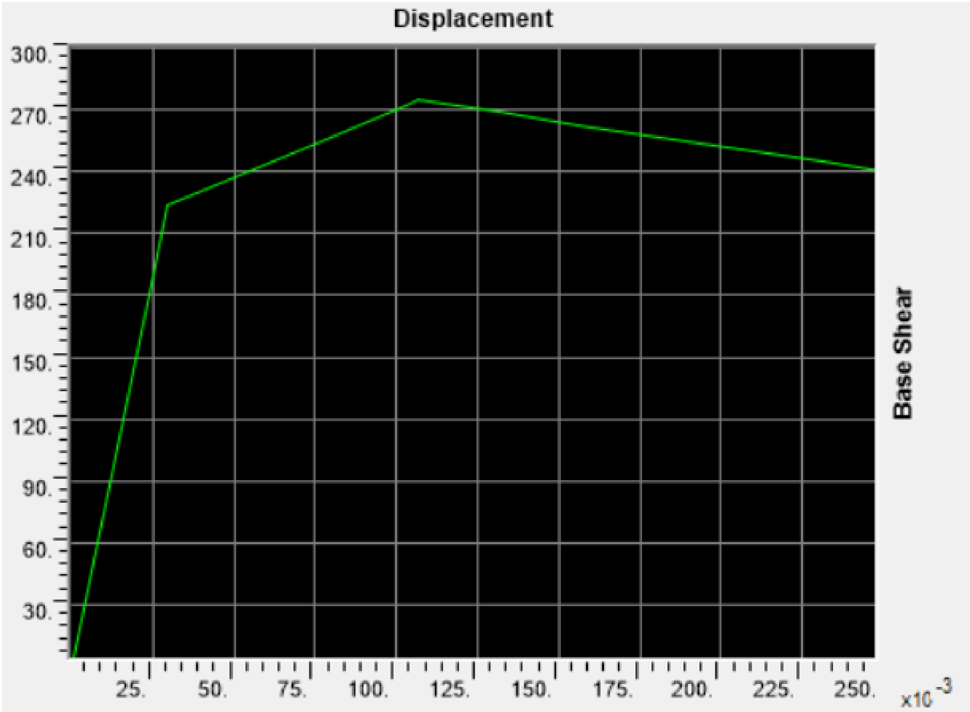

Figure 3-9: Pushover curve of the column under 1700 kN axial compressive load (units are in kN&m)

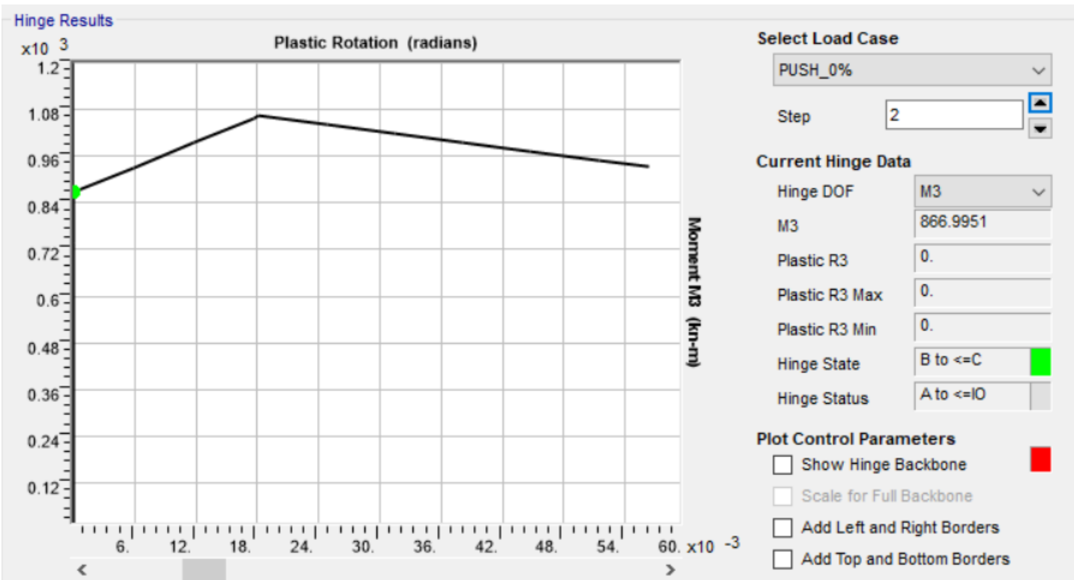

Figure 3-10: Hinge moment-rotation curve for the column under 1700 kN axial compressive load

3.7 Pushover Analysis of The Structure

The strong column-weak beam (SCWB) design principle is a critical concept in seismic design for steel MRFs. The intention behind SCWB is to ensure that beams yield and dissipate energy before columns do, thereby preventing a soft-story mechanism that could lead to catastrophic structural failure. The pushover analysis was performed on the designed structure to verify whether the designed building adheres to this principle.

Hinges were assigned to beams and columns following the ASCE 41-17 guideline, which allows the tracking of plastic behavior. In the beams, P-M3 hinges are placed at the ends, while in the columns, P-M2-M3 hinges are applied, capturing the interaction between axial force and moments. A pushover analysis is carried out by applying a gradually increasing lateral equivalent earthquake force until a target displacement of %0.75, %1, %3, and %5 of the roof DR is reached. The hinge states color description can be seen in Figures 3-11, and the structure moment frame column and beam hinge states can be seen in Figures 3-12 and 3-13. The hinge states shown are calculated according to the ASCE41-17.

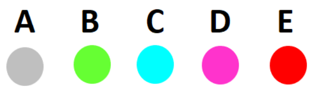

Figure 3-11: The hinge state colors

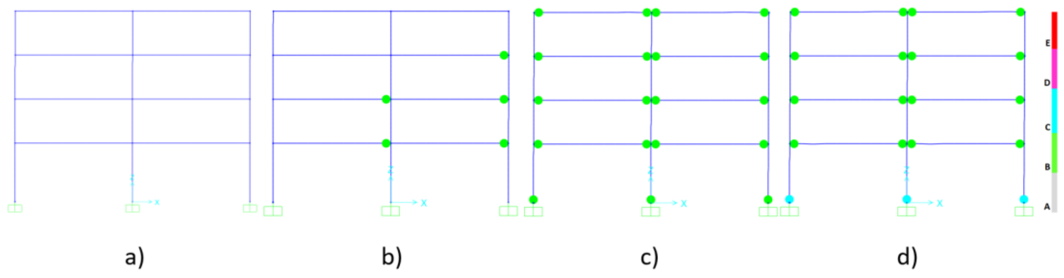

Figure 3-12: States on Different Roof DRs in X direction of Pushover Loading
a) 0.75% Roof DR b) 1% Roof DR c) 3% Roof DR d)5% Roof DR

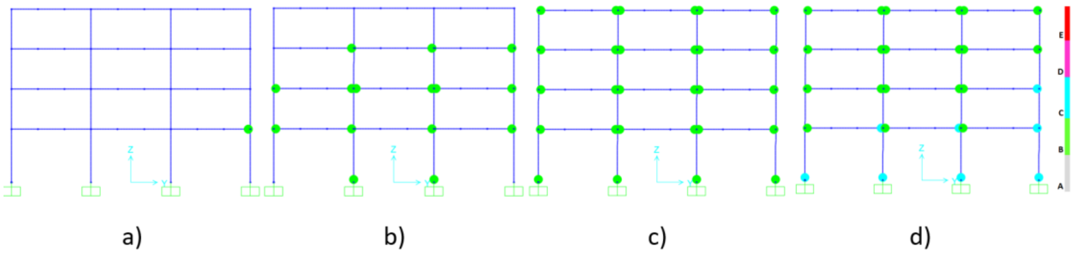

Figure 3-13: States on Different Roof DRs in Y direction of Pushover Loading
a) 0.75% Roof DR b) 1% Roof DR c) 3% Roof DR d)5% Roof DR

The results showed that the beams yielded earlier than the columns, which indicates that the design follows the SCWB principle.

The yielding of beams is desirable because it ensures that energy is dissipated through plastic deformations in the beams before the columns, reducing the likelihood of column failure. Overall, the pushover analysis supports that the structure adheres to the strong column-weak beam principle, indicating that the moment-resisting frames are properly designed to sustain seismic forces.

3.8 Nonlinear Time History Analysis of the Structure

The time-history analysis is carried out utilizing the earthquake data of station 3129 (Lat:36.19117, Long:36.1343). The earthquakes in the EW and NS directions are applied individually, not simultaneously. For the structure's natural periods in the X and Y directions (1.11975 s and 1.03693 s, respectively), there is a close match between the design spectral values and the Kahramanmaraş earthquake data in the EW direction. However, the earthquake data in the NS direction significantly deviates from the design values in the natural periods of structure in both directions, as shown in Figures 1-3a and 1-3b.

The horizontal directions of the earthquake, EW, and NS are applied to the structure individually, both in X and Y directions, respectively. The hinge states are shown in Figures 3-14 and 3-15. The hinge states are calculated according to ASCE41-17.

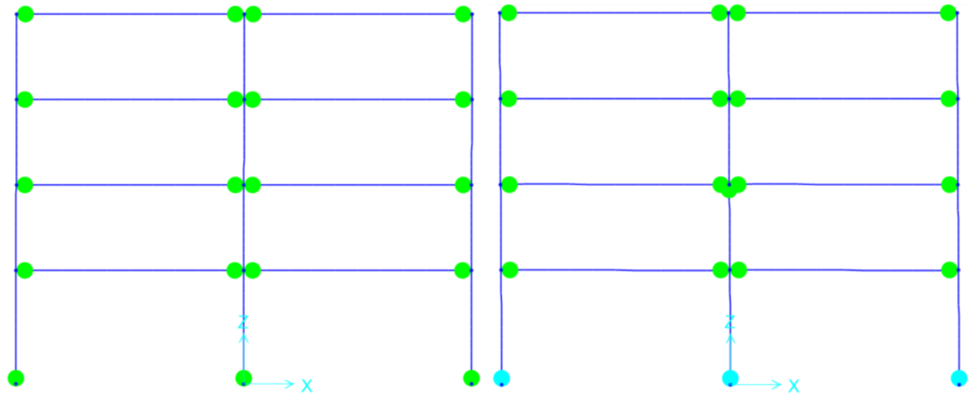

a) b)

Figure 3-14: Hinge states after the horizontal earthquakes are applied individually in X direction a) EW earthquake b) NS earthquake

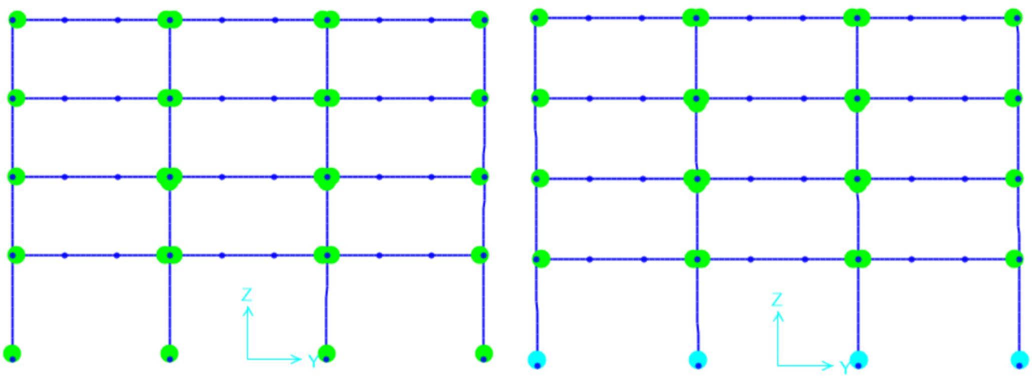

a) b)

Figure 3-15: Hinge states after the horizontal earthquakes are applied individually in Y direction a) EW earthquake b) NS earthquake

Figure 3-14 illustrates the moment-resisting frame in the X-direction of the earthquake placed on axis 1, while Figure 3-15 depicts the moment-resisting frame in the Y-direction of the earthquake placed on axis E. During the seismic evaluation, it was observed that the building exhibited differential performance under the North-South (NS) and East-West (EW) earthquake loads due to variations in the earthquake spectral acceleration values when compared to the design spectra.

The spectral acceleration values in the NS direction of the earthquake closely aligned with the design spectral values, indicating that the seismic demands in this direction were within the range anticipated during the design process. As a result, the structure demonstrated acceptable performance, with no significant signs of overloading in both directions. The plastic hinge formation in the moment-resisting frames (MRFs) remained within B-C level.

In contrast, the spectral acceleration values in the EW direction exceeded the design spectra. Under the EW directional earthquake loading, the structure sustained more severe damage as the plastic hinge formation level is above the C point defined in ASCE41-17, which represents the significant level of inelastic deformation.

When the 3-dimensional earthquake is applied to the structure (EW in X direction, NS in Y direction, UD in Z direction), the hinge states of the moment-resisting frames in the X and Y directions are presented in Figures 3-16 and 3-17, respectively. Even though the states show that the hinge state in the Y direction is between B and C points, the columns experience the 'Collapse' level, as can be seen in Table B-1 in Appendix B.

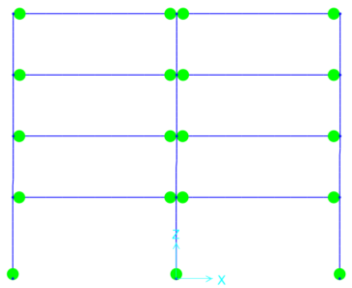

Figure 3-16: Hinge states in the X direction moment-resisting frame after the 3-direction of the earthquake are applied simultaneously (1-4 axes)

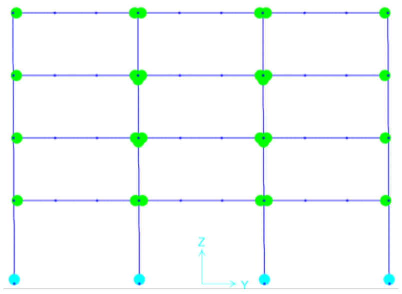

Figure 3-17: Hinge states in the Y direction moment-resisting frame after the 3-direction of the earthquake are applied simultaneously in A, E axes

CHAPTER 4

INFILL WALL MODELLING APPROACH

Two prevalent modeling methods, micro- and macro-modelling, are utilized for infill wall implementation on the structures. As highlighted in the study by J-R Wu et al. (2022) and M. Mohammadi et al. (2021), macro modeling – employing either equivalent single-strut or multi-strut approaches – effectively captures the overall structure response. Representing infill walls as a single strut is a widely accepted practice, which is also adopted by the Turkish Earthquake Code of 2018.

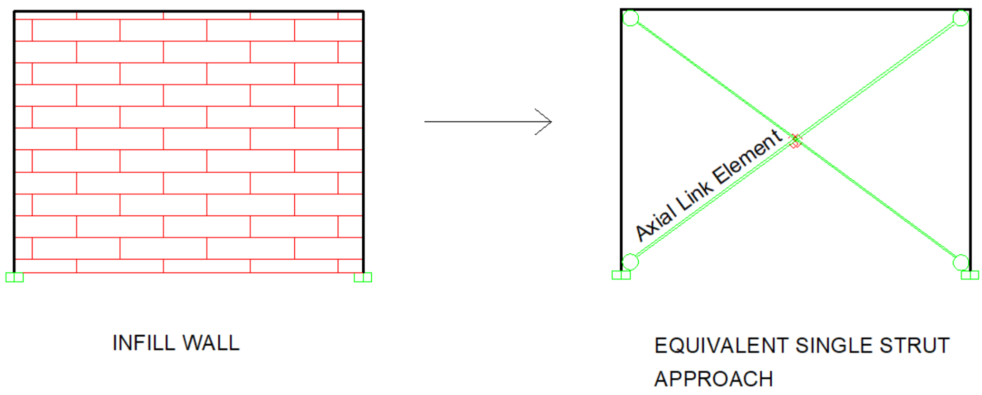

Figure 4-1: Equivalent single strut modeling representing the infill wall

A link model in the SAP2000 will be utilized to capture the compressive axial truss behavior of the equivalent strut for the infill wall, as seen in Figure 4-1. Firstly, the link model will be calibrated, then the influence on the MRF will be investigated.

4.1 Link Element Modelling

A 2-node link element is essentially a straight line connecting two points (Figure 4-2). It represents a simplified representation of the wall's behavior, assuming it acts primarily in compression. To simulate the nonlinear behavior of the model, a multi-linear plastic link element is selected. The force-deformation relationship is calculated according to the Eq. 4-1 and Eq. 4-3 and values given in TBEC2018 Section 15C.2.

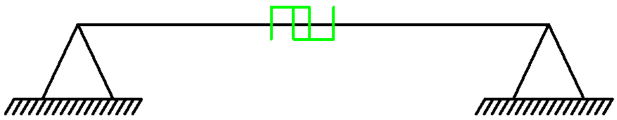

Figure 4-2: Simply modeling of a single strut

Table 4-1: The Mechanical Properties Of The Column And Beam Materials

E_{steel}	200000 MPa	Young's Modulus of beam and column material
υ	0.3	Poisson's Ratio
Fy	235 MPa	Yield Stress
Ic	1.072E0+9	Moment of Inertia of the Column HE500B

Table 4-2: The Mechanical Properties Of The Infill Wall

E_{inf}	2000 MPa	Young's Modulus of beam and column material
fc	5 MPa	Compressive strength of the masonry unit
T_{inf}	200 mm	Thickness of the infill wall
h_{inf}	4000 mm	Height of the infill wall
I_{inf}	6000 mm	Length of the infill wall
r_{inf}	7211.1 mm	Length of the strut (off-diagonal of the infill wall)
Θ	33.69 degrees	The angle of the diagonal with the horizontal
μ	0.67 mm^{-1}	Friction coefficient of the infill to the columns

$$Relative\ Stiffness\ of\ the\ infill\ , \lambda_d = \left[\frac{E_{infill} t_{infill} sin2\theta}{4E_{steel} I_c h_{inf}}\right]^{\frac{1}{4}} \quad \text{(Eq. 4-1)}$$

$$\lambda_d = \left[\frac{2000 * 200 * \sin(2 * 33.69)}{4 * 200000 * 1.072 * 10^9 * 4000}\right]^{1/4} = 5.73 * 10^{-4} \quad \text{(Eq. 4-2)}$$

$$a_d = 0.175 * (\lambda h_c)^{-0.4} * r_{inf} \quad \text{(Eq. 4-3)}$$

$$a_d = 0.175 * (5.73 * 10^{-4} * 4000)^{-0.4} * 7211.1 = 905.78\ mm \quad \text{(Eq. 4-4)}$$

The material axial force behavior is calculated using the related formulas proposed by M. Mohammadi et al. (2021) shown in Eq 4-5, 4-6, 4-7 and 4-8.

$$F_{MD} = f_c * a_d * t_{inf} = 5 * 905.78 * 200 = 905.78\ kN \quad \text{(Eq. 4-5)}$$

$$F_{UD} = 0.25 * F_{MD} = 0.25 * 905.78 = 226.44\ kN \quad \text{(Eq. 4-6)}$$

$$\delta_{MD} = 12.4 * 10^{-4} * \sin(2\theta) * L_{Dstrut} \quad \text{(Eq. 4-7)}$$

$$\delta_{MD} = 12.4 * 10^{-4} * \sin(2 * 33.69) * 7211.1 = 8.25\ mm$$

$$\delta_{UD} = 0.4 * \arctan(\mu) * \delta_{MD} = 0.4 * \arctan(0.67) * 8.25 \quad \text{(Eq. 4-8)}$$

$$\delta_{UD} = 111.67\ mm$$

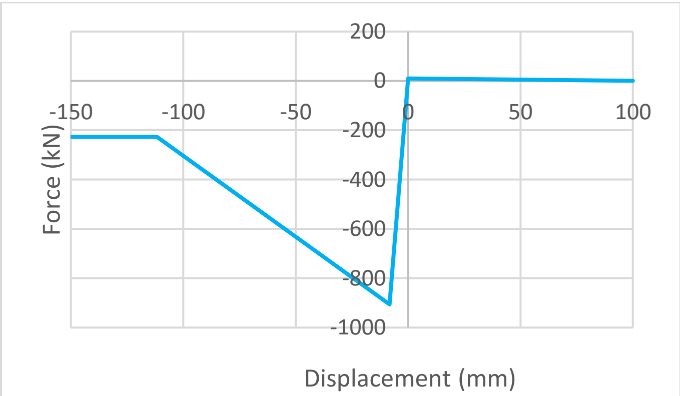

Figure 4-3: The force-displacement curve of the single strut compression element

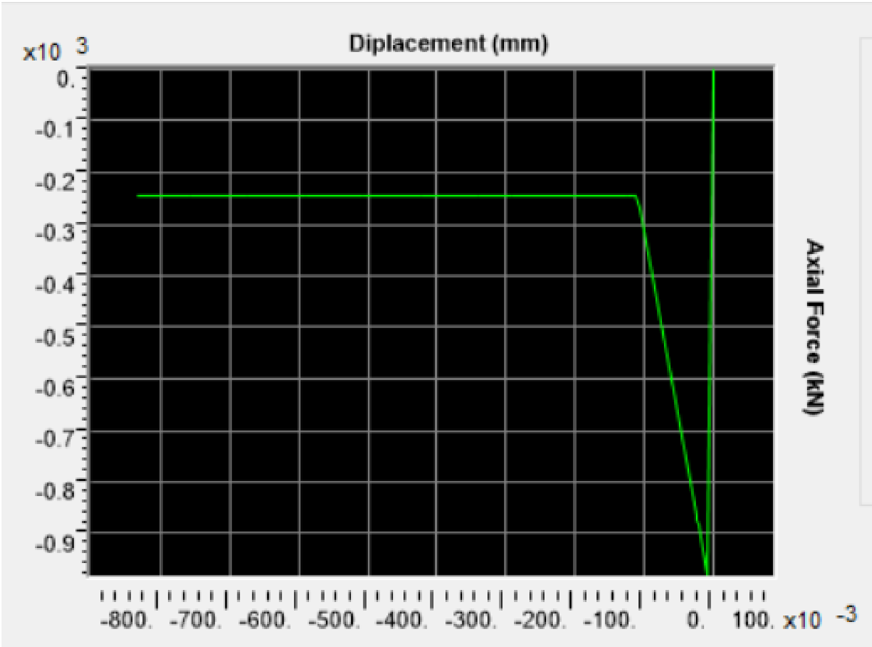

Figure 4-4: The axial behavior of the single strut compression element under compression load provided by SAP2000

The response of the single strut element shows a parallel behavior with the axial response obtained from SAP2000, as depicted in Figure 4-3 and Figure 4-4.

In order to investigate the cyclic behavior of the link element, a cyclic property of the link element is assigned. 'Concrete' hysteresis type is selected with an Energy Degradation Factor of 0. The 'Concrete' hysteresis model is intended for masonry materials, and this model provides a different and independent behavior for the tension and compression side. The only parameter for this type of model is the energy degradation factor, f, which should be defined as 0. $0 \leq f \leq 1.0$. A value of $f = 0$ indicates a clean gap while unloading of the compression force and dissipating the least amount of energy. This behavior is similar to a gap element, where the element provides no resistance once the load reverses, representing a loss of contact. If the energy degradation factor, f, is equal to 0, subsequent compression loading follows the previous unloading. Figure 4-5 shows the unloading and reloading path for the single strut.

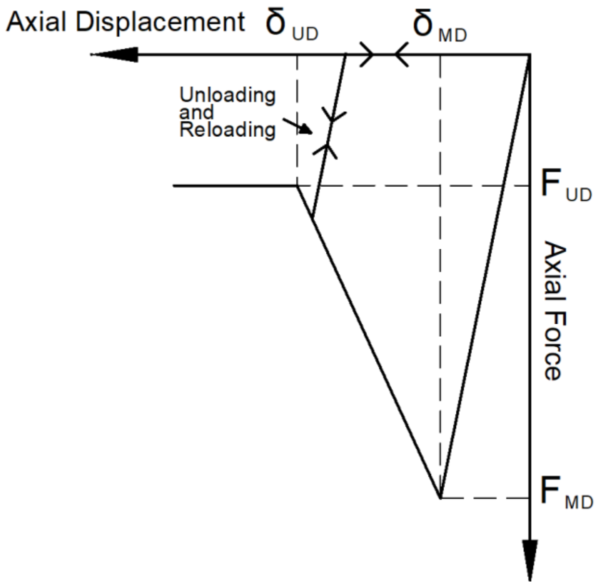

Figure 4-5: Force displacement relation of the single strut element

A user-defined time-history displacement is defined as shown in the Figure 4-6.

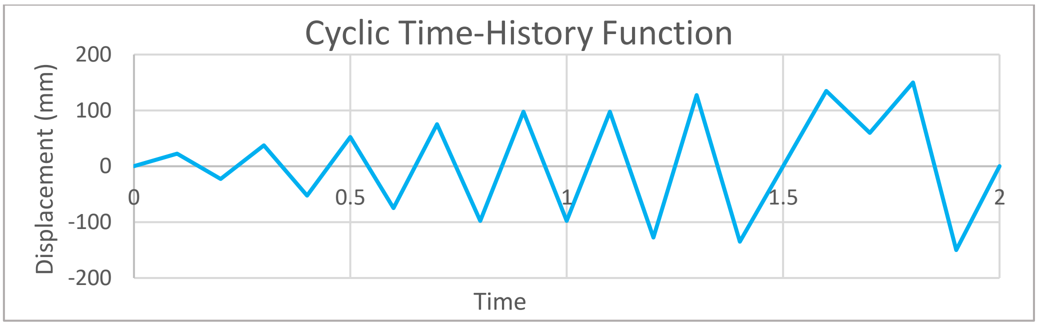

Figure 4-6: The user-defined time-history function

The hysteretic curve shows resistance on the compression side, while the tension side shows no resistance - it only appears as a flat line at very low forces (Figure 4-7). The inability to carry tensile forces leads to increased deformation when it is under tensile loading. This asymmetrical shape of the hysteretic curve indicates that the link can dissipate energy and provide stiffness only in compression. The unloading to zero follows a nearly parallel line to the compression elastic line, as adopted in the model by Mohammadi et. al (2021).

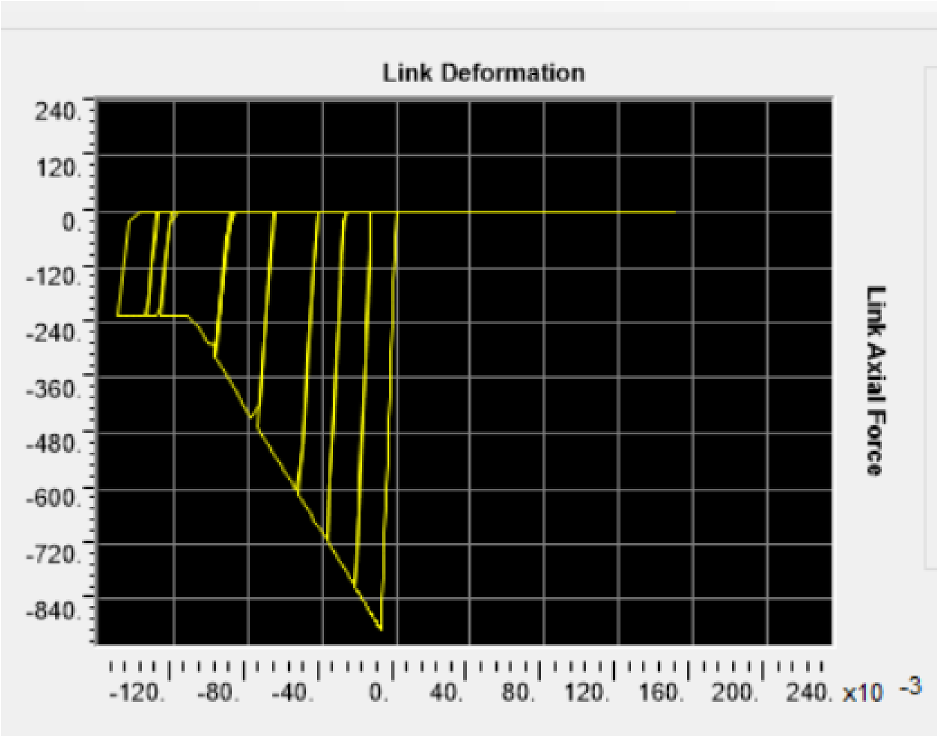

Figure 4-7: The hysteresis graph of the single strut element

4.2 MRF with Equivalent Strut Element

The study involves analyzing the performance of 1-story MRFs with different equivalent single-strut models of infill walls. The analysis is conducted to assess the impact of infill wall thickness on the structural response under pushover loading. The MRF structure is forced to displace up to a 5% drift ratio.

Model 1 incorporates an equivalent strut representing a masonry infill wall with a thickness of 200 mm. Model 1 will be named IW20, indicating an MRF with a 20 cm thickness infill wall.

Model 2 contains equivalent struts with a reduced thickness of 100 mm. Model 2 will be named IW10, representing the MRF with a 10 cm thickness infill wall.

Model 3 does not include any infill walls in order to understand the behavior of bare MRF without the additional stiffness of single struts. Model 3 will be named as BF, indicating the bare frame.

The cross-sections of the columns and beam used in all MRFs are HE500B and IPE450, respectively. The material quality is S235.

Auto PM2M3 hinges are assigned to the columns, and auto M3 hinges are assigned to the beam. The 'Drift Ratio vs. Base Shear' graph is plotted on the MRF with an equivalent single strut and without a strut element, as shown in Figure 4-8.

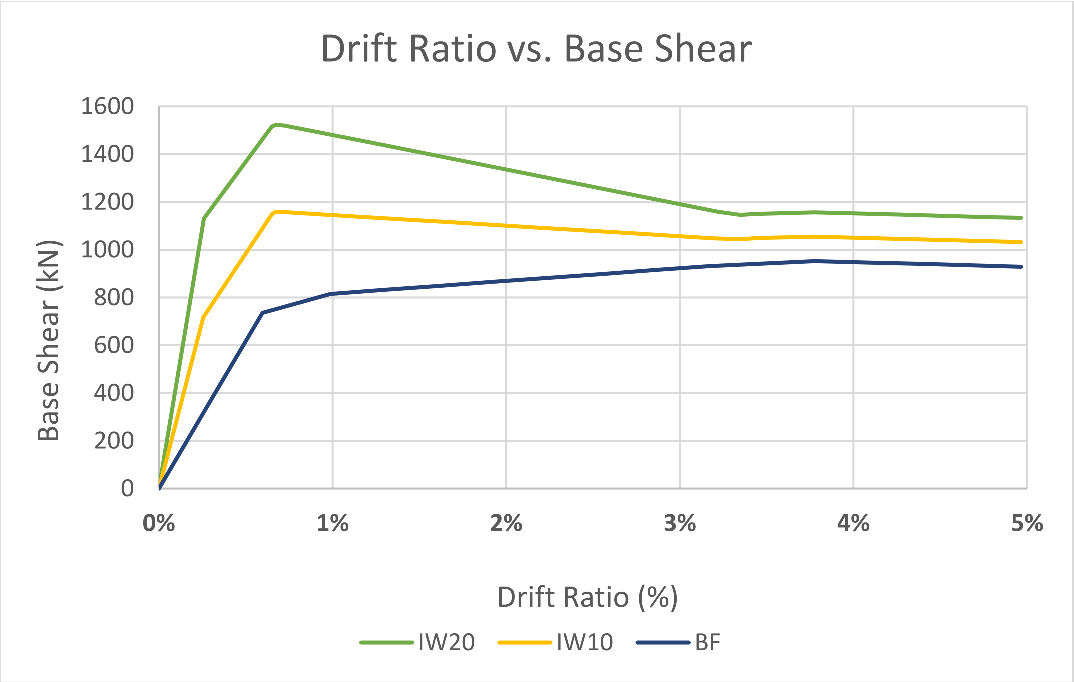

Figure 4-8: Drift ratio vs Base Shear of the MRF structures with different thicknesses of infill walls

The model IW20 exhibits the highest peak base shear force of 1522.7 kN at the drift ratio of 0.6%. The analysis reveals that thicker infill walls contribute to higher stiffness and strength in MRFs, with the 20 cm infill wall model demonstrating up to 87% and 31% higher peak base shear at the lower drift ratios compared to the model without infill walls and the model with 10 cm infill wall, respectively.

On the other hand, the post-peak responses of the models reveal their ductility mechanism. The IW20 and IW10 model exhibits a reduction in strength after the drift ratio of 0.7%. The strength reduction ratio experienced by the IW20 and IW10 models is 24% and 9% up to 3.5% drift ratios. This emphasizes that the infill wall contributes to the lateral load capacity in the lower drift ratios; after that point, they crack immediately, and the strength reduction on the structure begins.

After a 3.5% drift ratio, the strength of the BF is approximately 20%, and 10% is less than the IW20 and IW10 models.

These findings underscore the importance of carefully considering infill wall thickness in the seismic analysis. The BF model shows lower strength, although more ductility; while thicker walls enhance stiffness and strength, they may also lead to immediate strength loss after low drift ratios and less ductile behavior. Therefore, achieving an optimal balance between stiffness, strength, and ductility is crucial for ensuring a structure's seismic resilience.

CHAPTER 5

INFILL WALL IMPLEMENTATION ANALYSIS RESULTS

5.1 Column Hinge Status

Hinge rotation values are crucial parameters for assessing the performance of steel columns and beams during and after the earthquake. These values are utilized to evaluate the extent of inelastic deformations that occur in structural elements and determine the performance level of the elements after the earthquake. These values are compared with the limit values specified in TBEC2018 to evaluate whether the structural elements remain within "acceptable" limits. This assessment provides information about whether the building can continue to be used safely or whether retrofitting is required.

Table 5.1 and Table 5.2 address plastic hinge formation and yield rotation in steel columns and beams.

The yield rotation for the steel beams:

$$For\ all\ shapes:\ \theta_y = \frac{W_p F_{ye} l_b}{6EI_b} \qquad \text{(Eq. 5-1)}$$

The yield rotation for steel columns:

$$For\ all\ shapes:\ \theta_y = \frac{W_p F_{ye} l_c}{6EI_c}\left[1 - \frac{|P|}{P_{ye}}\right] \qquad \text{(Eq. 5-2)}$$

At the same time, since high axial loads have a major impact on the stability of columns and increase the risk of columns buckling, the columns where the P/Pc>0.5 are not allowed for nonlinear deformation. Not allowing nonlinear deformation in columns with P/Pc > 50 aims to minimize the risk of buckling and collapse by preserving the stability of these columns under high axial loads. This restriction increases structure safety and stability, making the structure more durable during an earthquake.

Table 5-1: Acceptance Criteria for Nonlinear Procedures – Structural Steel Beams

Beam (Bending)	*Deformation Limits*		
	LD	*CD*	*CP*
High Ductility Level	$1\theta_y$	$6\theta_y$	$9\theta_y$
Limited Ductility Level	$0.25\theta_y$	$3\theta_y$	$4\theta_y$

Table 5-2: Acceptance Criteria for Nonlinear Procedures – Structural Steel Columns

Column (Flexure)	*Plastic Rotation Li*		
	LD	*CD*	*CP*
$P/Pc < 0.20$			
High Ductility Level	$1\theta_y$	$6\theta_y$	$9\theta_y$
Limited Ductility Level	$0.25\theta_y$	$3\theta_y$	$4\theta_y$
$0.20 \leq P/Pc < 0.50$			
High Ductility Level	$1.5(1\text{-}1.66P/Pc)\theta_y$	$9(1\text{-}1.66P/Pc)\theta_y$	$13.5(1\text{-}1.66P/Pc)\theta_y$
Limited Ductility Level	$0.25\theta_y$	$0.7\theta_y$	$1\theta_y$
Slip Zone	$1\theta_y$	$9\theta_y$	$12\theta_y$

Three distinct structural models consisting of 2 sets of 3 different buildings are considered for the analysis, as depicted in Figure 5-1. In the first model, the high

MRF system is evaluated as a bare frame. The second model contains infill walls only at the intermediate openings in the upper 3 stories. The third model consisted of a continuous wall configuration with infill walls placed at each level of intermediate spans.

The difference between the models in the first set and the second set is that the material quality of the first set and the second set are different from each other. The steel material quality of the columns and beams is S235 for the first set of models, while the material quality of the columns and beams in the second set is selected as S355 and S275, respectively.

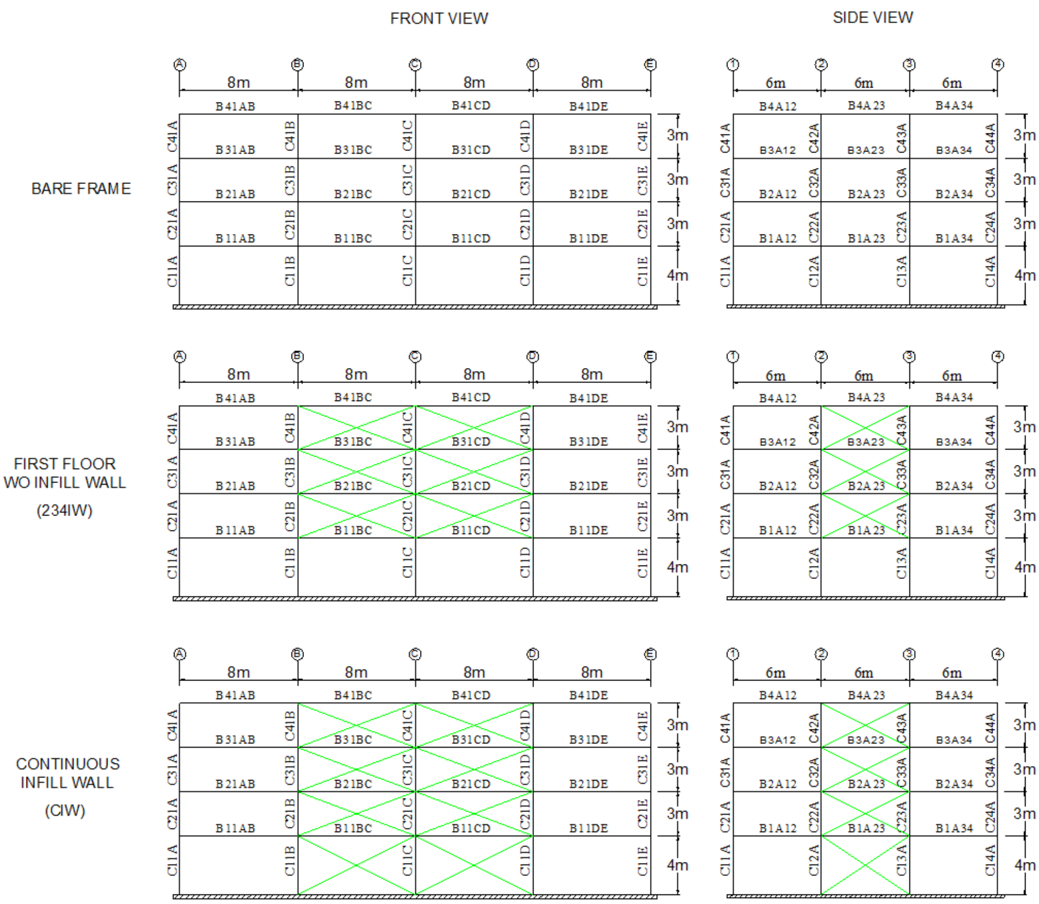

Figure 5-1: Three different configurations of analysis buildings

The time-history analysis is carried out utilizing the earthquake data of station 3129 (Lat:36.19117, Long:36.1343) since the building is designed with the soil design parameters in Antakya, Defne. The analysis starts with the 'Vertical load' case, which includes the G+0.3Q+0.3S loads. After these loads are applied, the earthquake time history analysis is continued. In the analyses, P-Delta effect is considered. The hinge values resulting from the time-history analysis are evaluated according to Tables 5-1 and 5-2 as specified in TBEC2018 Section 5.

Column C11A in the bare frame example is calculated according to Eq. 5-2.

P=1302.44 kN in compression affects the column.

$$\theta_{y,x} = \frac{W_{px} F_{ye} l_c}{6EI_{cx}}\left[1 - \frac{P}{P_{ye}}\right] = \frac{4815000 * 235 * 4000}{6 * 200000 * 1.072 * 10^9}\left[1 - \frac{|-1302.44|}{5616.5}\right]$$
$$= 0.0027\, rad$$

$$\frac{P}{P_c} = \frac{1302.44}{4798.64} = 0.27 \leq 0.50$$

Table 5-3: The calculated values of the sample column C11A

Column (Flexure)	*Plastic Rotation*		
	LD	*CD*	*CP*
0.20 ≤ P/Pc < 0.50			
High Ductility Level	1.5(1-1.66P/Pc)θy	9(1-1.66P/Pc)θy	13.5(1-1.66P/Pc)θ_y
	0.00223	0.01336	0.02004

The absolute hinge rotation of C11A in the direction of X is -0.041506 rad.

$$\theta_{C11A,X} = -0.041506\, rad$$

Since the hinge rotation of C11A in the axial compressive load of 1302.44 kN is -0.041506 rad, which is higher than the Collapse Prevention level limit of 0.02004 rad, the column experiences a Full Collapse (Table 5-3).

Column C11B as a sample is calculated as presented below:

P=158.733 axial tensile load affects the column.

$$\theta_{y,x} = \frac{W_{px}F_{ye}l_c}{6EI_{cx}}\left[1-\frac{P}{P_{ye}}\right] = \frac{4815000 * 235 * 4000}{6 * 200000 * 1.072 * 10^9}\left[1-\frac{|158.733|}{5616.50}\right]$$
$$= 0.00342\, rad$$

$$\frac{P}{P_c} = \frac{158.733}{4798.64} = 0.03 \leq 0.20$$

Table 5-4: The calculated rotation values of the sample column C11B

Column (Flexure)	*Plastic Rotation Limits* (*rad*)		
	LD	*CD*	*CP*
P/Pc < 0.20			
High Ductility Level	1θy	6θy	9θy
	0.00342	0.02051	0.03077

The absolute hinge rotation of column C11B is 0.05093 rad.

$$\theta_{C11B,X} = 0.005093\, rad$$

Since the hinge rotation of column C11B is 0.005093 rad, which is higher than the limit value of Limited Damage State and less than the limit value of Controlled

Damage, the column is in the performance level of Controlled Damage (CD) (Table 5-4).

The other column and beam hinge rotations and performance levels are calculated in a similar manner. The results obtained from the SAP2000 software are presented in the appendix. The number of columns for each building is presented in Figure 5-2.

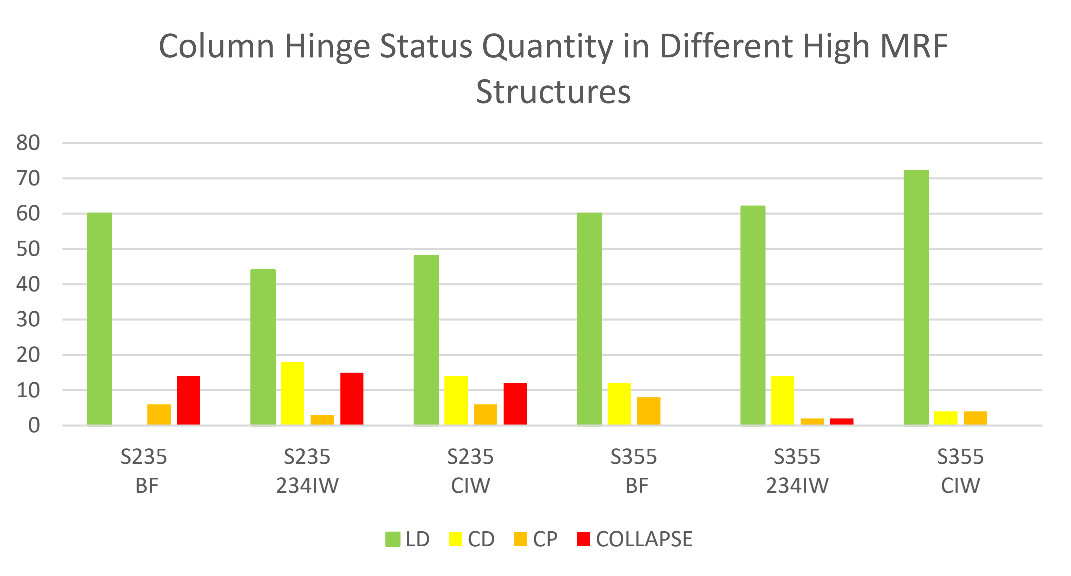

Figure 5-2: The column hinge status of the MRF structures with different infill wall configurations after the time-history analysis

S235 Bare Frame model contains 14 columns in the 'Collapse' level. Adding infill wall only to the 1st story of the S235 Bare Frame model results in a slightly more number of columns in 'Collapse' state. Also, 27% of the columns in the above floors, which are in the 'LD' state, changed to the 'CD' performance level as an adverse effect of the infill wall placed only on the 1st floor.

At the same time, increasing the column material grade from S235 (Fye=235 MPa) to S355 (Fye=355 MPa) has a significantly positive effect on the structure. Performance levels of 12 columns in the first story are changed from 'Collapse' to 'CD' and 'CP' levels.

In the S355 Bare Frame model, no ‘Collapse’ occurred in any of the columns. This model exhibits a response without any collapsed columns, indicating significant improvement in seismic performance compared to the S235 bare frame. The presence of 8 columns in the CP level on the 1st story shows how severe the earthquake intensity is, as 40% of the total columns in the first story are in the CP level. The continuous infill wall shows a positive effect on the S355 MRF structure, reducing the total number of columns in CD and CP levels by 60% and increasing the number of columns in LD level by 13%. However, the structure without an infill wall on the 1st floor shows an adverse effect, increasing the number of ‘Collapse’ columns on the 1st floor by 10%. It should be noted that the maximum utilization of columns in the building with material strength S355 is 41.1%, which is 31.6% lower than that of the building with material strength S235.

In the end, the bar chart underscores that the continuous infill wall included MRF structure’s seismic performance is improved in the lower states of performance levels such as LD and CD. However, beyond the Advanced Damage Zone, the beneficial effect of the infill wall is diminished, and the structure is more susceptible to seismic loads. The performance limit states of all columns can be reached in Appendix A.

5.2 Floor Displacement Profile

The average displacements for each floor level are computed by evaluating the maximum displacement values recorded at the corners of each floor. An average floor displacement is determined by using the maximum displacement values at these nodes. It provides a representative value for each floor's lateral movement under the applied loads.

Figure 5-3 illustrates the displacement profile of a structure where all the structural components have S235. In contrast, Figure 5-4 presents the displacement profile for a structure where the columns are upgraded to steel grade S355 while the beams remain S235.

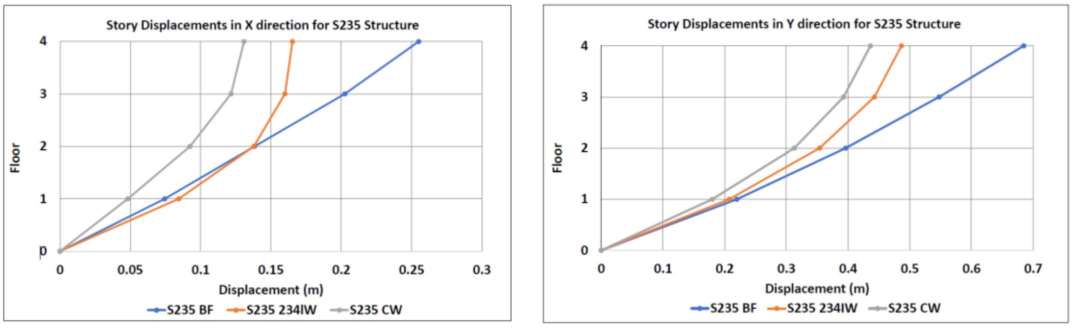

Figure 5-3: Displacement Profile of the S235 Structure

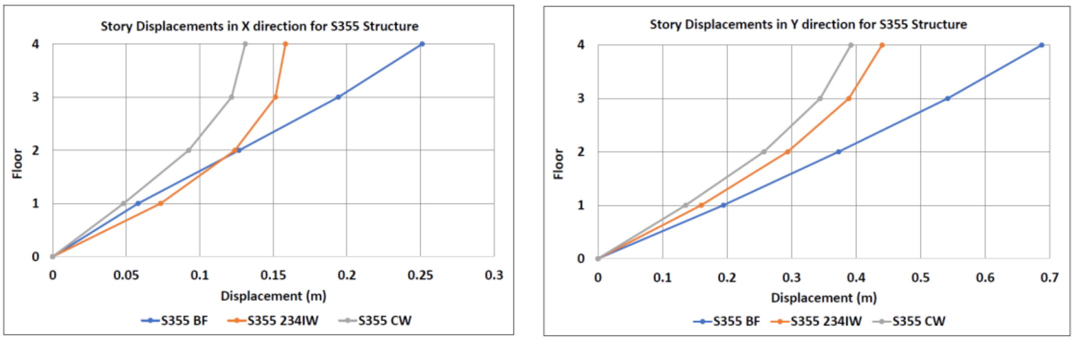

Figure 5-4: Displacement Profile of the S355 Structure

The displacement profile in the X direction indicates that the absence of infill walls on the first floor has a slightly adverse effect on the overall displacement behavior. In contrast, the presence of continuous infill walls has a beneficial impact by significantly reducing lateral displacements.

In the Y direction, the displacement profile reveals greater lateral movement, which can be attributed to the higher seismic demand in the NS direction of the earthquake loading. Notably, the best scenario belongs to the structure with continuous infill walls, as it results in a substantial reduction in lateral displacement compared to the BF and 234IW configurations.

CHAPTER 6

BASEMENT FLOOR EFFECT ON THE SEISMIC PERFORMANCE OF A LOW-RISE SPECIAL MRF STRUCTURE

The basement floor is the initial level of the building, located beneath ground level. With the improved soil-structure interaction, the basement helps the structure be more securely placed on the ground, especially in areas with loose or liquefiable soils. Also, it lowers the structure's center of mass, reducing overturning moments during seismic events. This contributes to the overall stability of the building. The basement floor can serve as an integral part of the foundation, helping to distribute seismic forces more evenly across the structure, and may act as a damping mechanism by absorbing and dissipating the seismic energy before it reaches the superstructure.

In this study, a basement floor will be added to the 6 buildings, including 2 sets of bare frames, a model with continuous infill walls, and a model with the soft story – with S235 and S355 column material structure, taken as the basis in the previous chapters. The first floor will be doubled as a basement floor of the same height, which is 4m. Beams and moment releases will be doubled, similar to the other floors. Shear walls used in the basement floor will not be explicitly modeled. However, the effect of shear walls and surrounding ground will be achieved by using supports that will fix the lateral movement, as done in the study conducted by P. Jones et. al (2010) (Figure 6-1).

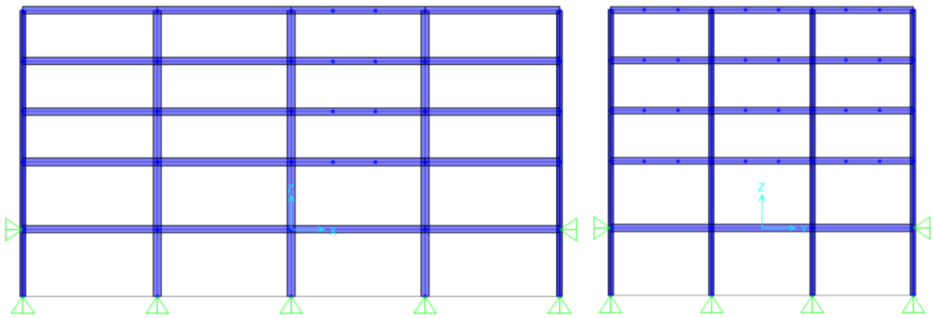

Figure 6-1: The side view of the building with the lateral supports on the 1st floor, representing the basement walls not explicitly modeled

Nonlinear time history analysis is carried out on all 6 building models using earthquake ground motion records obtained from station 3129 (Lat:36.19117, Long:36.1343) in Hatay/Defne. Nonlinear time-history analysis continues after the 'Vertical load' case, which consists of G+0.3Q+0.3S loads. For the basement floor, no wind load is considered. All analyses consider the P-Delta effect.

The first set of MRF structures with the material quality of S235 is as follows:

- **Bare Frame Model (BF235):** This model only contains a bare MRF frame with the beams and columns material strength of S235 constructional steel.
- **1st Floor wo Infill Wall (234IW235):** This model contains the infill wall equivalent struts for the 2nd, 3rd, and 4th floors. The equivalent strut modeling is not included on the 1st floor.
- **Continuous Infill Wall (CIW235):** The infill wall equivalent struts are included in all the floors of the building.
- **Bare Frame Basement (BF235Base):** This model has a basement floor with the bare MRF on it.
- **1st Floor wo Infill Wall Basement (234IW235Base):** This model has a basement floor in addition to the infill walls on the 2nd, 3rd, and 4th floors. The 1st floor of the building does not contain the infill wall modeling.
- **Continuous Infill Wall Basement (CIW235Base):** This model has a basement floor with infill wall struts on all floors of the buildings.

The hinge results that occurred in the columns of the building are presented in Figure 6-2. The performance level difference between the structures without a basement and with a basement draws attention.

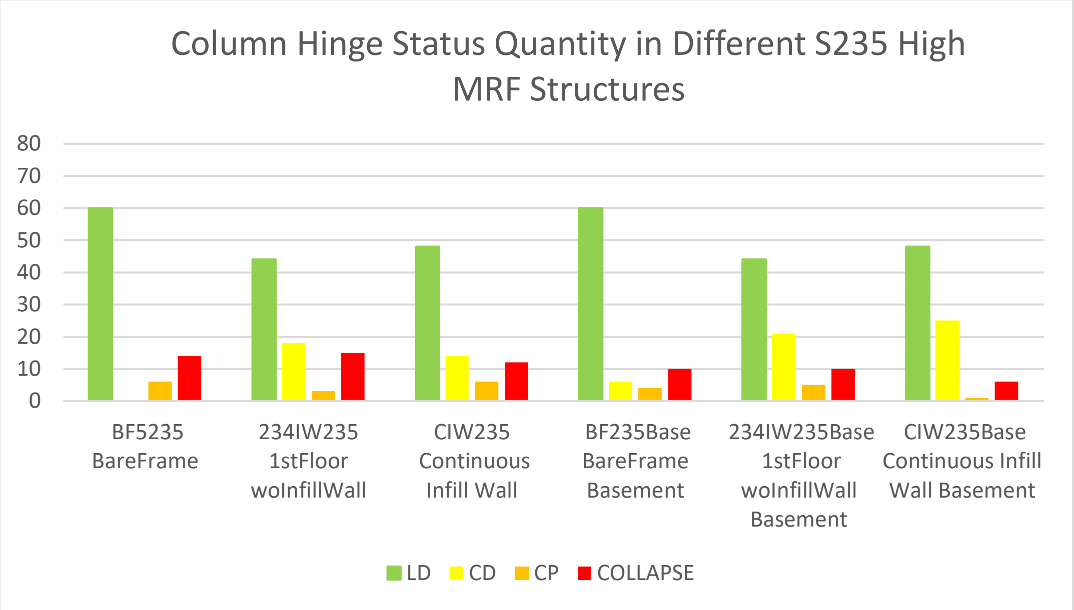

Figure 6-2: The column hinge status quantity of S235 MRF structures with different configurations of infill wall and basement implementation

The computation of average displacements across different floor levels is calculated with the maximum displacement at the corners of each floor. Figures 6-3 and 6-4 illustrate the displacement profile of the structure where all the structural components have S235 in X and Y directions, respectively.

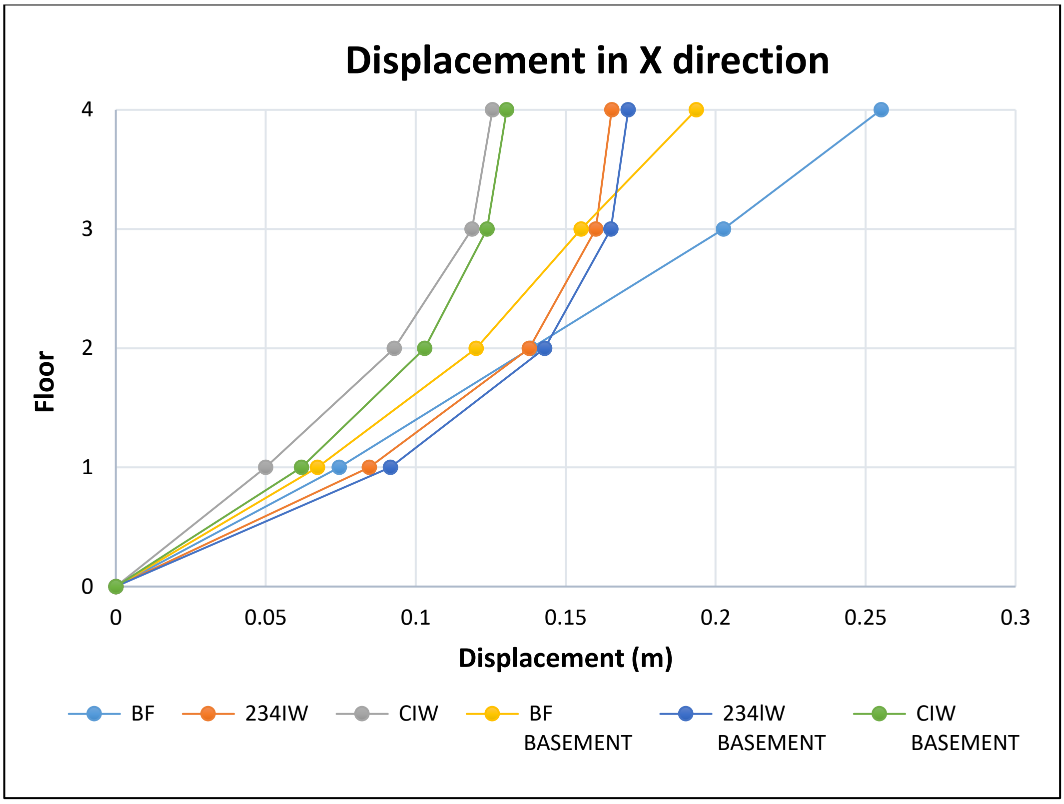

Figure 6-3: The displacement profile in X direction for S235 Structure

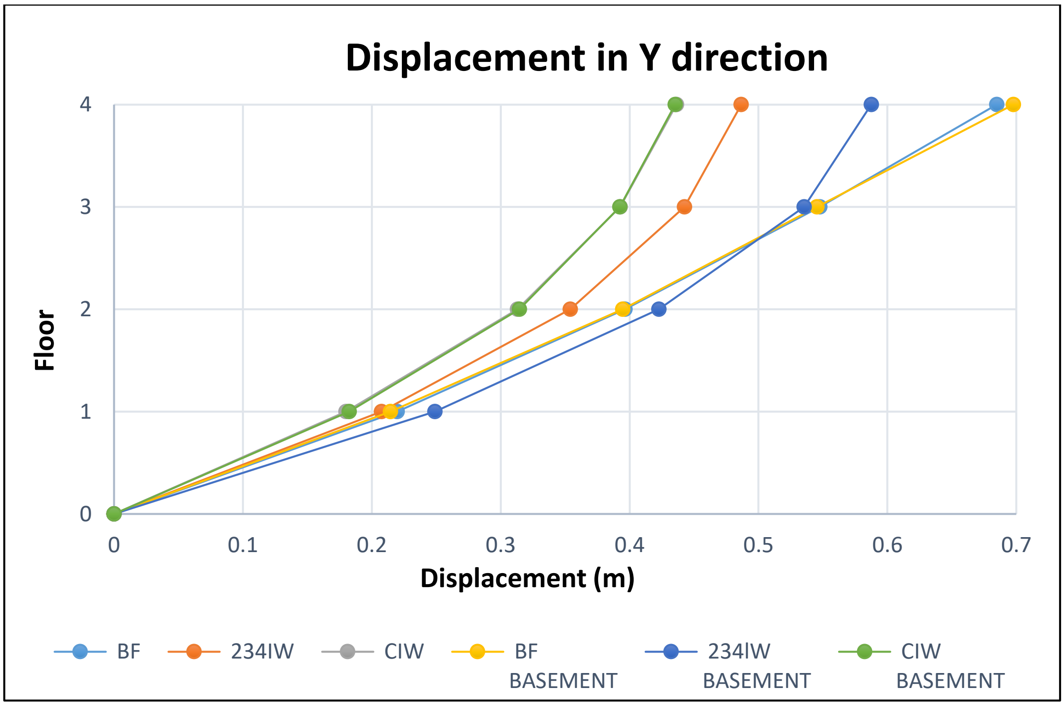

Figure 6-4: The displacement profile in Y direction for S235 Structure

BF235 model contains 14 'collapsed' columns on the 1st floor. Adding a basement decreased the number of collapsed columns by 29% to 10. It should be noted that 6 out of 20 basement columns have exhibited the 'CD' performance state, indicating these elements dissipated a portion of the input energy prior to its transmission to the superstructure. Also, it is observed that the lateral displacement in the BF is reduced when the basement is implemented to the structure.

234IW235 model has 10 columns in the 'Collapse' Zone. The basement floor has a positive effect on the columns, with a decrease in the number of 'Collapse' columns from 15 to 10 on the 1st floor. The columns on the above floors, which are in the 'Advanced Damage Zone,' were changed to 'Significant Damage Zone, ' resulting in a favorable structural behavior that no column in the 'CP' state on the above floors.

The positive effect of the basement floor is more prominent in the Continuous Infill Wall configuration. While the 12 columns on the 1st floor are in a 'Collapse' state, the basement floor has decreased the number by 50% to 5. All 6 columns in the 'CP' state shown in the chart are located in the 1st column. Adding the basement floor caused 5 out of 6 columns in the overall performance state to change from 'CP' to 'CD', showing an 83% positive impact. The total number of 'LD' columns does not change, while the 'CD' column number is increased by 44%.

In general, it can be said that the basement has a positive effect on the MRF structures, with the transition of the columns' performance states from the 'Advanced Damage Zone' to the 'Significant Damage Zone'. This led to improvement in the overall seismic performance of the structures, attributed to the increased energy dissipation capacity and reduced lateral movement.

The second set of MRF structures using the material quality of S355 in the columns and S275 in the beams are summarized below:

- **Bare Frame Model (BF355):** This model only contains a bare MRF frame with the beams and columns material strength of S275 and S355 constructional steel, respectively.

- **1st Floor wo Infill Wall (234IW355):** This model contains the infill wall equivalent struts for the 2nd, 3rd, and 4th floors. The equivalent strut modeling is not included on the 1st floor.
- **Continuous Infill Wall (CIW355):** The infill wall equivalent struts are included in all the floors of the building.
- **Bare Frame Basement (BF355Base):** This model has a basement floor with the bare MRF on it.
- **1st Floor wo Infill Wall Basement (234IW355Base):** This model has a basement floor in addition to the infill walls on the 2nd, 3rd, and 4th floors. The 1st floor of the building does not contain the infill wall modeling.
- **Continuous Infill Wall Basement (CIW355Base):** This model has a basement floor with infill wall struts on all floors of the buildings.

The hinge results that occurred in the columns of the building are presented in Figure 6-5.

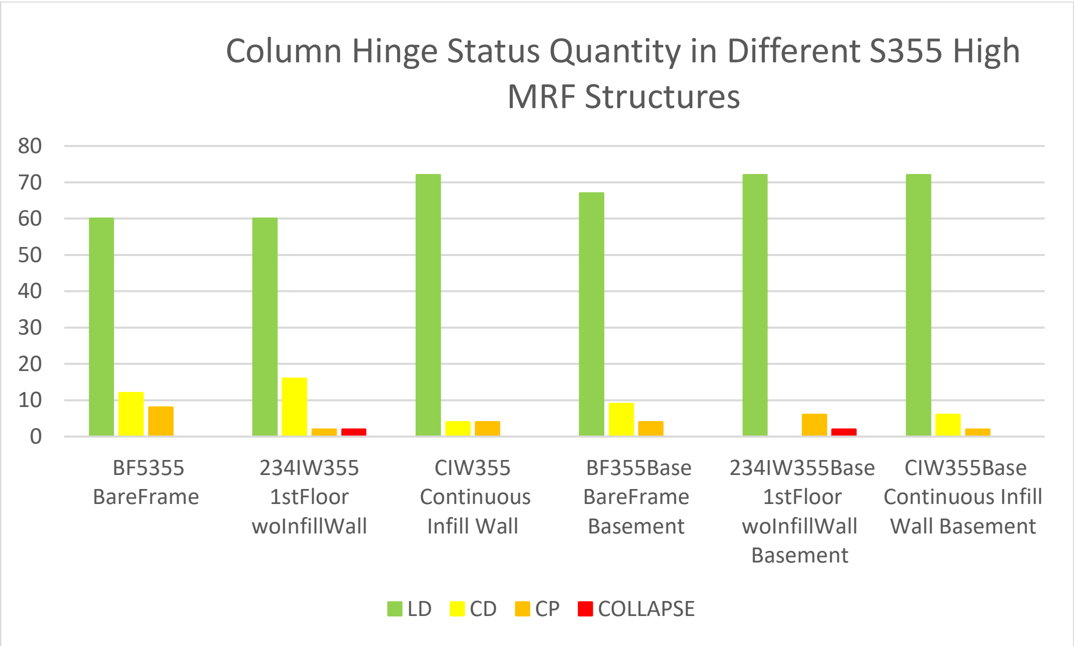

Figure 6-5: The column hinge status quantity of S355 MRF structures with different configurations of infill wall and basement implementation

The displacement profile, shown in Figures 6-6 and 6-7, is determined by averaging the displacement of corner nodes per floor, illustrating the structure's response with columns and beams made of S355 and S235 steel material, respectively.

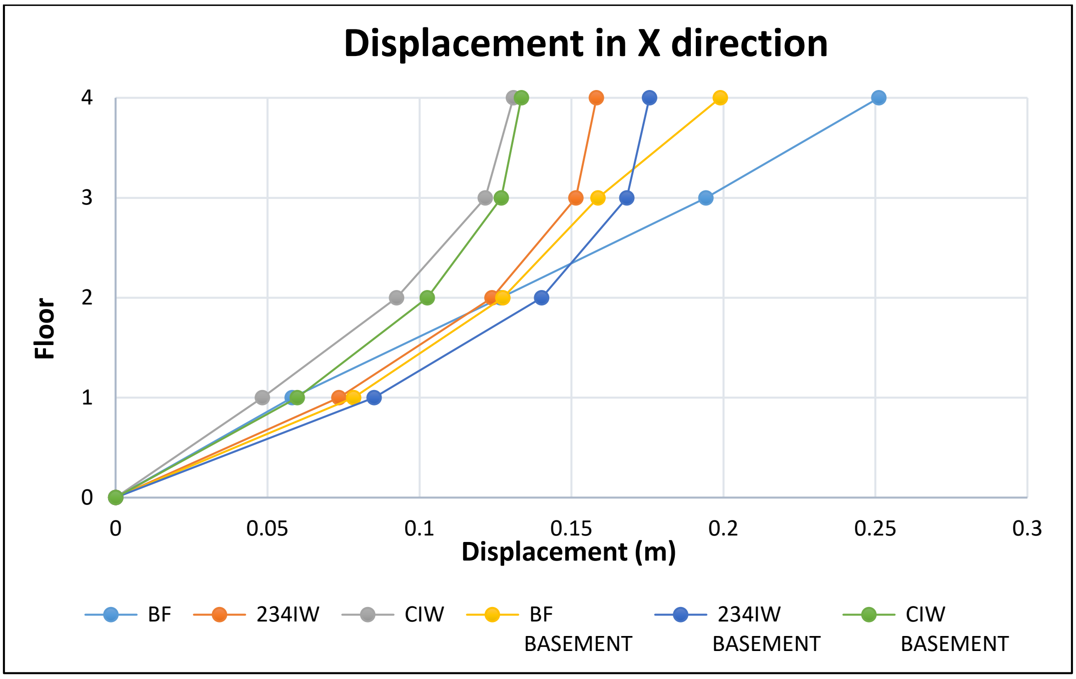

Figure 6-6: The displacement profile in X direction for S355 Structure

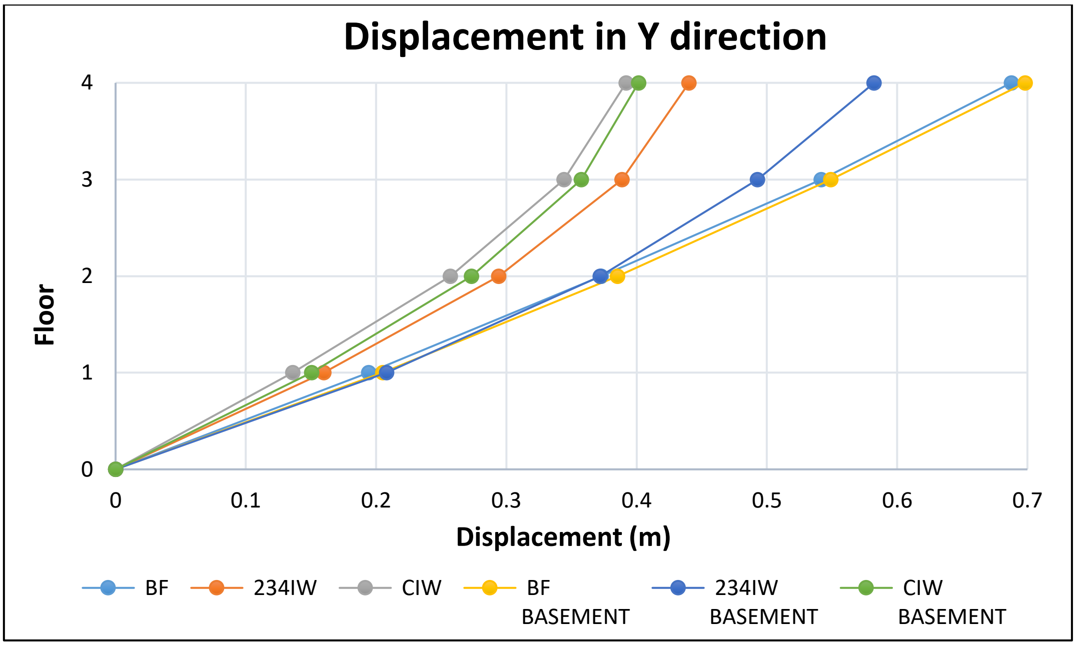

Figure 6-7: The displacement profile in Y direction for S355 Structure

BF355 model exhibited 8 columns in total in the ‘CP’ limit states. Adding the basement floor showed a good contribution to the energy dissipation and reduced half of the columns in the ‘CP’ states to the lower states. Additionally, the total number of columns in the ‘LD’ state has increased by 11.7%, showing a conducive impact on the overall seismic response. The basement implementation also shows that the top floor lateral displacement of the BF355 model is decreased by 20% in X direction.

In the 234IW355 model, 2 columns are in the ‘Collapse Zone.’ While the total number of ‘Collapsed’ columns did not change, the total number of columns in the ‘LD’ state increased from 60 to 72 by 20%.

CIW355 model is classified as in the ‘Advanced Damage Zone’ at the beginning. After the inclusion of the basement floor, the seismic response of the 2 more columns showed an improvement in terms of performance states and transitioned to a ‘Significant Damage Zone,’ suggesting that the basement floor has a beneficial impact on the overall response by reducing the limit states of the columns. Although the total number of columns in the ‘LD’ state remains constant, half of the columns previously in the ‘CP’ state were shifted to the ‘CD’ limit state.

In conclusion, the implementation of a basement floor resulted in a notable enhancement of the overall structural behavior. The basement effectively absorbed the energy, reducing the damage on the columns in the superstructure. The performance limit states of the columns on the basement floor can be reached in Appendix B. The moment-resisting beams hinge states for the S235 Bare Frame and the S235 Continuous Infill Wall with the Basement are also shared in Appendix B.

CHAPTER 7

SUMMARY AND CONCLUSIONS

7.1 Summary

On January 6, 2023, two devastating earthquakes in Turkey severely affected the southern part of the country, with magnitudes of 7.8 and 7.6. Over 50,000 deaths were reported in Turkey. Besides that, 58,000 buildings collapsed, along with 200,000 with severe damage. In this thesis, the seismic performance of a steel building designed according to the Turkish Building Earthquake Regulation (2018) and Principles of Design, Calculation, and Construction of Steel Structures (2018) is assessed under earthquake data taken from station 3129 located in Hatay/Defne region. The same design methodology is used as the reference building designed by Erkan Özer, Cavidan Yorgun, and Cüneyt Vatansever (2018). The design is significantly affected by the change in soil class, causing alterations to the column cross-sections.

The analysis and design are conducted considering the Load and Resistance Factor Design method as described in DCCPSS 2018, Section 5.3.1. The soil class is ZA and PGA value is 0.452g for 475 years return period where the building is located in Defne/Antakya. The dead loads, live loads, and snow loads are considered in the design with different combinations in accordance with the DCCSPP 5.3.1, TBEC 4.4, and TBEC9.2.5. The fictitious loads caused by imperfections are considered in the vertical load combinations. The inspection of the irregularities of the building is conducted to ensure that the building meets the requirements to use Equivalent Earthquake Load Method. Since the A1 torsional irregularity coefficient, $\eta_{bi} \leq 2.0$, and there is no type B2 stiffness irregularity, the Equivalent Earthquake Load Method is used. The Structural Response Coefficient is given as 8, and the Overstrength Factor, D is given as 3 for special moment-resisting steel frames. The

Seismic Load Reduction Factor, Ra of 8 is found to be used as a basis for reducing the linear elastic seismic loads. The relative story drifts at the end of the design is checked and meet the requirements under defined cross-sectional properties. Second-order effects are also considered, and the building meets the requirements of the second-order limitations. The strength and service limit status checks are conducted under vertical loads and service loads. For all structural members, the dimensioning of the members is presented under the most governing combination. At the end of the design, the check of the strong column – weak beam principle is carried out, in which TBEC Section 9.3.2 emphasizes that the columns shall be designed to be stronger than the beams. While performing this check, expected material strengths are used with the Ry values specified in TBEC Table 9.2 for the beam elements. The cross-sections of the structural elements result in the altering of the column sections to HEB500, which was HEB450 in the reference model designed for Maslak/İstanbul previously.

All the analyses and assessments conducted throughout the study are performed by using the SAP2000 program, which is a well-known commercial program in the industry. The material nonlinearity and P-Delta effect are incorporated into the assessment. Therefore, plastic hinges at the ends of the beams and columns are located to capture inelastic deformation in the structural members. Deformation-controlled hinges are selected to obtain the expected ductile response of the columns. This approach helps in evaluating the different performance levels of the building's structural elements while simulating the gradual degradation of stiffness and strength. In order to ensure the accuracy of the model response, the hinge models assigned to the beams and columns of the building are verified according to the ASCE41-17. The verification is completed in a single column to make it easier to track the response. The yielding and plastic rotation angles of a 4-meter-long column (the same height as the 1st story of the building in question) are calculated and compared with the values presented by SAP2000. The results are very similar, suggesting that the 'Nonlinear Beam Column Hinges' as an Auto Hinge Property could be utilized in the assessment. Also, it should be noted that a higher P/Pye value leads to a greater reduction in yield rotation, indicating earlier plastification on the column. ASCE41-17 Section 9 defines two limits for the τ_b value, which is the additional reduction factor for the flexural stiffness for the members whose P/Pye ratio is under 0.5 and above 0.5. Additionally, the expected moment capacity of the section depends on the P/Pye value with a limit of 0.2. The higher axial force on the member has a noticeably detrimental impact on the member's elastic limits.

The influence of infill walls is considered on the overall structural behavior, and two sets of numerical models were generated for investigation. One set employed S235 structural steel for all structural members, while the other set utilized a higher strength of S275 steel for beams and S355 steel for columns. The infill wall modeling may be implemented in the structures using either micro-modeling or macro-modeling. Micro-modeling of infill walls includes a detailed numerical model and simulation. This method can give more accurate results, especially in the local response of the structural elements. Macro-modeling, on the other hand, simplifies the infill-wall modeling using equivalent strut approaches. Different strut models are presented in the literature. In this study, one couple of the equivalent strut approaches is used with the strut width value, calculated as per TBEC2018 Section 15C. The material properties are taken from the code 15C.2.2 for the blend brick assumption. The material axial behavior is calculated by taking reference to the equations proposed by M. Mohammadi et al. (2021). One single compression-only truss member is generated using the ‘Link’ property in SAP2000. Under the static pushover and hysteretic loading case, the behavior of the strut is simulated. According to the results obtained from pushover analysis, the strut is found to go the high axial compression loads in a very limited displacement, indicating a very steep curve in the elastic region. After reaching the elastic limit, the strength capacity immediately drops by nearly 75% and shows a perfectly plastic response after that point. The tension force capacity is assigned as very low. In order to investigate the cyclic behavior of the link element, the ‘Concrete’ hysteresis type is assigned with the Energy Degradation Factor of 0, as also recommended by SAP2000. The selected hysteretic behavior demonstrates that the tension and compression behavior of the strut are independent of each other. When the strut shows resistance under the compression load, there is no resistance under the tension load, similar to the gap element, representing a loss of contact under tension loading. Also, the member follows the same unloading curve during subsequent compression loading. Three different simple MRF models are generated with different infill wall thicknesses – without infill wall, 100 mm, and 200 mm - to compare the influence of the infill thickness on the %DR of the MRFs. Based on the analysis results, it was observed that the wall thickness has a significant impact on the %DR value under the same Base Shear. A thicker infill wall leads to a lower %DR value, indicating that it limits the lateral movement of the MRFs by providing additional lateral strength.

After investigating the equivalent single strut approach of infill wall modeling, the designed building is utilized in 3 different configurations to examine the infill wall effect on the overall structural seismic response. The model explanations are presented below:

- First set of building configurations with the material strength of S235
    - The designed bare frame with the structural elements' strength of S235
    - The designed building includes infill wall in 2nd, 3rd and 4th story. Only 1st story does not include the infill wall simulating the soft story. The infill walls are placed in the middle bays of the stories.
    - The infill wall is continuously placed across all stories in the middle bays of the building.
- Second set of building configurations with column material strength of S355
    - The bare frame with the column and beam strength of S355 and S275, respectively.
    - Infill walls are placed to the bare frame in the 2nd, 3rd, and 4th stories. Only 1st story does not include the infill wall simulating the soft story. The infill walls are placed in the middle bays of the stories.

- The infill wall is continuously placed across all stories in the middle bays of the building.

The thickness of the infill wall is selected as 200 mm, and the material axial behavior of the equivalent single strut models is calculated based on this thickness. The time-history analysis is conducted using the earthquake data of station 3129 (Lat:36.19117, Long:36.1343) located in Antakya/Defne since the building is designed with the soil parameters and PGA values of the Antakya/Defne region. The column hinge rotation values are assessed according to the TBEC2018 Section 5C.1. As stated in the aforementioned section of TBEC2018, plastic deformation on the columns with $P/Pc > 0.5$ is not allowed. This limitation aims to reduce the risk of buckling and collapse under high axial loads of columns. Since the peak vertical ground acceleration observed in the earthquake data is significantly high -0.73g-, it is worth noting that the P values recorded within the columns approach approximately 50% of their capacity, albeit not precisely reaching this threshold. The seismic performance of the buildings is compared between the different configurations by considering the performance states of the columns. Adding the infill wall to the building affects the structure's seismic performance positively in the lower states while having a negative effect beyond the 'Advanced Damage Zone.' Also, reducing the usage ratio of the columns by increasing the strength of the columns has a major impact on the 'Collapsed Column'. Also, the infill wall has a beneficial effect on lateral displacement by reducing it.

Additionally, the seismic performance of the basement level is evaluated in this study using the same numerical models and ground motion records. The basement floor is added to these different configurations by doubling the 1st floor. Beams and moment releases are the same for the basement floor. The shear walls to be placed on the basement floor are not explicitly modeled. Instead, supports that fix the lateral movements are defined to take into account the shear wall effect and the lateral support by surrounding ground, as done in the study carried out by P. Jones et. al (2010). The nonlinear time history analysis is conducted for all 6 different configurations. Implementation of a basement floor has a positive effect on reducing the number of 'Collapsed Columns' by dissipating a portion of the energy before it transmits to the superstructure. The basement floor implementation also significantly reduces the lateral displacement in the bare frame configuration. The positive effect is more prominent in the models with S355 material strengths. Especially with continuous infill walls, the basement floor significantly increases the number of ‘LD’ columns when compared to the models with S235 columns.

7.2 Conclusion

Based on the observations and results derived from the numerical analysis, the following conclusions can be drawn. All findings are based on the model designed in Chapter 2 and its various configurations adhering to the original design.

- As a result of the analyses made using the acceleration records recorded at station 3129 in Defne/Hatay during the February 6, 2023 Earthquakes, The overall structural performance evaluation of the special moment-resisting frame building designed according to TBEC2018 is made, and it is observed that the building considered is at the Collapse Performance Level and could not meet the targeted Controlled Damage Performance Level.
- The PGA value taken into consideration in the design for the Defne/Antakya region is 0.452g for a 475-year return period. It was observed during the time-history analysis that the accelerations occurring on February 6, 2023, were greater than the accelerations predicted by the earthquake regulations, resulting in the properly designed structural elements being insufficient to meet the moment demands.
- The implementation of infill walls in a building has a significant impact on its structural performance level. Infill walls add stiffness to the structure. If the walls are unevenly placed to the stories, this can lead to stiffness irregularities in the building, leading to high differential movement between different stories of the structure. Leaving the first floor without an infill wall had such a negative effect on the building's seismic performance, even in

cases where the building was constructed with high-strength materials. This resulted in reduced seismic performance in the columns of the first story, with a higher lateral drift ratio on the first floor. The continuity of the wall across all the floors has a positive effect on preventing the hinge states from going beyond the advanced damage zone.

- The basement floor implementation on the structure reduces the column plastification states in a significant manner. While effectively absorbing the energy with the basement columns, the hinge states of the columns on the upper structure remain in the 'Controlled Damage Zone,' which is the target performance level of such a building defined in the TBEC 2018.
- There are 2 sets of models generated – one set includes the S235 material strength in the columns and beams as designed, and the other one includes the S355 and S275 material strength in the columns and beams, respectively. Restricting the column capacity usage to below 50% has been observed to enhance the seismic performance of a building by increasing the yield rotation and reducing the lateral displacement.

In conclusion, it has been observed that the special MRF steel structures designed considering the minimum conditions of the earthquake regulations and steel standards, the relevant structure will not exhibit sufficient earthquake performance. Therefore, the PGA values should be revised to reflect the high seismic design parameters. Additionally, the infill wall should be continuous across the whole story in order to prevent stiffness irregularity, resulting in a high differential movement and high-performance states of columns. Furthermore, as a result of the basement effect investigation, the basement floor has a significant effect on the first-floor lateral movement by reducing it. Also, this application enhances the structural performance by absorbing the energy at the basement level before its transmission to the upper structure. Hence, the application of the basement floor should be considered for the special MRF steel structures to help increase seismic performance.

7.3 Future Recommendations

1. Extension to Mid-Rise and High-Rise Buildings: This study focuses on the seismic behavior of low-rise buildings. It is recommended to extend the analysis to mid-rise and high-rise buildings. This would provide a more comprehensive understanding of seismic performance across different building heights and help generalize the findings to a wider range of structures.

2. Consideration of Interior Wall Effects: The current study evaluates only the impact of exterior walls under seismic loading. Future research could incorporate the effects of interior walls to comprehensively evaluate their influence on the overall seismic response of the building.

3. Incorporation of Window Openings in External Walls: In this study, external walls were modeled without considering window openings, assuming walls only in the middle spans. A future study could focus on considering the effects of window openings on external walls, as they might influence the stiffness and seismic response of the building. Understanding these effects could lead to more accurate seismic performance.

REFERENCES

AFAD, 2023. 06 Şubat 2023 Pazarcık-Elbistan (Kahramanmaraş) Mw: 7.7 – Mw: 7.6 Depremleri Raporu. 140 s.

Aldemir, A., Erdil, B., & Yücel, Ö. B. (2024). Türkiye’deki Depreme Dayanıklı Betonarme Çerçeveli Bina Tasarımına Retrospektif Bir Bakış. Çukurova Üniversitesi Mühendislik Fakültesi Dergisi, 39(1), 271-285. https://doi.org/10.21605/cukurovaumfd.1460500

Aldemir, A., Unutmaz, B., Koçkar, M. K., Erkal, B. G., Şahin, U., Sandıkkaya, M. A., ... & Çiçek, E. (2023). ŞUBAT 2023–Kahramanmaraş Pazarcık (Mw= 7.7) ve Kahramanmaraş Elbistan (Mw= 7.6) Depremleri İnceleme Raporu. Hacettepe Üniversitesi, İnşaat Mühendisliği Bolumu: Ankara, Türkiye, 1-170.

Aydınoğlu, N., Gülenç, C. (2023). Şubat 2023 Depremlerinde Binalarin Ağir Hasar Ve Yikimlarinda Tasarim, Yapim Ve Denetim Hatalari Yaninda Depremlerin Büyüklüğünden Ve Yönetmeliklerden Kaynaklanan Sorunlara Ilişkin Bir Irdeleme: Antakya Örneği, Boğaziçi Üniversitesi, Kandilli Rasathanesi ve Deprem Araştırma Enstitüsü Deprem Mühendisliği Anabilim Dalı

Aydınoğlu, N. M., Celep, Z., Özer, E., & Özaydın, K. (2018). Türkiye Bina Deprem Yönetmeliği Eğitim Sunumları. TMMOB İnşaat Mühendisleri Odası.

Binici, B., Yakut, A., Kadas, K., Demirel, O., Akpinar, U., Canbolat, A., ... & Canbay, E. (2023). Performance of RC buildings after Kahramanmaraş Earthquakes: lessons toward performance-based design. Earthquake Engineering and Engineering Vibration, 22(4), 883-894.

Çağlar, N., Sert, S., & Serdar, A. H. (2021). Basement-storey effect on the seismic response of RC buildings on soft surface soil. Arabian Journal for Science and Engineering, 46(11), 11291-11302.

Çelik Yapıların Tasarım, Hesap ve Yapım Esaslarına Dair Yönetmelik (RG no. 29614), Turkiye Cumhuriyeti Çevre ve Şehircilik Bakanlığı, Ankara, 2016.

Elkady, A., & Lignos, D. G. (2012, December). Dynamic stability of deep slender steel columns as part of special MRFs designed in seismic regions: Finite element modeling. In Proc. first international conference on performance-based and life-cycle structural engineering (PLSE), Hong Kong.

Jones, P., & Zareian, F. (2010). Relative safety of high-rise and low-rise steel moment-resisting frames in Los Angeles. The Structural Design of Tall and Special Buildings, 19(1-2), 183-196.

Mercado, J. A., & Arboleda-Monsalve, L. G. (2018). Numerical Insights into Seismic Performance of Low-Rise Buildings with Basements. In IFCEE 2018 (pp. 286-296).

Mohammadi, M., Mirzaei, M., & Pashaie, M. R. (2021, December). Seismic performance and fragility analysis of infilled steel frame structures using a new multi-strut model. In Structures (Vol. 34, pp. 1403-1415). Elsevier.

Odası, T. İ. M. (2018). Türkiye Bina Deprem Yönetmeliği (TBDY-2018) Eğitim Kitabı, Ankara. ZI-3/24.

Structural Engineering Institute, Structural Engineering Institute Seismic Retrofit of Existing Buildings Standards Committee, & American Society of Civil Engineers. (2017). ASCE standard, ASCE/SEI, 41-17: Seismic Evaluation and Retrofit of Existing Buildings. American Society of Civil Engineers. https://doi.org/10.1061/9780784414859

TBDY 2018, "Türkiye Bina Deprem Yönetmeliği (Mayıs 2018), Resmi Gazete

Wu, J. R., Di Sarno, L., Freddi, F., & D'Aniello, M. (2022). Modeling of masonry infills in existing steel moment-resisting frames: Nonlinear force-displacement relationship. Engineering Structures, 267, 114699.

Yakut, A. ve Binici, B. (2023). "Ülkemizde Riskli Yapıların Genel Özellikleri ve Deprem Performansı".. Çevre, Şehir ve İklim Dergisi. Yıl: 2. Sayı: 4. ss. (220-237)

Zervent, A., Yücel, Ö. B., Aldemir, A., Erdil, B. (2024). Türkiye'deki Depreme Dayanıklı Çelik Çerçeveli Bina Tasarımına Retrospektif Bir Bakış. Çukurova Üniversitesi Mühendislik Fakültesi Dergisi, 39(2), 453-466. https://doi.org/10.21605/cukurovaumfd.1514474

Zorlu, M., & Akbaş, B. (2017). Yeni Türkiye Bina Deprem Yönetmeliği'ne Göre Çelik Yapı Tasarımı. Uluslararası Katılımlı, 7, 292-305.

https://tadas.afad.gov.tr

APPENDICES

A. The Check of Strong Column Weak Beam Principle

X-Direction of Earthquake:

This system, which has a high ductility level according to TBEC 9.3.2, will check whether its columns are stronger than its beams in the X direction moment-resisting frame.

$$\frac{\sum M_{pc}^{*}}{\sum M_{pb}^{*}} > 1.0$$

In the evaluation of this condition, the 1st Floor C/2 column is taken as a basis. The joint connection is visualized in Figure 2-5.

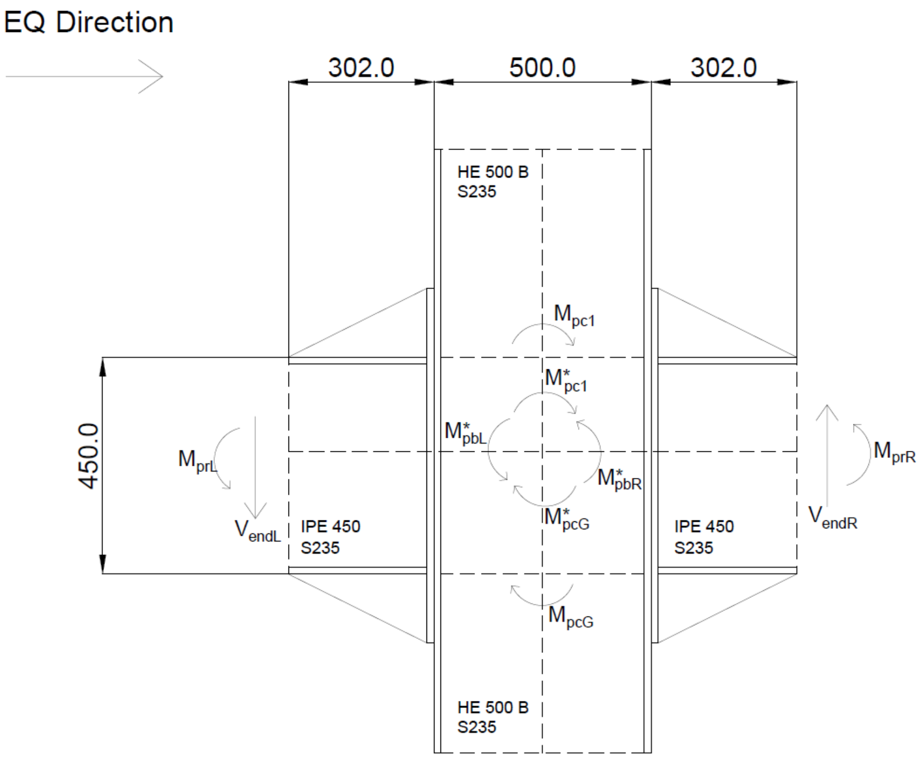

Figure A-1: Strong column - Weak beam principle

The expected flexural strength of the beam, M_{pr},

$$M_{pr} = M_{prR} = M_{prL} = C_{pr} R_y F_y Z$$

While performing SCWB check, possible (expected), material strengths will be utilized in the design of steel structural components and their connections.

$$C_{pr} = \frac{F_y + F_u}{2F_y} = \frac{235 + 360}{2 * 235} = 1.27 > 1.2 \rightarrow C_{pr} = 1.2$$

The possible yield stress of structural steel, R_yF_y, will be determined depending on the structural steel class and element type. For S235, R_y=1.4 according to TBEC2018 Table 9.2.

$$M_{pr} = M_{prR} = M_{prL} = C_{pr} R_y F_y Z = 1.2 * 1.4 * 235 * (1702 * 10^3) * 10^{-6}$$
$$= 671.95\ kNm$$

$$l_n = L - 2 * \frac{d_c}{2} - 2l_n = 8 - 2 * \frac{0.500}{2} - 2 * 0.302 = 6.896\ m$$

$$V_{ucR} = \frac{2M_{prR}}{l_n} + V_{dR} = \frac{2 * 671.95}{6.896} - 90.201 = 104.68\ kN \qquad \text{(Eq. A-1)}$$

$$V_{ucL} = \frac{2M_{prL}}{l_n} + V_{dL} = \frac{2 * 671.95}{6.896} + 50.273 = 245.15\ kN \qquad \text{(Eq. A-2)}$$

In equation, A-1 and A-2, the V_{dR} and V_{dL} shear forces are calculated only under the influence of vertical load combination (1.2G+0.5Q+0.2S).

$$\sum M_{uv} = (V_{endR} + V_{endL})\left(L_h + \frac{d_c}{2}\right) = (104.68 + 245.154)(6.896 + \frac{0.5}{2})$$
$$= 193.108\ kNm$$

$$\sum M_{pb} = 2(1.1 R_y F_{yb} W_{pb}) = 2 * 1.1 * 1.4 * 235 * \left(1702 * 10^3\right) * 10^{-6}$$
$$= 1231.908\ kNm$$

$$\sum M_{pb}^* = \sum M_{pb} + \sum M_{uv} = 1231.908 + 193.108 = 1425.016\ kNm$$

The flexural capacity of the column, M_{pc}:

$$M_{pc} = W_{pc}\left(F_{yc} - \frac{P_{end}}{A_g}\right)$$

Axial compression force, P_{endG}, under the combination of 1.455G+0.5Q+0.2S+D($E_d^{(X)+}$0.3$E_d^{(Y)}$):

$$P_{ucG} = 1190.572 + 3 * 1.036 * (\sim 0) = 1190.572\ kNm$$

$$M_{pcG} = (4815 * 10^3)\left(235 - \left(\frac{1190.572 * 10^3}{23900}\right)\right) * 10^{-6} = 891.67\ kN$$

$$P_{uc1} = 1056.216 + 3 * 1.036 * (\sim 0) = 1056.216\ kNm$$

$$M_{pc1} = (4815 * 10^3)\left(235 - \left(\frac{1056.216 * 10^3}{23900}\right)\right) * 10^{-6} = 918.74\ kN$$

$$M_{pcG}^{*} = 891.67\left(\frac{2.0}{2.0 - \frac{0.50}{2}}\right) = 1019.05\ kNm$$

$$M_{pc1}^{*} = 918.74\left(\frac{1.5}{1.5 - \frac{0.50}{2}}\right) = 1102.49\ kNm$$

$$\frac{\sum M_{pc}^{*}}{\sum M_{pb}^{*}} = \frac{1019.05 + 1102.49}{1425.016} = 1.49 > 1.0\ \checkmark$$

Y-Direction of Earthquake:

The same system, which has a high ductility level according to TBEC 9.3.2, will check whether its columns are stronger than its beams also in the Y direction moment-resisting frame.

In the evaluation of this condition, the 1st Floor E/3 column is taken as a basis.

The expected flexural strength of the beam, M_{pr},

$$M_{pr} = M_{prR} = M_{prL} = C_{pr} R_y F_y Z$$

While performing SCWB checl, possible (expected) material strengths will be utilized in the design of steel structural components and their connections.

$$C_{pr} = \frac{F_y + F_u}{2F_y} = \frac{235 + 360}{2 * 235} = 1.27 > 1.2 \rightarrow C_{pr} = 1.2$$

The possible yield stress of structural steel, R_yF_y, will be determined depending on the structural steel class and element type. For S235, R_y=1.4 according to TBEC2018 Table 9.2.

$$M_{pr} = M_{prR} = M_{prL} = C_{pr} R_y F_y Z = 1.2 * 1.4 * 235 * (1702 * 10^3) * 10^{-6}$$
$$= 671.95\ kNm$$

$$l_n = L - 2 * \frac{d_c}{2} - 2l_h = 6 - 2 * \frac{0.500}{2} - 2 * 0.302 = 4.896\ m$$

$$V_{ucR} = \frac{2M_{prR}}{l_n} + V_{dR} = \frac{2 * 671.95}{4.896} - 73.331 = 201.16\ kN \qquad \text{(Eq. A-3)}$$

$$V_{ucL} = \frac{2M_{prL}}{l_n} + V_{dL} = \frac{2 * 671.95}{4.896} + 72.3 = 346.79\ kN \qquad \text{(Eq. A-4)}$$

In equations A-3 and A-4, the V_{dR} and V_{dL} shear forces are calculated only under the influence of vertical load combination (1.2G+0.5Q+0.2S).

$$\sum M_{uv} = (V_{ucR} + V_{ucL})\left(l_h + \frac{d_c}{2}\right) = (201.16 + 346.79)(0.302 + \frac{0.5}{2})$$
$$= 302.47\ kNm$$

$$\sum M_{pb} = 2(1.1 R_y F_{yb} W_{pb}) = 2 * 1.1 * 1.4 * 235 * \left(1702 * 10^3\right) * 10^{-6}$$
$$= 1231.908\ kNm$$

$$\sum M_{pb}^* = \sum M_{pb} + \sum M_{uv} = 1231.908 + 302.47 = 1534.38\ kNm$$

The flexural capacity of the column, M_{pc}:

$$M_{pc} = W_{pc}\left(F_{yc} - \frac{P_{uc}}{A_g}\right)$$

Axial compression force, P_{ucG}, under the combination of 1.455G+0.5Q+0.2S+D($E_d^{(X)}$-0.3$E_d^{(Y)}$):

$$P_{ucG} = 775.05 + 3 * 1.036 * (\sim 0) = 775.05\ kN$$

$$M_{pcG} = (4815 * 10^3)\left(235 - \left(\frac{775.05 * 10^3}{23900}\right)\right) * 10^{-6} = 975.38\ kNm$$

$$P_{end1} = 572.661 + 3 * 1.036 * (\sim 0) = 572.661\ kN$$

$$M_{pc1} = (4815 * 10^3)\left(235 - \left(\frac{572.661 * 10^3}{23900}\right)\right) * 10^{-6} = 1016.15\ kNm$$

$$M^*_{pcG} = 775.05\left(\frac{2.0}{2.0 - \frac{0.50}{2}}\right) = 885.77\ kNm$$

$$M^*_{pc1} = 572.661\left(\frac{1.5}{1.5 - \frac{0.50}{2}}\right) = 687.19\ kNm$$

$$\frac{\sum M^*_{pc}}{\sum M^*_{pb}} = \frac{885.77 + 687.19}{1534.38} = 1.03 > 1.0\ \checkmark$$

B. Infill Wall Implementation Hinge Status Results for Each Column

Table B-1: S235 Bare Frame Hinge Results in the Columns

EQ Data Station	3129											
Element Type	Floor	Element ID	Performance Level	Floor	Element ID	Performance Level	Floor	Element ID	Performance Level	Floor	Element ID	Performance Level
Column	1	C11A	COLLAPSE	2	C21A	LD	3	C31A	LD	4	C41A	LD
Column	1	C11B	CP	2	C21B	LD	3	C31B	LD	4	C41B	LD
Column	1	C11C	CP	2	C21C	LD	3	C31C	LD	4	C41C	LD
Column	1	C11D	CP	2	C21D	LD	3	C31D	LD	4	C41D	LD
Column	1	C11E	COLLAPSE	2	C21E	LD	3	C31E	LD	4	C41E	LD
Column	1	C12A	COLLAPSE	2	C22A	LD	3	C32A	LD	4	C42A	LD
Column	1	C12B	COLLAPSE	2	C22B	LD	3	C32B	LD	4	C42B	LD
Column	1	C12C	COLLAPSE	2	C22C	LD	3	C32C	LD	4	C42C	LD
Column	1	C12D	COLLAPSE	2	C22D	LD	3	C32D	LD	4	C42D	LD
Column	1	C12E	COLLAPSE	2	C22E	LD	3	C32E	LD	4	C42E	LD
Column	1	C13A	COLLAPSE	2	C23A	LD	3	C33A	LD	4	C43A	LD
Column	1	C13B	COLLAPSE	2	C23B	LD	3	C33B	LD	4	C43B	LD
Column	1	C13C	COLLAPSE	2	C23C	LD	3	C33C	LD	4	C43C	LD
Column	1	C13D	COLLAPSE	2	C23D	LD	3	C33D	LD	4	C43D	LD
Column	1	C13E	COLLAPSE	2	C23E	LD	3	C33E	LD	4	C43E	LD
Column	1	C14A	COLLAPSE	2	C24A	LD	3	C34A	LD	4	C44A	LD
Column	1	C14B	CP	2	C24B	LD	3	C34B	LD	4	C44B	LD
Column	1	C14C	CP	2	C24C	LD	3	C34C	LD	4	C44C	LD
Column	1	C14D	CP	2	C24D	LD	3	C34D	LD	4	C44D	LD
Column	1	C14E	COLLAPSE	2	C24E	LD	3	C34E	LD	4	C44E	LD

Table B-2: S235 1st Floor without Infill Wall Hinge Results in the Columns

Element Type	Floor	Element ID	Performance Level	Floor	Element ID	Performance Level	Floor	Element ID	Performance Level	Floor	Element ID	Performance Level
Column	1	C11A	COLLAPSE	2	C21A	CD	3	C31A	CD	4	C41A	LD
Column	1	C11B	COLLAPSE	2	C21B	LD	3	C31B	LD	4	C41B	LD
Column	1	C11C	CD	2	C21C	LD	3	C31C	LD	4	C41C	LD
Column	1	C11D	COLLAPSE	2	C21D	LD	3	C31D	LD	4	C41D	LD
Column	1	C11E	COLLAPSE	2	C21E	CD	3	C31E	CD	4	C41E	LD
Column	1	C12A	COLLAPSE	2	C22A	CD	3	C32A	CD	4	C42A	LD
Column	1	C12B	COLLAPSE	2	C22B	LD	3	C32B	LD	4	C42B	LD
Column	1	C12C	CP	2	C22C	LD	3	C32C	LD	4	C42C	LD
Column	1	C12D	CP	2	C22D	LD	3	C32D	LD	4	C42D	LD
Column	1	C12E	COLLAPSE	2	C22E	CD	3	C32E	CD	4	C42E	LD
Column	1	C13A	COLLAPSE	2	C23A	CD	3	C33A	CD	4	C43A	LD
Column	1	C13B	COLLAPSE	2	C23B	LD	3	C33B	LD	4	C43B	LD
Column	1	C13C	COLLAPSE	2	C23C	LD	3	C33C	LD	4	C43C	LD
Column	1	C13D	COLLAPSE	2	C23D	LD	3	C33D	LD	4	C43D	LD
Column	1	C13E	COLLAPSE	2	C23E	CD	3	C33E	CD	4	C43E	LD
Column	1	C14A	COLLAPSE	2	C24A	CD	3	C34A	CD	4	C44A	LD
Column	1	C14B	COLLAPSE	2	C24B	LD	3	C34B	LD	4	C44B	LD
Column	1	C14C	CD	2	C24C	LD	3	C34C	LD	4	C44C	LD
Column	1	C14D	COLLAPSE	2	C24D	LD	3	C34D	LD	4	C44D	LD
Column	1	C14E	COLLAPSE	2	C24E	CD	3	C34E	CD	4	C44E	LD

Table B-3: S235 Continuous Infill Wall Hinge Results in the Columns

Element Type	Floor	Element ID	Performance Level	Floor	Element ID	Performance Level	Floor	Element ID	Performance Level	Floor	Element ID	Performance Level
Column	1	C11A	COLLAPSE	2	C21A	CD	3	C31A	LD	4	C41A	LD
Column	1	C11B	COLLAPSE	2	C21B	LD	3	C31B	LD	4	C41B	LD
Column	1	C11C	CD	2	C21C	LD	3	C31C	LD	4	C41C	LD
Column	1	C11D	COLLAPSE	2	C21D	LD	3	C31D	LD	4	C41D	LD
Column	1	C11E	COLLAPSE	2	C21E	CD	3	C31E	LD	4	C41E	LD
Column	1	C12A	COLLAPSE	2	C22A	CD	3	C32A	CD	4	C42A	LD
Column	1	C12B	CP	2	C22B	LD	3	C32B	LD	4	C42B	LD
Column	1	C12C	CP	2	C22C	LD	3	C32C	LD	4	C42C	LD
Column	1	C12D	CP	2	C22D	LD	3	C32D	LD	4	C42D	LD
Column	1	C12E	COLLAPSE	2	C22E	CD	3	C32E	CD	4	C42E	LD
Column	1	C13A	COLLAPSE	2	C23A	CD	3	C33A	CD	4	C43A	LD
Column	1	C13B	CP	2	C23B	LD	3	C33B	LD	4	C43B	LD
Column	1	C13C	CP	2	C23C	LD	3	C33C	LD	4	C43C	LD
Column	1	C13D	CP	2	C23D	LD	3	C33D	LD	4	C43D	LD
Column	1	C13E	COLLAPSE	2	C23E	CD	3	C33E	CD	4	C43E	LD
Column	1	C14A	COLLAPSE	2	C24A	CD	3	C34A	LD	4	C44A	LD
Column	1	C14B	COLLAPSE	2	C24B	LD	3	C34B	LD	4	C44B	LD
Column	1	C14C	CD	2	C24C	LD	3	C34C	LD	4	C44C	LD
Column	1	C14D	COLLAPSE	2	C24D	LD	3	C34D	LD	4	C44D	LD
Column	1	C14E	COLLAPSE	2	C24E	CD	3	C34E	LD	4	C44E	LD

Table B-4: Bare Frame Hinge Results in the Columns

Element Type	Floor	Element ID	Performance Level	Floor	Element ID	Performance Level	Floor	Element ID	Performance Level	Floor	Element ID	Performance Level
Column	1	C11A	CP	2	C21A	LD	3	C31A	LD	4	C41A	LD
Column	1	C11B	CD	2	C21B	LD	3	C31B	LD	4	C41B	LD
Column	1	C11C	CD	2	C21C	LD	3	C31C	LD	4	C41C	LD
Column	1	C11D	CD	2	C21D	LD	3	C31D	LD	4	C41D	LD
Column	1	C11E	CP	2	C21E	LD	3	C31E	LD	4	C41E	LD
Column	1	C12A	CP	2	C22A	LD	3	C32A	LD	4	C42A	LD
Column	1	C12B	CD	2	C22B	LD	3	C32B	LD	4	C42B	LD
Column	1	C12C	CD	2	C22C	LD	3	C32C	LD	4	C42C	LD
Column	1	C12D	CD	2	C22D	LD	3	C32D	LD	4	C42D	LD
Column	1	C12E	CP	2	C22E	LD	3	C32E	LD	4	C42E	LD
Column	1	C13A	CP	2	C23A	LD	3	C33A	LD	4	C43A	LD
Column	1	C13B	CD	2	C23B	LD	3	C33B	LD	4	C43B	LD
Column	1	C13C	CD	2	C23C	LD	3	C33C	LD	4	C43C	LD
Column	1	C13D	CD	2	C23D	LD	3	C33D	LD	4	C43D	LD
Column	1	C13E	CP	2	C23E	LD	3	C33E	LD	4	C43E	LD
Column	1	C14A	CP	2	C24A	LD	3	C34A	LD	4	C44A	LD
Column	1	C14B	CD	2	C24B	LD	3	C34B	LD	4	C44B	LD
Column	1	C14C	CD	2	C24C	LD	3	C34C	LD	4	C44C	LD
Column	1	C14D	CD	2	C24D	LD	3	C34D	LD	4	C44D	LD
Column	1	C14E	CP	2	C24E	LD	3	C34E	LD	4	C44E	LD

Table B-5: S235 1st Floor without Infill Wall Hinge Results in the Columns

Element Type	Floor	Element ID	Performance Level	Floor	Element ID	Performance Level	Floor	Element ID	Performance Level	Floor	Element ID	Performance Level
Column	1	C11A	CD	2	C21A	LD	3	C31A	LD	4	C41A	LD
Column	1	C11B	CD	2	C21B	LD	3	C31B	LD	4	C41B	LD
Column	1	C11C	LD	2	C21C	LD	3	C31C	LD	4	C41C	LD
Column	1	C11D	CD	2	C21D	LD	3	C31D	LD	4	C41D	LD
Column	1	C11E	CD	2	C21E	LD	3	C31E	LD	4	C41E	LD
Column	1	C12A	CP	2	C22A	LD	3	C32A	LD	4	C42A	LD
Column	1	C12B	CD	2	C22B	LD	3	C32B	LD	4	C42B	LD
Column	1	C12C	CD	2	C22C	LD	3	C32C	LD	4	C42C	LD
Column	1	C12D	CD	2	C22D	LD	3	C32D	LD	4	C42D	LD
Column	1	C12E	CP	2	C22E	LD	3	C32E	LD	4	C42E	LD
Column	1	C13A	COLLAPSE	2	C23A	LD	3	C33A	LD	4	C43A	LD
Column	1	C13B	CD	2	C23B	LD	3	C33B	LD	4	C43B	LD
Column	1	C13C	CD	2	C23C	LD	3	C33C	LD	4	C43C	LD
Column	1	C13D	CD	2	C23D	LD	3	C33D	LD	4	C43D	LD
Column	1	C13E	COLLAPSE	2	C23E	LD	3	C33E	LD	4	C43E	LD
Column	1	C14A	CD	2	C24A	LD	3	C34A	LD	4	C44A	LD
Column	1	C14B	CD	2	C24B	LD	3	C34B	LD	4	C44B	LD
Column	1	C14C	LD	2	C24C	LD	3	C34C	LD	4	C44C	LD
Column	1	C14D	CD	2	C24D	LD	3	C34D	LD	4	C44D	LD
Column	1	C14E	CD	2	C24E	LD	3	C34E	LD	4	C44E	LD

Table B-6: S355 Continuous Infill Wall Hinge Results in the Columns

Element Type	Floor	Element ID	Performance Level	Floor	Element ID	Performance Level	Floor	Element ID	Performance Level	Floor	Element ID	Performance Level
Column	1	C11A	CD	2	C21A	LD	3	C31A	LD	4	C41A	LD
Column	1	C11B	LD	2	C21B	LD	3	C31B	LD	4	C41B	LD
Column	1	C11C	LD	2	C21C	LD	3	C31C	LD	4	C41C	LD
Column	1	C11D	LD	2	C21D	LD	3	C31D	LD	4	C41D	LD
Column	1	C11E	CD	2	C21E	LD	3	C31E	LD	4	C41E	LD
Column	1	C12A	CP	2	C22A	LD	3	C32A	LD	4	C42A	LD
Column	1	C12B	LD	2	C22B	LD	3	C32B	LD	4	C42B	LD
Column	1	C12C	LD	2	C22C	LD	3	C32C	LD	4	C42C	LD
Column	1	C12D	LD	2	C22D	LD	3	C32D	LD	4	C42D	LD
Column	1	C12E	CP	2	C22E	LD	3	C32E	LD	4	C42E	LD
Column	1	C13A	CP	2	C23A	LD	3	C33A	LD	4	C43A	LD
Column	1	C13B	LD	2	C23B	LD	3	C33B	LD	4	C43B	LD
Column	1	C13C	LD	2	C23C	LD	3	C33C	LD	4	C43C	LD
Column	1	C13D	LD	2	C23D	LD	3	C33D	LD	4	C43D	LD
Column	1	C13E	CP	2	C23E	LD	3	C33E	LD	4	C43E	LD
Column	1	C14A	CD	2	C24A	LD	3	C34A	LD	4	C44A	LD
Column	1	C14B	LD	2	C24B	LD	3	C34B	LD	4	C44B	LD
Column	1	C14C	LD	2	C24C	LD	3	C34C	LD	4	C44C	LD
Column	1	C14D	LD	2	C24D	LD	3	C34D	LD	4	C44D	LD
Column	1	C14E	CD	2	C24E	LD	3	C34E	LD	4	C44E	LD

C. Basement Floor Implementation Hinge Status Results for Each Column

Table C-1: S235 Bare Frame with Basement Hinge Results

EQ Data Station	3129																		
Element Type	Floor	Element ID	Performance Level	Element Type	Floor	Element ID	Performance Level	Floor	Element ID	Performance Level	Floor	Element ID	Performance Level	Floor	Element ID	Performance Level			
Column	Basement	CB1A	LD	Column	1	C11A	COLLAPSE	2	C21A	LD	3	C31A	LD	4	C41A	LD			
Column	Basement	CB1B	LD	Column	1	C11B	CD	2	C21B	LD	3	C31B	LD	4	C41B	LD			
Column	Basement	CB1C	LD	Column	1	C11C	CD	2	C21C	LD	3	C31C	LD	4	C41C	LD			
Column	Basement	CB1D	LD	Column	1	C11D	CD	2	C21D	LD	3	C31D	LD	4	C41D	LD			
Column	Basement	CB1E	LD	Column	1	C11E	COLLAPSE	2	C21E	LD	3	C31E	LD	4	C41E	LD			
Column	Basement	CB2A	LD	Column	1	C12A	COLLAPSE	2	C22A	LD	3	C32A	LD	4	C42A	LD			
Column	Basement	CB2B	CD	Column	1	C12B	COLLAPSE	2	C22B	LD	3	C32B	LD	4	C42B	LD			
Column	Basement	CB2C	CD	Column	1	C12C	CP	2	C22C	LD	3	C32C	LD	4	C42C	LD			
Column	Basement	CB2D	CD	Column	1	C12D	CP	2	C22D	LD	3	C32D	LD	4	C42D	LD			
Column	Basement	CB2E	LD	Column	1	C12E	COLLAPSE	2	C22E	LD	3	C32E	LD	4	C42E	LD			
Column	Basement	CB3A	LD	Column	1	C13A	COLLAPSE	2	C23A	LD	3	C33A	LD	4	C43A	LD			
Column	Basement	CB3B	CD	Column	1	C13B	COLLAPSE	2	C23B	LD	3	C33B	LD	4	C43B	LD			
Column	Basement	CB3C	CD	Column	1	C13C	CP	2	C23C	LD	3	C33C	LD	4	C43C	LD			
Column	Basement	CB3D	CD	Column	1	C13D	CP	2	C23D	LD	3	C33D	LD	4	C43D	LD			
Column	Basement	CB3E	LD	Column	1	C13E	COLLAPSE	2	C23E	LD	3	C33E	LD	4	C43E	LD			
Column	Basement	CB4A	LD	Column	1	C14A	COLLAPSE	2	C24A	LD	3	C34A	LD	4	C44A	LD			
Column	Basement	CB4B	LD	Column	1	C14B	CD	2	C24B	LD	3	C34B	LD	4	C44B	LD			
Column	Basement	CB4C	LD	Column	1	C14C	CD	2	C24C	LD	3	C34C	LD	4	C44C	LD			
Column	Basement	CB4D	LD	Column	1	C14D	CD	2	C24D	LD	3	C34D	LD	4	C44D	LD			
Column	Basement	CB4E	LD	Column	1	C14E	COLLAPSE	2	C24E	LD	3	C34E	LD	4	C44E	LD			

Table C-2: S235 1st Floor without Infill Wall with Basement Hinge Results

EQ Data Station	3129															
Element Type	Floor	Element ID	Performance Level	Element Type	Floor	Element ID	Performance Level	Floor	Element ID	Performance Level	Floor	Element ID	Performance Level	Floor	Element ID	Performance Level
Column	Basement	CB1A	LD	Column	1	C11A	COLLAPSE	2	C21A	CD	3	C31A	CD	4	C41A	LD
Column	Basement	CB1B	LD	Column	1	C11B	COLLAPSE	2	C21B	LD	3	C31B	LD	4	C41B	LD
Column	Basement	CB1C	LD	Column	1	C11C	CD	2	C21C	LD	3	C31C	LD	4	C41C	LD
Column	Basement	CB1D	CD	Column	1	C11D	CP	2	C21D	LD	3	C31D	LD	4	C41D	LD
Column	Basement	CB1E	LD	Column	1	C11E	COLLAPSE	2	C21E	CD	3	C31E	CD	4	C41E	LD
Column	Basement	CB2A	LD	Column	1	C12A	COLLAPSE	2	C22A	CP	3	C32A	CD	4	C42A	LD
Column	Basement	CB2B	CD	Column	1	C12B	CD	2	C22B	LD	3	C32B	LD	4	C42B	LD
Column	Basement	CB2C	CD	Column	1	C12C	CD	2	C22C	LD	3	C32C	LD	4	C42C	LD
Column	Basement	CB2D	CD	Column	1	C12D	CD	2	C22D	LD	3	C32D	LD	4	C42D	LD
Column	Basement	CB2E	LD	Column	1	C12E	COLLAPSE	2	C22E	CP	3	C32E	CD	4	C42E	LD
Column	Basement	CB3A	LD	Column	1	C13A	COLLAPSE	2	C23A	CD	3	C33A	CD	4	C43A	LD
Column	Basement	CB3B	CD	Column	1	C13B	CD	2	C23B	LD	3	C33B	LD	4	C43B	LD
Column	Basement	CB3C	CD	Column	1	C13C	CP	2	C23C	LD	3	C33C	LD	4	C43C	LD
Column	Basement	CB3D	CD	Column	1	C13D	CD	2	C23D	LD	3	C33D	LD	4	C43D	LD
Column	Basement	CB3E	LD	Column	1	C13E	COLLAPSE	2	C23E	CD	3	C33E	CD	4	C43E	LD
Column	Basement	CB4A	LD	Column	1	C14A	COLLAPSE	2	C24A	CD	3	C34A	CD	4	C44A	LD
Column	Basement	CB4B	LD	Column	1	C14B	COLLAPSE	2	C24B	LD	3	C34B	LD	4	C44B	LD
Column	Basement	CB4C	LD	Column	1	C14C	CD	2	C24C	LD	3	C34C	LD	4	C44C	LD
Column	Basement	CB4D	CD	Column	1	C14D	CP	2	C24D	LD	3	C34D	LD	4	C44D	LD
Column	Basement	CB4E	LD	Column	1	C14E	COLLAPSE	2	C24E	CD	3	C34E	CD	4	C44E	LD

Table C-3: S235 Continuous Infill Wall with Basement Hinge Results

EQ Data Station	3129																
Element Type	Floor	Element ID	Performance Level	Element Type	Floor	Element ID	Performance Level	Floor	Element ID	Performance Level	Floor	Element ID	Performance Level	Floor	Element ID	Performance Level	
Column	Basement	CB1A	CD	Column	1	C11A	CP	2	C21A	CD	3	C31A	LD	4	C41A	LD	
Column	Basement	CB1B	LD	Column	1	C11B	CD	2	C21B	LD	3	C31B	LD	4	C41B	LD	
Column	Basement	CB1C	LD	Column	1	C11C	CD	2	C21C	LD	3	C31C	LD	4	C41C	LD	
Column	Basement	CB1D	LD	Column	1	C11D	CD	2	C21D	LD	3	C31D	LD	4	C41D	LD	
Column	Basement	CB1E	LD	Column	1	C11E	COLLAPSE	2	C21E	CD	3	C31E	LD	4	C41E	LD	
Column	Basement	CB2A	CP	Column	1	C12A	COLLAPSE	2	C22A	CD	3	C32A	CD	4	C42A	LD	
Column	Basement	CB2B	CD	Column	1	C12B	CD	2	C22B	LD	3	C32B	LD	4	C42B	LD	
Column	Basement	CB2C	CD	Column	1	C12C	CD	2	C22C	LD	3	C32C	LD	4	C42C	LD	
Column	Basement	CB2D	CD	Column	1	C12D	CD	2	C22D	LD	3	C32D	LD	4	C42D	LD	
Column	Basement	CB2E	LD	Column	1	C12E	COLLAPSE	2	C22E	CD	3	C32E	CD	4	C42E	LD	
Column	Basement	CB3A	CP	Column	1	C13A	COLLAPSE	2	C23A	CD	3	C33A	CD	4	C43A	LD	
Column	Basement	CB3B	CD	Column	1	C13B	CD	2	C23B	LD	3	C33B	LD	4	C43B	LD	
Column	Basement	CB3C	CD	Column	1	C13C	CD	2	C23C	LD	3	C33C	LD	4	C43C	LD	
Column	Basement	CB3D	CD	Column	1	C13D	CD	2	C23D	LD	3	C33D	LD	4	C43D	LD	
Column	Basement	CB3E	LD	Column	1	C13E	COLLAPSE	2	C23E	CD	3	C33E	CD	4	C43E	LD	
Column	Basement	CB4A	CD	Column	1	C14A	CD	2	C24A	CD	3	C34A	LD	4	C44A	LD	
Column	Basement	CB4B	LD	Column	1	C14B	CD	2	C24B	LD	3	C34B	LD	4	C44B	LD	
Column	Basement	CB4C	LD	Column	1	C14C	CD	2	C24C	LD	3	C34C	LD	4	C44C	LD	
Column	Basement	CB4D	LD	Column	1	C14D	CD	2	C24D	LD	3	C34D	LD	4	C44D	LD	
Column	Basement	CB4E	LD	Column	1	C14E	COLLAPSE	2	C24E	CD	3	C34E	LD	4	C44E	LD	

Table C-4: S355 Bare Frame with Basement Hinge Results

EQ Data Station	3129																
Element Type	Floor	Element ID	Performance Level	Element Type	Floor	Element ID	Performance Level	Floor	Element ID	Performance Level	Floor	Element ID	Performance Level	Floor	Element ID	Performance Level	
Column	Basement	CB1A	LD	Column	1	C11A	CD	2	C21A	LD	3	C31A	LD	4	C41A	LD	
Column	Basement	CB1B	LD	Column	1	C11B	LD	2	C21B	LD	3	C31B	LD	4	C41B	LD	
Column	Basement	CB1C	LD	Column	1	C11C	LD	2	C21C	LD	3	C31C	LD	4	C41C	LD	
Column	Basement	CB1D	LD	Column	1	C11D	LD	2	C21D	LD	3	C31D	LD	4	C41D	LD	
Column	Basement	CB1E	LD	Column	1	C11E	CD	2	C21E	LD	3	C31E	LD	4	C41E	LD	
Column	Basement	CB2A	LD	Column	1	C12A	CP	2	C22A	LD	3	C32A	LD	4	C42A	LD	
Column	Basement	CB2B	LD	Column	1	C12B	CD	2	C22B	LD	3	C32B	LD	4	C42B	LD	
Column	Basement	CB2C	LD	Column	1	C12C	CD	2	C22C	LD	3	C32C	LD	4	C42C	LD	
Column	Basement	CB2D	LD	Column	1	C12D	LD	2	C22D	LD	3	C32D	LD	4	C42D	LD	
Column	Basement	CB2E	LD	Column	1	C12E	CP	2	C22E	LD	3	C32E	LD	4	C42E	LD	
Column	Basement	CB3A	LD	Column	1	C13A	CP	2	C23A	LD	3	C33A	LD	4	C43A	LD	
Column	Basement	CB3B	LD	Column	1	C13B	CD	2	C23B	LD	3	C33B	LD	4	C43B	LD	
Column	Basement	CB3C	LD	Column	1	C13C	CD	2	C23C	LD	3	C33C	LD	4	C43C	LD	
Column	Basement	CB3D	LD	Column	1	C13D	LD	2	C23D	LD	3	C33D	LD	4	C43D	LD	
Column	Basement	CB3E	LD	Column	1	C13E	CP	2	C23E	LD	3	C33E	LD	4	C43E	LD	
Column	Basement	CB4A	LD	Column	1	C14A	CD	2	C24A	LD	3	C34A	LD	4	C44A	LD	
Column	Basement	CB4B	LD	Column	1	C14B	LD	2	C24B	LD	3	C34B	LD	4	C44B	LD	
Column	Basement	CB4C	LD	Column	1	C14C	CD	2	C24C	LD	3	C34C	LD	4	C44C	LD	
Column	Basement	CB4D	LD	Column	1	C14D	LD	2	C24D	LD	3	C34D	LD	4	C44D	LD	
Column	Basement	CB4E	LD	Column	1	C14E	CD	2	C24E	LD	3	C34E	LD	4	C44E	LD	

Table C-5: S355 1st Floor without Infill Wall with Basement Hinge Results

EQ Data Station	3129

Element Type	Floor	Element ID	Performance Level	Element Type	Floor	Element ID	Performance Level	Floor	Element ID	Performance Level	Floor	Element ID	Performance Level	Floor	Element ID	Performance Level
Column	Basement	CB1A	LD	Column	1	C11A	CP	2	C21A	LD	3	C31A	LD	4	C41A	LD
Column	Basement	CB1B	LD	Column	1	C11B	LD	2	C21B	LD	3	C31B	LD	4	C41B	LD
Column	Basement	CB1C	LD	Column	1	C11C	LD	2	C21C	LD	3	C31C	LD	4	C41C	LD
Column	Basement	CB1D	LD	Column	1	C11D	LD	2	C21D	LD	3	C31D	LD	4	C41D	LD
Column	Basement	CB1E	LD	Column	1	C11E	CP	2	C21E	LD	3	C31E	LD	4	C41E	LD
Column	Basement	CB2A	LD	Column	1	C12A	COLLAPSE	2	C22A	LD	3	C32A	LD	4	C42A	LD
Column	Basement	CB2B	LD	Column	1	C12B	LD	2	C22B	LD	3	C32B	LD	4	C42B	LD
Column	Basement	CB2C	LD	Column	1	C12C	LD	2	C22C	LD	3	C32C	LD	4	C42C	LD
Column	Basement	CB2D	LD	Column	1	C12D	LD	2	C22D	LD	3	C32D	LD	4	C42D	LD
Column	Basement	CB2E	LD	Column	1	C12E	COLLAPSE	2	C22E	LD	3	C32E	LD	4	C42E	LD
Column	Basement	CB3A	LD	Column	1	C13A	CP	2	C23A	LD	3	C33A	LD	4	C43A	LD
Column	Basement	CB3B	LD	Column	1	C13B	LD	2	C23B	LD	3	C33B	LD	4	C43B	LD
Column	Basement	CB3C	LD	Column	1	C13C	LD	2	C23C	LD	3	C33C	LD	4	C43C	LD
Column	Basement	CB3D	LD	Column	1	C13D	LD	2	C23D	LD	3	C33D	LD	4	C43D	LD
Column	Basement	CB3E	LD	Column	1	C13E	CP	2	C23E	LD	3	C33E	LD	4	C43E	LD
Column	Basement	CB4A	LD	Column	1	C14A	CP	2	C24A	LD	3	C34A	LD	4	C44A	LD
Column	Basement	CB4B	LD	Column	1	C14B	LD	2	C24B	LD	3	C34B	LD	4	C44B	LD
Column	Basement	CB4C	LD	Column	1	C14C	LD	2	C24C	LD	3	C34C	LD	4	C44C	LD
Column	Basement	CB4D	LD	Column	1	C14D	LD	2	C24D	LD	3	C34D	LD	4	C44D	LD
Column	Basement	CB4E	LD	Column	1	C14E	CP	2	C24E	LD	3	C34E	LD	4	C44E	LD

Table C-6: S355 Continuous Infill Wall with Basement Hinge Results

EQ Data Station	3129

Element Type	Floor	Element ID	Performance Level	Element Type	Floor	Element ID	Performance Level	Floor	Element ID	Performance Level	Floor	Element ID	Performance Level	Floor	Element ID	Performance Level
Column	Basement	CB1A	LD	Column	1	C11A	CD	2	C21A	LD	3	C31A	LD	4	C41A	LD
Column	Basement	CB1B	LD	Column	1	C11B	LD	2	C21B	LD	3	C31B	LD	4	C41B	LD
Column	Basement	CB1C	LD	Column	1	C11C	LD	2	C21C	LD	3	C31C	LD	4	C41C	LD
Column	Basement	CB1D	LD	Column	1	C11D	LD	2	C21D	LD	3	C31D	LD	4	C41D	LD
Column	Basement	CB1E	LD	Column	1	C11E	CD	2	C21E	LD	3	C31E	LD	4	C41E	LD
Column	Basement	CB2A	LD	Column	1	C12A	CD	2	C22A	LD	3	C32A	LD	4	C42A	LD
Column	Basement	CB2B	LD	Column	1	C12B	LD	2	C22B	LD	3	C32B	LD	4	C42B	LD
Column	Basement	CB2C	LD	Column	1	C12C	LD	2	C22C	LD	3	C32C	LD	4	C42C	LD
Column	Basement	CB2D	LD	Column	1	C12D	LD	2	C22D	LD	3	C32D	LD	4	C42D	LD
Column	Basement	CB2E	LD	Column	1	C12E	CD	2	C22E	LD	3	C32E	LD	4	C42E	LD
Column	Basement	CB3A	LD	Column	1	C13A	CP	2	C23A	LD	3	C33A	LD	4	C43A	LD
Column	Basement	CB3B	LD	Column	1	C13B	LD	2	C23B	LD	3	C33B	LD	4	C43B	LD
Column	Basement	CB3C	LD	Column	1	C13C	LD	2	C23C	LD	3	C33C	LD	4	C43C	LD
Column	Basement	CB3D	LD	Column	1	C13D	LD	2	C23D	LD	3	C33D	LD	4	C43D	LD
Column	Basement	CB3E	LD	Column	1	C13E	CP	2	C23E	LD	3	C33E	LD	4	C43E	LD
Column	Basement	CB4A	LD	Column	1	C14A	CD	2	C24A	LD	3	C34A	LD	4	C44A	LD
Column	Basement	CB4B	LD	Column	1	C14B	LD	2	C24B	LD	3	C34B	LD	4	C44B	LD
Column	Basement	CB4C	LD	Column	1	C14C	LD	2	C24C	LD	3	C34C	LD	4	C44C	LD
Column	Basement	CB4D	LD	Column	1	C14D	LD	2	C24D	LD	3	C34D	LD	4	C44D	LD
Column	Basement	CB4E	LD	Column	1	C14E	CD	2	C24E	LD	3	C34E	LD	4	C44E	LD

Table C-7: S235 Bare Frame Moment-Resisting Beams Hinge Results

EQ Data Station	3129													
Element Type	Cross-sections	Length	Floor	Element ID	Performance Level	Floor	Element ID	Performance Level	Floor	Element ID	Performance Level	Floor	Element ID	Performance Level
Beam	IPE450	8 m	1	B11BC	CD	2	B21BC	CD	3	B31BC	CD	4	B41BC	CD
Beam	IPE450	8 m	1	B11CD	CD	2	B21CD	CD	3	B31CD	CD	4	B41CD	CD
Beam	IPE450	8 m	1	B12BC	CD	2	B22BC	CD	3	B32BC	CD	4	B42BC	CD
Beam	IPE450	8 m	1	B12CD	CD	2	B22CD	CD	3	B32CD	CD	4	B42CD	CD
Beam	IPE450	8 m	1	B13BC	CD	2	B23BC	CD	3	B33BC	CD	4	B43BC	CD
Beam	IPE450	8 m	1	B13CD	CD	2	B23CD	CD	3	B33CD	CD	4	B43CD	CD
Beam	IPE450	8 m	1	B14BC	CD	2	B24BC	CD	3	B34BC	CD	4	B44BC	CD
Beam	IPE450	8 m	1	B14CD	CD	2	B24CD	CD	3	B34CD	CD	4	B44CD	CD
Beam	IPE450	6 m	1	B1A12	LD	2	B2A12	LD	3	B3A12	LD	4	B4A12	LD
Beam	IPE450	6 m	1	B1A23	LD	2	B2A23	LD	3	B3A23	LD	4	B4A23	LD
Beam	IPE450	6 m	1	B1A34	LD	2	B2A34	LD	3	B3A34	LD	4	B4A34	LD
Beam	IPE450	6 m	1	B1E12	LD	2	B2E12	LD	3	B3E12	LD	4	B4E12	LD
Beam	IPE450	6 m	1	B1E23	LD	2	B2E23	LD	3	B3E23	LD	4	B4E23	LD
Beam	IPE450	6 m	1	B1E34	LD	2	B2E34	LD	3	B3E34	LD	4	B4E34	LD

Table C-8: S355 Continuous Infill Wall with Basement Moment-Resisting Beams Hinge Results

EQ Data Station	3129													
Element Type	Cross-sections	Length	Floor	Element ID	Performance Level	Floor	Element ID	Performance Level	Floor	Element ID	Performance Level	Floor	Element ID	Performance Level
Beam	IPE450	8 m	1	B11BC	LD	2	B21BC	LD	3	B31BC	LD	4	B41BC	LD
Beam	IPE450	8 m	1	B11CD	CD	2	B21CD	LD	3	B31CD	LD	4	B41CD	LD
Beam	IPE450	8 m	1	B12BC	CD	2	B22BC	LD	3	B32BC	LD	4	B42BC	LD
Beam	IPE450	8 m	1	B12CD	CD	2	B22CD	LD	3	B32CD	LD	4	B42CD	LD
Beam	IPE450	8 m	1	B13BC	CD	2	B23BC	LD	3	B33BC	LD	4	B43BC	LD
Beam	IPE450	8 m	1	B13CD	CD	2	B23CD	LD	3	B33CD	LD	4	B43CD	LD
Beam	IPE450	8 m	1	B14BC	LD	2	B24BC	LD	3	B34BC	LD	4	B44BC	LD
Beam	IPE450	8 m	1	B14CD	CD	2	B24CD	LD	3	B34CD	LD	4	B44CD	LD
Beam	IPE450	6 m	1	B1A12	LD	2	B2A12	LD	3	B3A12	LD	4	B4A12	LD
Beam	IPE450	6 m	1	B1A23	LD	2	B2A23	LD	3	B3A23	LD	4	B4A23	LD
Beam	IPE450	6 m	1	B1A34	LD	2	B2A34	LD	3	B3A34	LD	4	B4A34	LD
Beam	IPE450	6 m	1	B1E12	LD	2	B2E12	LD	3	B3E12	LD	4	B4E12	LD
Beam	IPE450	6 m	1	B1E23	LD	2	B2E23	LD	3	B3E23	LD	4	B4E23	LD
Beam	IPE450	6 m	1	B1E34	LD	2	B2E34	LD	3	B3E34	LD	4	B4E34	LD